



TECHNISCHE
UNIVERSITÄT
WIEN

Master Thesis

Biomedical Engineering

Side-group Modification of Selenobenzoacenes: Synthesis and Characterization of a New Class of Soluble Semiconductors

performed at the
Institute of Applied Synthetic Chemistry
at the **TU Wien**

under the supervision of
Univ.Prof. Dipl.-Ing. Dr.techn. Johannes **Fröhlich**
and
Ass. Prof. Dipl.-Ing. Dr.techn. Christian **Hametner**

by
Dipl.-Ing. Dr.techn. Brigitte **Holzer**



Vienna, July 2023

Danksagung

An dieser Stelle möchte ich mich herzlich bei nachstehenden Personen bedanke, ohne deren Unterstützung die Anfertigung dieser Arbeit nicht möglich gewesen wäre.

Johannes Fröhlich danke ich für die Unterstützung und Möglichkeit diese Arbeit durchzuführen. Vielen Dank für den zugestandenen Freiraum bei den Forschungsaktivitäten!

Mein besonderer Dank gilt Christian Hametner für die zahlreichen Ratschläge und Korrekturen während der Arbeit.

Weiters möchte ich mich bei Berthold Stöger für die Kooperation sowie für das Messen zahlreicher Einkristalle bedanken.

Für die gute Zusammenarbeit möchte ich mich bei meinen (ehemaligen) LaborkollegInnen bedanken. Besonders möchte ich mich bei Hannes Mikula, Daniel Lumpi, Ernst Horkel, Thomas Kader, Dorian Bader, Birgit Meindl, Nikolaus Poremba, Katharina Pfennigbauer, Lavinia Klement und allen anderen Mitgliedern der FGHF für das angenehme Arbeitsklima und die Unterstützung in vielen Belangen in den letzten Jahren bedanken.

Bei Thomas Schwartz, Lavinia Klement, Jacqueline Bitai, Anna-Maria Schober (Wagner), Barbara Dellago, Marlene Matthuber, Fabio Stipkovits, David Schönbauer, Thomas Anderl (Raab) und Michael Schmitz, deren Bachelorarbeiten und (Wahl)Praktika ich betreuen durfte, gebührt mein Dank für die produktive und unterhaltsame Zeit im Labor.

Für die Unterstützung während der gesamten Arbeit möchte ich mich zudem beim allgemeinen Personal der TU bedanken; ohne sie wäre ein Laborbetrieb in dieser Form nicht möglich. Insbesondere gilt mein Dank Sabine Stiedry und Tanja Halbarth.

Abschließend möchte ich mich bei meinen Eltern Erika und Artur Holzer bedanken– vielen Dank für das mir entgegengebrachte Verständnis und Vertrauen.

Meinem Partner Maximilian Wohlgemuth möchte ich von ganzem Herzen für die Unterstützung und die stete Motivation in den letzten Jahren danken.

Kurzfassung

Organische Halbleiter haben aufgrund ihrer mechanischen Flexibilität und ihres geringen Gewichts im Vergleich zu ihren anorganischen Gegenstücken an großem Interesse gewonnen. Kommerzielle Geräte wie flexible Displays auf Basis organischer Halbleiter sind bereits erhältlich. Darüber hinaus bieten organische Halbleiter eine noch viel breitere Anwendbarkeit und könnten in flexiblen Sensoren sowie biologischen und medizinischen elektronischen Geräten verwendet werden. Insbesondere im Bereich der biomedizinischen Technik können organische Halbleiter als Biosensoren, Electronic Skin, thermische oder implantierbare Sensoren oder Detektoren für ionisierende Strahlung eingesetzt werden.

Unter den organischen Halbleitern ist TIPS-Pentacen (Abb. 1) ein hervorragendes Material für organische Feldeffekttransistoren (OFETs). Jedoch erschwert seine mangelnde Stabilität eine breitere Anwendung. Die Einführung von Heteroatomen wie Schwefel in Acenhalbleitern hat zur Entwicklung von stabilen und hocheffizienten Halbleitermaterialien geführt, allerdings auf Kosten ihrer Löslichkeit. Der Ersatz von Schwefel durch schwerere Atome verbessert nachweislich die Halbleitereigenschaften von Thioacenen aufgrund des großen Atomradius, der hohen Polarisierbarkeit sowie der effizienten intermolekularen Wechselwirkungen im Festkörper. Solche Verbindungen stellen eine neue Substanzklasse für Detektoren für ionisierende Strahlung dar.

Im Rahmen dieser Arbeit sollten trialkylsilylethynylsubstituierte Selen-basierte Analoga von TIPS-Pentacen synthetisiert werden. Diese Zielverbindungen wurden so konzipiert, dass sie (i) Trialkylsilylethynylgruppen zur Erhöhung der Löslichkeit sowie (ii) Selen-

Heteroatome mit großem Strahlungseingangsquerschnitt enthalten. Die erhaltenen Zielverbindungen sollen somit aus Lösung prozessierbar sowie für die Anwendung in Sensoren zur Detektion von ionisierender Strahlung vorteilhaft sein. Zusätzlich wurden Benzothiophen-basierte Analoga untersucht, um den Einfluss des Heteroatoms in dieser Serie zu untersuchen.

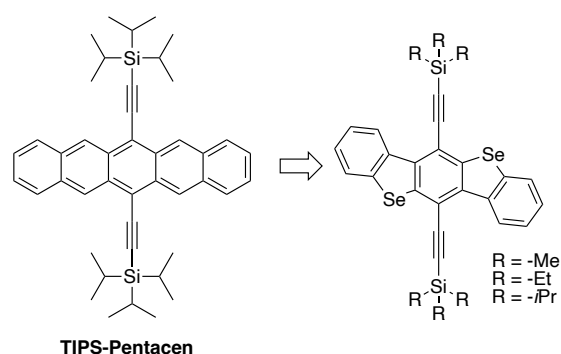


Abbildung 1 TIPS-Pentacene sowie Trialkylsilylethynyl-substituierte Zielmoleküle.

Für die Synthese dieser Materialien wurden zwei verschiedene Ansätze verfolgt. Einerseits wurden intramolekulare Ringschlussreaktionen basierend auf nukleophiler Substitution, C-H- oder C-F-Aktivierung untersucht. Andererseits wurde die Synthese der Zielmoleküle durch nukleophile Addition der Trialkylsilylethynylgruppe an geeignete aromatische Chinone und anschließende Reduktion der resultierenden Diole effizient realisiert.

Weiters wurden Einkristalle aller Zielverbindungen auf ihre intermolekulare Packungsanordnung untersucht. Alle Zielverbindungen wurden hinsichtlich ihrer molekular-elektronischen Eigenschaften mittels UV-Vis-Spektroskopie und Cyclovoltammetrie charakterisiert. Die Ergebnisse dieser Studie legen eine neue vielversprechende Substanzklasse für die Anwendung als lösliche und stabile Lochleiter in biomedizinischen Geräten nahe.

Abstract

Organic semiconductors have gained considerable interest due to their mechanical flexibility and light compared to their inorganic counterparts. Commercial devices such as flexible displays based on organic semiconductors are already available. However, these materials offer a much broader applicability and may be used in sensors as well as biological and medical electronic devices. Especially in the field of biomedical engineering, organic semiconductors may be applied as biosensors, electronic skins, or ionizing radiation detectors.

Among organic semiconductors, TIPS-pentacene (Fig. 1) is a benchmark material in organic field effect transistors (OFETs). However, its lack of stability hampers its broader application. The introduction of heteroatoms in acene semiconductors has led to stable and highly efficient semiconducting material, however at the expense of their solubility. The replacement of sulfur atoms by heavier atoms has been shown to improve the semiconducting properties of thioacenes due to the large atomic radius, high polarizability as well as efficient intermolecular electronic coupling in the solid state. Furthermore, such compounds incorporating a high atomic number atom represent a new substance class for ionizing radiation detectors.

Within this thesis, trialkylsilylethynyl substituted selenium-based analogues of TIPS-pentacene were designed and synthesized. The novel potential semiconductors were designed to include (i) trialkylsilylethynyl groups facilitating the solubility of the target compounds rendering these compounds solution-processable and (ii) selenium heteroatoms ensuring a large

radiation capture cross section beneficial for application in ionizing radiation detectors. Additionally, benzothiophene-based analogues were investigated to evaluate the influence of the heteroatom in this series.

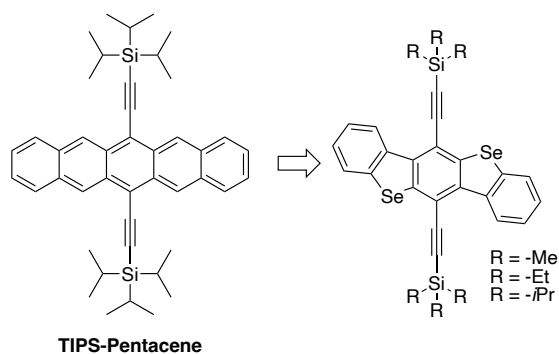


Figure 1: TIPS-Pentacene and trialkylsilylethynyl-substituted target compounds.

To realize these materials, two different synthetic approaches were assessed. Intramolecular ring closure reactions based on nucleophilic substitution, C-H or C-F activation were evaluated. Furthermore, a convenient synthetic approach toward the target molecules by nucleophilic addition of the trialkylsilylethynyl group to suitable aromatic quinones and subsequent reduction of the resulting diols is presented.

Single crystals of all target compounds were investigated regarding their intermolecular packing arrangement. Additionally, all target compounds were characterized in terms of molecular electronic properties using UV-Vis spectroscopy and cyclic voltammetry. The results of this study suggest a new promising substance class for the application as soluble and stable p-channel organic semiconductors applicable in biomedical devices.

Abbreviations

ACN	acetonitrile
BBBS	benzo[1,2- <i>b</i> :4,5- <i>b'</i>]bis[<i>b</i>]benzoselenophene
BBBT	benzo[1,2- <i>b</i> :4,5- <i>b'</i>]bis[<i>b</i>]benzothiophene
DCM	dichloromethane
DCE	1,2-dichloroethane
DIPA	diisopropylamine
DMF	dimethylformamide
DMSO	dimethylsulfoxide
EtOAc	ethyl acetate
eq.	equivalents
Et ₃ N	triethylamine
EtOH	ethanol
GC-MS	gas chromatography – mass spectrometry
<i>i</i> PrOH	isopropanol
KOtBu	potassium <i>tert</i> -butoxide
<i>n</i> BuLi	<i>n</i> -butyllithium
NP	normal phase
MeOH	methanol
NBS	<i>N</i> -bromosuccinimide
NMP	<i>N</i> -methyl-2-pyrrolidone
NMR	nuclear magnetic resonance
<i>t</i> BuLi	<i>tert</i> -butyllithium
TIPS-pentacene	6,13-bis(triisopropylsilylethynyl)pentacene

General Remarks

Labelling of substances

Identification of substances is achieved by strict sequential numbering. Substances previously reported in literature receive Arabic numerals, whereas substances unknown to literature are labelled in Roman numerals.

References to literature citations

References to literature are given within the text by superscript Arabic numbers.

Nomenclature

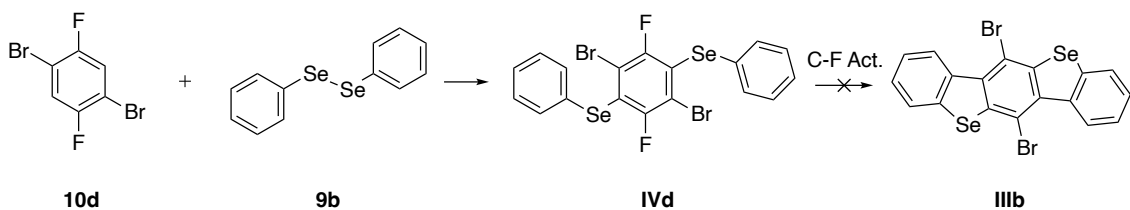
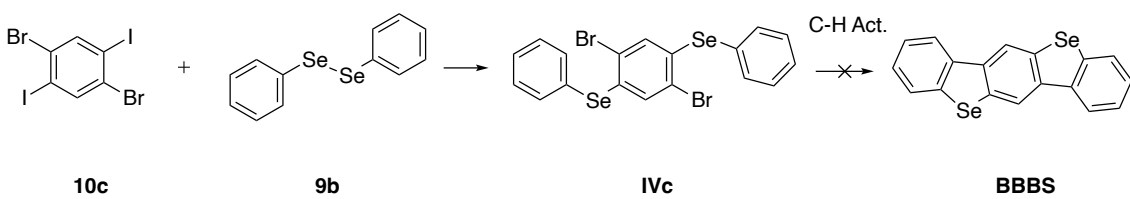
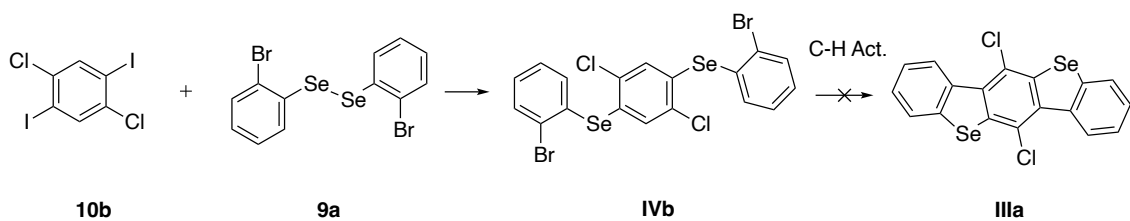
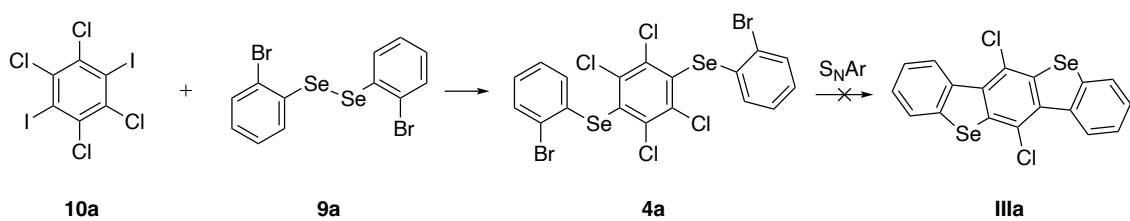
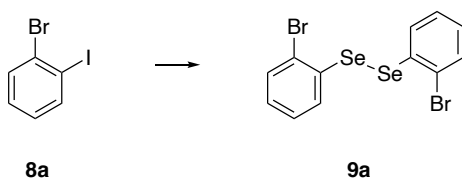
The nomenclature of chemical compounds not described in literature is based on the rules of Chemical Abstracts. Other compounds, reagents and solvents may be described by simplified terms, trivial or trade names.

Table of Contents

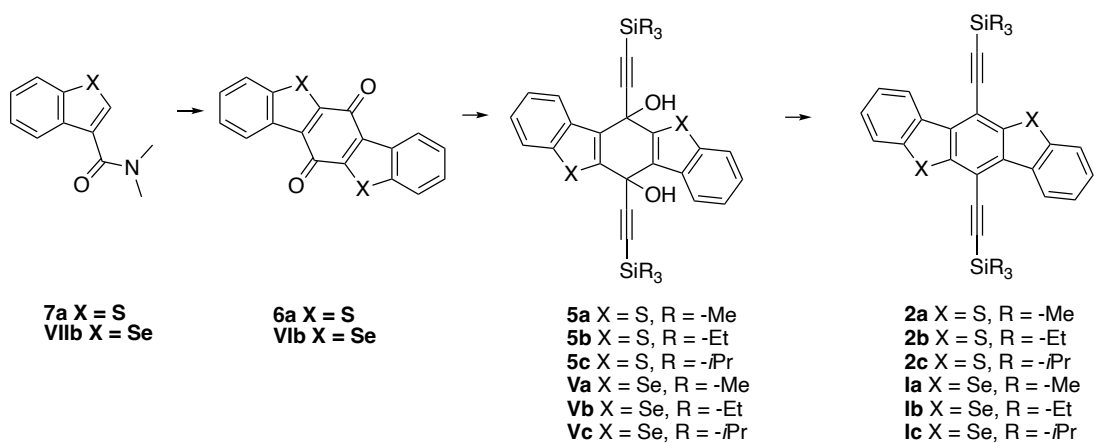
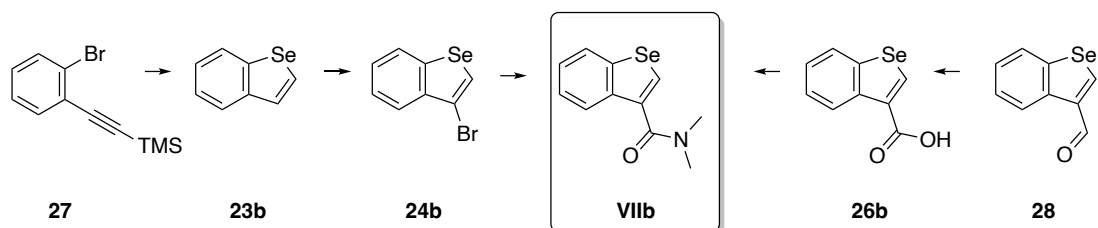
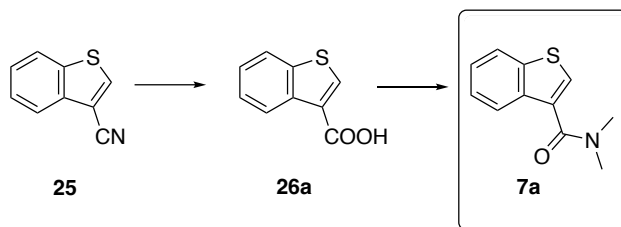
1	FORMULA SCHEME	2
1.1	INTRAMOLECULAR CYCLIZATION APPROACHES	2
1.2	SYNTHESIS VIA QUINONES	3
2	INTRODUCTION	4
2.1	INTRODUCTION – ORGANIC ELECTRONICS	4
2.2	ORGANIC FIELD EFFECT TRANSISTORS	5
2.3	THE RISE OF THE APPLICATION OF OFETs IN BIOMEDICAL DEVICES	9
2.4	OBJECTIVES	13
3	SPECIFIC PART	14
3.1	RETROSYNTHETIC ANALYSIS	14
3.2	INTRAMOLECULAR CYCLIZATION APPROACH TOWARD 6,12-DISUBSTITUTED BENZO[1,2- <i>B</i> :4,5- <i>B'</i>]BIS[1]BENZOSELENOPHENES	15
3.2.1	SYNTHESIS OF BIS(PHENYLSELENO)BENZENES	16
3.2.2	INTRAMOLECULAR CYCLIZATION VIA NUCLEOPHILIC AROMATIC SUBSTITUTION	19
3.2.3	INTRAMOLECULAR CYCLIZATION VIA C-H ACTIVATION	20
3.2.4	INTRAMOLECULAR CYCLIZATION VIA C-F ACTIVATION	22
3.3	SYNTHESIS VIA QUINONES	24
3.3.1	SYNTHESIS OF FUSED AROMATIC QUINONES	24
3.3.2	SYNTHESIS OF TRIALKYLSILYLETHYNYL-SUBSTITUTED TARGET COMPOUNDS	27
3.4	ANALYSIS OF TARGET COMPOUNDS	28
3.4.1	SINGLE CRYSTAL STRUCTURES	28
3.4.2	ASSESSMENT OF THE HOMO-LUMO ENERGY GAP	31
3.5	SUMMARY & OUTLOOK	34
4	EXPERIMENTAL PART	36
4.1	MATERIALS AND METHODS	36
4.1.1	REACTANTS AND SOLVENTS	36
4.1.2	CHROMATOGRAPHIC METHODS	36
4.2	ANALYTIC METHODS	36
4.2.1	MASS SPECTROMETERS	36
4.2.2	NMR SPECTROSCOPY	36
4.2.3	UV-VIS SPECTROSCOPY	36
4.2.4	CYCLIC VOLTAMMETRY	36
4.3	SYNTHESIS AND CHARACTERIZATION OF ALL COMPOUNDS	37
4.3.1	SYNTHETIC INTERMEDIATES FOR RING-CLOSURE STRATEGY	37
4.3.2	SYNTHETIC STRATEGY TOWARD TARGET COMPOUNDS VIA QUINONE	39
4.1	REFERENCES	49
4.2	APPENDIX	52

1 Formula Scheme

1.1 Intramolecular Cyclization Approaches



1.2 Synthesis *via* Quinones



2 Introduction

2.1 Introduction – Organic Electronics

In the past few decades, the field of organic semiconductors gained significant interest due to their potential application in next generation technologies. The ultra-thin, lightweight and large-area features of these flexible devices make them suitable for various applications, including rollable display screens, intelligent identification cards, and wearable and implantable electronics that can be worn or embedded in the body.^[1] Unlike traditional silicon technologies, significant advancements have been made in developing flexible electronic devices through cost-effective and energy-efficient manufacturing processes. These devices include organic field-effect transistors (OFETs), organic light-emitting diodes (OLEDs), and organic photovoltaic (OPV) devices and memories.

The first organic semiconductors can be dated back to 1862, when Henry Letheby made the initial discovery polyaniline. As a physician, he was interested in the poisonous nature of aniline and observed a conductive bluish-green material by anodic oxidation of aniline in sulfuric acid, which decolorized when reduced.^[2] The first report on organic semiconductors can be dated back to the 1950s, when the electrical conductivity of charge-transfer complexes of polycyclic aromatic compounds and halogens was investigated by the group of Matsunaga: a high conductivity of 0.12 S cm^{-1} was reported in perylene–iodine complexes.^[3] However, already at that time the low stability of these organic materials was reported. In 1977, the highly conducting nature of chemically doped polyacetylene exhibiting metallic conductivity (10^5 S cm^{-1}) was shown by Hideki Shirakawa, Alan Heeger, and Alan MacDiarmid.^[4] As stated in the conclusions of the publication, these findings have led “to the development of a large new class of conducting organic polymers with electrical properties that can be controlled over the full range from insulator to semiconductor to metal.”^[4] For this discovery, Shirakawa, Heeger, and MacDiarmid were awarded the 2000 Nobel prize in Chemistry for “The discovery and development of conductive polymers”.^[5] This significant breakthrough paved the way for the design, synthesis and introduction in commercial products of a variety of organic semiconducting materials (OSC) including polythiophene, polyphenylene sulfide, and others (Figure 2).

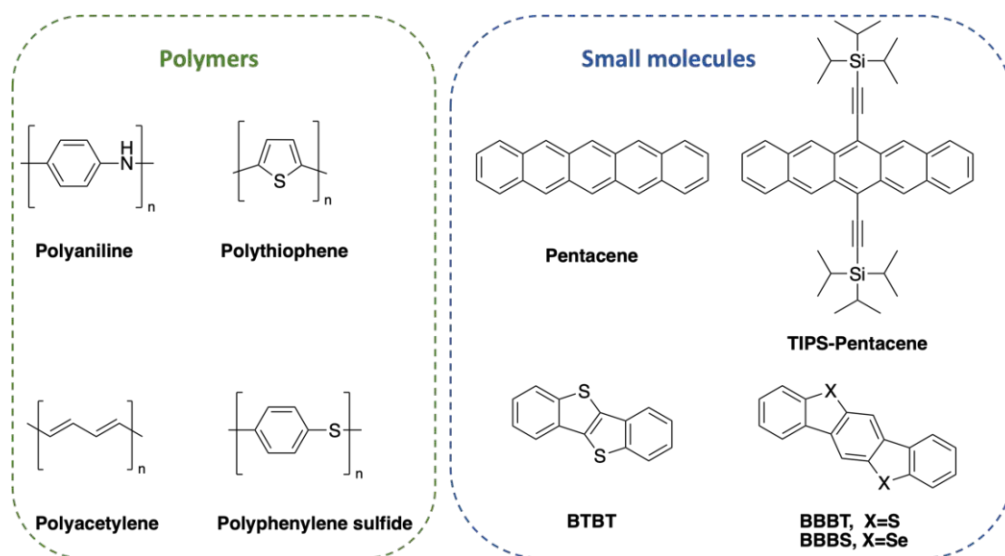


Figure 2: Polymer and small molecule-based semiconducting materials.

2.2 Organic Field Effect Transistors

While photoconductivity and electroluminescence of organic compounds have been known since the 1900s, these materials have been regarded as “semiconducting materials” with energy gaps.^[6] The concept of a field-effect transistor (FET) was introduced by J.E. Lilienfeld in 1920, but it was not until 1986 that the Mitsubishi Electric researchers Hiroshi Koezuka et al. reported the first application of the semiconducting nature of polythiophene (Figure 2) in switching devices (organic field-effect transistor, OFET).^[7] Nevertheless, the device performance as well as the stability of these prototypical OFETs were poor rendering them unsuitable for practical applications. The great breakthroughs in the field of OFETs were observed in the late the 1990s, as several research groups including Bell Laboratories in the United States reported on significant enhancement in device performance. These improvements allowed the consideration of implementing organic semiconductors in large-area electronic circuits.^[8] In addition to polymeric semiconductors, small molecule based semiconductors such as pentacene (Figure 2) were used in OFETs demonstrating charge carrier mobilities of up to $1.5 \text{ cm}^2 \text{ V}^{-1} \text{ s}^{-1}$.^[9] Especially pentacene, known for its easy availability and good reproducibility in OFET performances, has emerged as the standard organic semiconductor and found extensive use in various OFET studies.

Organic Semiconductors in OFETs

There are two classes of OSCs that are commonly applied in organic electronics: molecular and polymeric semiconductors (Figure 2). Polymeric semiconductors offer advantages such as facile intra- and interchain transport, ease of solution processing with suitable functionalization, and a wide range of possibilities for chemical modifications. However, they often require reaction conditions, that result in a high level of polydispersity and regiochemical isomers, which significantly impact the device performance. Consequently, sophisticated synthetic and purification methods are essential to ensure the desired level of purity. In contrast, small molecule semiconductors have well-defined structures and are generally easier to synthesize, purify and processed either by vacuum or solution deposition techniques. The monodisperse nature of these molecular entities facilitates the investigation of structure-property relations, although film formation and solid-state packing can be highly sensitive to minor chemical modifications.^[10]

Molecular design strategies of organic compounds allow tailoring the properties of organic semiconductors. Using the tools of organic chemistry, semiconductors can be realized that exhibit good stability, processability, solubility in organic solvents and device performance. These qualities are crucial for the development of functional devices. Among small molecules, pentacene is one of the most studied OSCs for high-performance field-effect transistors due to its high charge carrier mobility of up to $35 \text{ cm}^2 \text{ V}^{-1} \text{ s}^{-1}$.^[11] Pentacene has a highly delocalized rigid π -system and crystallizes in the herringbone packing structure. The good crystallization behavior of pentacene ensures good reproducibility of the packing arrangement of pentacene resulting in a two-dimensional isotropic electronic structure, which is also advantageous to achieve high performances.^[12] However, pentacene also has major disadvantages to be used as a semiconductor: (i) it is very prone to degradation processes induced by light and oxygen and (ii) its poor solubility limits its processability.^[6]

Over the past 20 years, new synthetic schemes have been developed to address some of these challenges encountered with pristine pentacene.^[13] Pentacene derivatives, such as 6,13-diethynylsubstituted pentacenes have emerged as solution-processable organic semiconductors. Among them, TIPS-pentacene (Figure 2) has become a benchmark semiconductor due to its high solubility (>100 mg/mL in chloroform) allowing the fabrication of OFET devices from solution. These devices demonstrate a hole mobility of $0.17 \text{ cm}^2 \text{ V}^{-1} \text{ s}^{-1}$ and an on/off current ratio of 10^5 .^[14] However, also substituted pentacene suffers from poor photostability, both in solution and in the solid state undergoing [4+4] dimerization and photooxidations.^[15] In addition, TIPS-pentacene exhibits an undesirable thermal transition at 124°C , which corresponds to a crystal to crystal phase transition. Heating the semiconductor above this temperature leads to thermal expansion causing cracks and substantial decrease in device performance.^[16]

To circumvent the limitations of acene-based semiconductors, molecular design strategies have been applied to incorporate heteroatoms in the π -conjugated backbone of acenes. The incorporation of heteroatoms, such as sulfur or selenium, is a common strategy to reduce the highest occupied molecular orbital (HOMO) energy level enabling the development of air-stable, high-performance organic semiconductors. Although the benzothiophene analogue of pentacene, benzo[1,2-*b*:4,5-*b'*]bis[*b*]benzothiophene (BBBT, Figure 2) proved to be a stable p-channel organic semiconductor with a small HOMO-LUMO energy gap, its solubility was rather low affording OFET devices after physical vapor deposition with low hole mobility of $2.4 \times 10^{-3} \text{ cm}^2 \text{ V}^{-1} \text{ s}^{-1}$.^[17] A similar device performance was observed for the selenium analogue benzo[1,2-*b*:4,5-*b'*]bis[*b*]benzoselenophene (BBBS, Figure 2) in this study.^[17] Therefore, to take advantage of the stability of this system, it is essential to adapt these compounds toward materials with an optimized molecular arrangement.

Molecular Orbital Design Considerations

While inorganic semiconducting compounds are strongly bonded through covalent bonds, organic materials are organized via intermolecular weak Van der Waals interactions in the solid state.^[18] This weak bonding in OSCs results in a lack of efficient molecular orbital overlap and leads to small bandwidths explaining the low intrinsic electrical conductivity of OSCs.^[19] The intermolecular charge transport is strongly influenced by the frontier molecular orbital energy levels and their distribution along the conjugated π electron backbone of the OSC in both small molecule and polymer.^[20] Both the electron density distribution along the molecule as well as the delocalization of the π -electron system orbitals significantly influence the HOMO energy level. Exemplarily, the energy scheme in Figure 3 shows the respective positions of the frontier orbitals of an OSC.

Charge transport in OSCs involves the addition or removal of electrons: an organic semiconductor is n-type (electron-transporting) when electron injection is easier than hole injection, which occurs when the LUMO is closer to the Fermi level than the HOMO. Contrary, if holes are more easily injected into an OSC than electrons, the material is p-type or hole transporting. While the HOMO wavefunction is delocalized over its entire π -conjugated backbone, the LUMO wavefunction is predominantly localized on electron-deficient substituents of a molecule. Therefore, the rational introduction of

substituents into a conjugated organic molecule is a practical means to manipulate molecular orbital energy levels: functional groups which can directly donate electron density either mesomerically or inductively can contribute to raising the HOMO energy level.^[20] By the introduction of electron accepting groups at the periphery of a molecule the LUMO energy level can be tuned. In general, in the case of hole transporting (p-type) organic semiconductors the level of HOMO is also crucial for the stability of the materials. Particularly if the HOMO energy level is above -4.97 eV, OSC become instable due to reactions with oxygen from the surrounding environment.^[21]

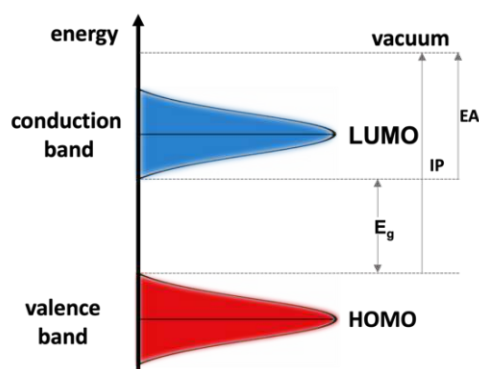


Figure 3: HOMO and LUMO energy levels in organic semiconductors. The optical bandgap E_g is the difference in energy between the highest energy of the valence band and the lowest energy of the conduction band (HOMO/LUMO energy gap). The ionization potential (IP) is the energy to remove one electron from the top of the valence band, whereas the electron affinity (E_A) is the energy released by adding one electron from the vacuum level to the bottom of the conduction band according to Bronstein et. al.^[20]

Packing Motives in Organic Semiconductors

Efficient charge transport in small-molecule organic semiconductors relies on frequent transfer of charge carriers between adjacent molecules. Consequently, the size and arrangement of molecular crystals play a critical role as it determines the extent of overlap of frontier orbitals that allows charges to be transported.^[22] The four most commonly observed packing motifs of pentacene derivatives are shown in Figure 4.

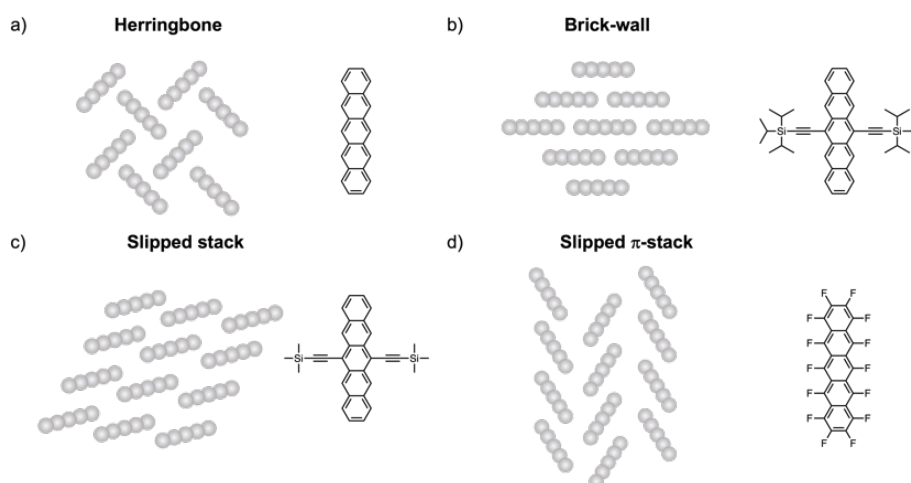


Figure 4: Common packing motifs of molecular semiconductors. a) Herringbone arrangement with charge transport dominated by edge-to-face interactions (pentacene), b) Brick-wall arrangement (TIPS-pentacene), c) Slipped-stack packing (TMS-pentacene) and d) Slipped π -stacking arrangement (perfluorinated pentacene).

Clearly, the introduced substituent in the pentacene backbone crucially impacts the packing arrangements and the semiconducting properties: in the herringbone (pentacene) and brick-wall (TIPS-pentacene) packing the highest charge carrier mobilities have been observed.^[22] Introducing a trimethylsilylethynyl group in pentacene results in slipped stacks,^[23] while for perfluorinated pentacene^[24] slipped π -stacks are observed.

While the presence of hydrogen bonds between adjacent molecules can aid in the self-assembly and reorganization of molecular packing resulting in efficient charge carrier transport, often limited solubility of OSCs is observed. Consequently, these materials are often difficult to process and cannot be used in direct OFET fabrication.^[25] Here, the introduction of side groups into the backbone of an OSC can facilitate its solubility.

Device Configuration

OFET devices consist of three different components: the OSC layer, electrodes (source, drain, and gate), and dielectric layer. The source and drain electrodes are in direct contact with the OSC, which forms the active channel for charge transport, whereas the gate electrode is isolated from the semiconductor by the dielectric, an insulator with high permittivity, and modulates the current flow across the source-drain electrodes.^[26] The OSC layer is employed with a film thickness lower than one micrometer. Typical device configurations of OFETs are given in Figure 5: bottom-gate bottom-contact (BG/BC), bottom-gate top-contact (BG/TC), top-gate bottom-contact (TG/BC), and top-gate top-contact (TG/TC).

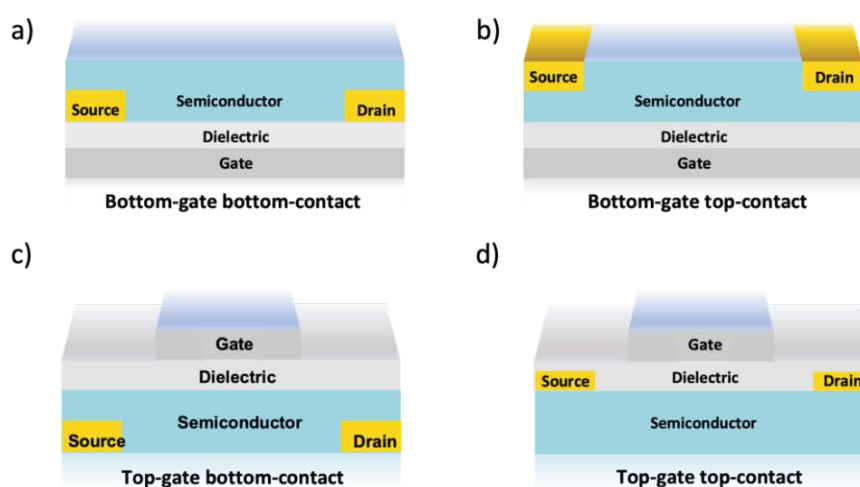


Figure 5: Schematic view of organic field-effect transistor configurations: (a) Bottom-gate bottom-contact (BGBC) (b) Bottom-gate top-contact (BGTC); (c) Top-gate bottom-contact (TGBC) and (d) Top-gate top-contact (TGTC) configuration.

Field-effect transistors can be considered as plane parallel capacitors, where one of the plates serves as the gate electrode, while the semiconductor element forms the second plate. The application of a bias at the gate electrode induces charge carriers in the OSC, while source and drain electrodes inject and retrieve charge carriers. When no voltage is applied between gate and source electrodes, ideally no current flows between the source and drain electrodes and the transistor is switched off. However, when a bias is applied, the transistor operates like a capacitor inducing charge carriers in the semiconducting layer forming a conducting channel. The conductance of the semiconductor increases with the

rising number of charge carriers in the channel and the transistor is switched on. Field-induced charge carriers in the semiconductor are only confined to the first few monolayers in proximity to the semiconductor/dielectric interface forming a two-dimensional conductive channel. Therefore, the ordering, orientation, and microstructure of the OSC at the molecular level significantly influence the device performance.

2.3 The Rise of the Application of OFETs in Biomedical Devices

Organic semiconductors provide remarkable properties such as flexibility, light weight, transparency, low-power consumption, ease of integration, high sensitivity, and large-area solution processability. These properties have fueled a broad range of technological application of OFETs as switches, amplifiers, transducers, drivers, and data-storage components for rollable displays and bendable smart cards.^[1] These advantages over inorganic material drive the usage of organic semiconductors in biomedical applications. Most of all the flexibility of these devices allows unprecedented, integrated device functions and architectures opening a **new perspective in medical applications**. Especially, OFETs provide an ideal bioelectronic interface that facilitates direct interactions between the semiconductor and external stimuli. This enables the **label-free detection of biological species** (such as antigens, biomarkers or whole cells) or physical signals (such as pressure or radiation energy) with high sensitivity.^[27]

Flexible electronics can retain comparatively steady electrical performance when subjected to mechanical bending, folding, twisting, compression and stretching.^[1] These **skin-like electronics** can be attached to human skin or within the body and may be applied in health monitoring, medical treatment, medical implants and biological studies. For example, the group of Bao has developed self-healing elastomers for robust electronic^[28] as well as an electronic skin-like device based on a stretchable transistor array, which remains stable under 1000 cycles of 100% strain.^[29] The similar properties of organic detectors to human tissue in density and composition render these devices ideal candidates for wearable sensitive ionizing radiation detectors in medical dosimetry applications.^[30] In the following section, **flexible ionizing radiation detectors** will be described that may allow experimental real-time and in situ dose monitoring during therapy.

Application as Ionizing Radiation Detectors

Over the past two decades, the use of radiation in modern medical imaging procedures and therapeutics has expanded rapidly.^[31] While providing accurate diagnosis and treatment decisions for patients, ionizing radiation represents a constant risk to medical personnel in certain departments such as cardiology, cardiovascular surgery, radiology, orthopedics and accident surgery.^[32] An especially high tumor risk was identified for radiation exposed orthopedic staff in a study investigating cumulative cancer incidence between 1976 and 2000. Here, a significant increase in cancer was observed in this group compared to personnel in other hospital departments.^[33]

Therefore, the detection of ionizing radiation is an increasingly important task in sectors including preventative radiological nuclear detection in hospitals, nuclear facilities, citizen and airport security, defense, environmental monitoring as well as nondestructive industrial testing.^[34,35]

Specifically, there is a growing demand for large-area, thin, flexible sensors capable of real-time and cost-efficient detection of ionizing radiation, which currently cannot be met by one single device.^[36] Various radiation detectors such as Geiger-Müller counters, dose rate meters, personal dosimeters, and portal monitors provide information on radiation doses for precautionary and monitoring purposes, either directly or indirectly. Typically, inorganic materials such as silicon, cadmium telluride, amorphous selenium, silicon carbide or diamond are used in solid-state devices due to their excellent detection performance. However, these materials have drawbacks in terms of limited active detection area, high weight, and power consumption. Additionally, their inability to provide real-time data renders radiation monitoring activities less effective.

Ionizing radiation detectors can be classified in two categories according to the used functional material, scintillators and semiconductors allowing an indirect or direct detection mechanism.^[37] In the case of scintillators, the incoming ionizing radiation is transduced into an electrical output signal in a two-steps process: first, a scintillator converts the incoming X-ray radiation into visible photons and then a photodiode converts the photons into an electrical signal. In the direct detection mode, an X-ray photon is typically absorbed by a OSC generating a high-energy electron which then releases its excess energy in the surroundings through the photoelectric effect and Compton scattering process. This results in the formation of electron-hole pairs and phonons. The generated electron-hole pairs are the charge carriers that are collected by the detector as a signal, while the phonons essentially represent losses. When an electric field is applied, the charge carriers drift toward their respective electrodes enabling the direct conversion of the incident photons to an electrical current.^[36]

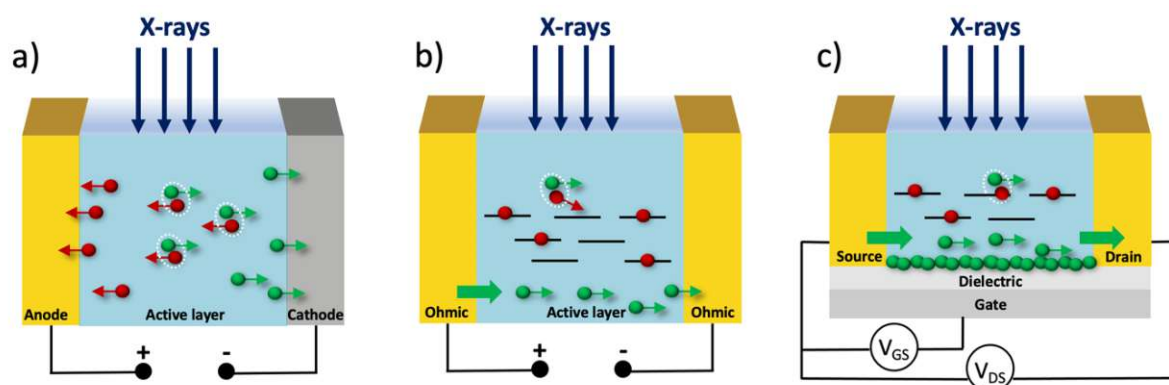


Figure 6: Schematic of the X-ray detection process in organic semiconductors: charge collection in a (a) photodiode, (b) photoconductor and (c) phototransistor architecture according to ^[37].

Different device architectures of organic direct ionizing radiation detectors are shown in Figure 6: photodiodes, photoconductors, and phototransistors. In photodiodes and photoconductors, the absorbing material is between two conductive electrodes (Figure 6 a,b). The sensitivity of these thin film organic semiconductors toward ionizing radiation can be improved, when using them in phototransistor architectures (Figure 6 c).^[34,38–40] In such devices, the gate electrode induces a charge current flowing in the channel between source and drain electrodes (as discussed in 2.2). Additional charges may be induced by the interaction with radiation rendering transistors X-ray detectors.^[37] Biasing the gate electrode with voltages progressively higher than the threshold, the charge density in

the transistor channel increases, leading to the enhancement of charge accumulation and gain of the detection performance. Setting the gate biasing below the threshold voltage, the charge carrier density in the transistor channel is low and the photocurrent results from the separation and collection of ionization charges generated by X-ray photon absorption.^[37] The advantage of transistor-based detectors lies in their ability to fully control the signal by the gate voltage.^[37]

Development of Semiconductors in Ionizing Radiation Detectors

The high demand for flexibility, conformability, low cost, low power consumption, and portability requires new materials and device architectures.^[34] In the past decade, both organic semiconductor thin crystals and polymers have shown great potential as active materials in highly sensitive ionizing radiation sensing devices, especially in X- and gamma-ray detectors.^[41–43] Despite having lower carrier mobility and a lower ionizing radiation absorption coefficient compared to inorganic semiconductors, their solution-processability onto unconventional flexible substrates (such as polyethylene terephthalate (PET), polyethylene naphthalate (PEN), polyimide (Kapton) foils) and over large areas through cost-effective processing techniques has made them interesting alternatives.^[44] Direct radiation detectors based on OFETs have been recently reported to outperform all the polymeric devices in sensitivity using a 100 nm-thick microcrystalline TIPS-pentacene active layer operating at room temperature and at very low bias voltages (<5 V), thanks to a photoconductive gain mechanism.^[38,45] Nevertheless, in such devices high-energy photon absorption is challenging since OSCs are made of atoms with low atomic number (Z). In order to develop a material that is suitable as a OSC for ionizing radiation detectors, the following main prerequisites have to be considered: (i) high resistivity and low leakage current, (ii) a small band gap to grant a low electron-hole ionization energy, a large number of photogenerated electron-hole pairs and thus a higher signal to noise ratio, (iii) a high atomic number and/or a large interaction volume for efficient radiation-atom interactions and thus effective detection, (iv) high intrinsic $\mu\tau$ (mobility lifetime) product, as an efficient collection of photogenerated charges is determined by which fraction effectively traverses the detector and reaches the electrodes, (v) homogenous, defect-free or defect-controlled materials, to ensure good charge transport properties and no conductive short circuits between the electrode, (vi) electrodes which produce no defects, impurities or barriers to the charge collection process and which can be used effectively to apply a uniform electric field across the device.^[37]

Considering the wide range of requirements, it becomes clear that not all can be met within one single material. One parameter that has been addressed in such devices is the improvement of high-energy photon absorption which is challenging as organic materials are constituted of atoms with low Z atomic numbers. This represents a constraint for the detection of high-energy radiation due to the resulting low stopping power. A wide range of strategies were recently suggested to enhance the absorbance of the organic layer, such as introducing in the active layer high-Z elements as nanoparticles or quantum dots, coupling the added high-Z elements with organic bulk heterojunctions, inserting carbon nanotubes in the active layer, and, more recently, by adding high-Z atoms directly into the molecule structure.^[40] In this context, chemical tailoring of known organic molecules such as TIPS-pentacene to synthesize new molecules with high-Z atoms was effectively realized by Anthony and co-

workers: germanium was substituted for silicon in TIPS-pentacene to produce TIPGe-Pentacene (Figure 7) to increase the material atomic number boosting the X-ray detection performance of organic thin films.^[34] Flexible devices with high mobility ($0.4 \text{ cm}^2 \text{ V}^{-1} \text{ s}^{-1}$) and enhanced X-ray sensitivity up to $9.0 \times 10^5 \text{ } \mu\text{C Gy}^{-1} \text{ cm}^{-3}$ could be obtained.

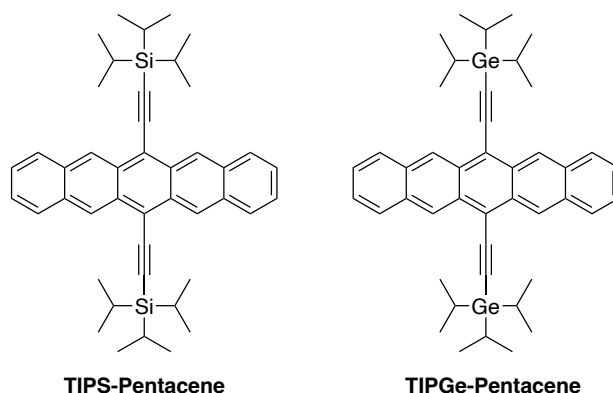


Figure 7: Organic semiconducting materials applied in OFET-based ionizing radiation detectors.^[46]

Despite the scientific efforts to push the performance of organic materials for the direct X-ray detection, there are only few studies that investigated the systematic integration of high-Z atoms in organic semiconductors for ionizing radiation detectors. Given these limitation of current materials, it becomes clear, that there are still challenges that have to be overcome: (i) the stability under atmospheric conditions and (ii) reducing the dark current to improve the lowest detectable dose.^[37] Within this work, the design and synthesis of a new class of soluble organic semiconductors and the structure-property relationships of the resulting compounds will be discussed, which ultimately add to the understanding of the underlying physical principles on a molecular basis. The investigation of structure-function relationships specific to X-ray radiation detection is a critical next step in advancing this field of research.

2.4 Objectives

The aim of this thesis is to synthesize and characterize organic semiconducting materials that overcome the drawbacks of prior materials as described above. The inclusion of five-membered heteroaromatic rings such as thiophene and selenophene in the linear backbone of pentacene has been shown to enhance photo- and thermal stability.^[17] This work aims to enhance the oxidation stability of carbon-based acenes by incorporating selenium as a high-Z atom in TIPS-pentacene like structures **1a-c** (Figure 8). Additionally, the introduction of suitable side chains such as trialkylsilyl ethynyl groups at the 6- and 12-position of these selenoacenes will ensure the solubility of these target compounds. The comparison of sulfur- (**2a-c**) and selenium- (**1a-c**) based materials will allow a direct evaluation of structure-property relationship through photophysical and electrochemical analysis. Furthermore, the assessment of the influence of the trialkylsilyl ethynyl groups on the intermolecular interactions in single crystals will allow insights in the packing motives of these materials.

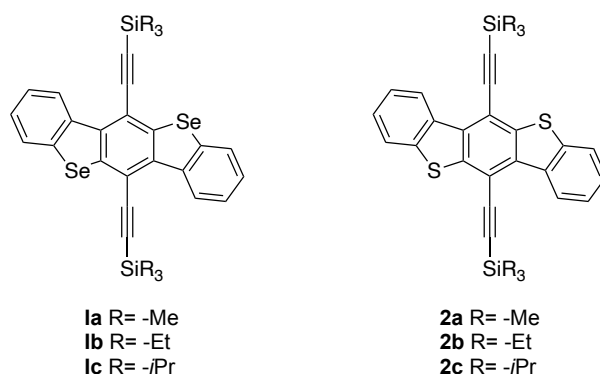


Figure 8: Molecular structures of trialkylsilyl ethynyl substituted target compounds **1a-c** and **2a-c**.

The synthesis of the target molecules will be pursued based on two strategies: (i) intramolecular ring closure reactions or (ii) synthesis of fused aromatic quinones followed by nucleophilic substitution and reductive aromatization. The first approach includes nucleophilic aromatic substitution, C-H or C-F activation starting from diphenyldiselenide and its derivatives. This strategy offers the advantage of functionalizing the BBBS system at the two relevant positions (6 and 12) by the choice of starting materials. The second strategy will follow a literature procedure for TIPS-BBBS systems,^[47] in which alkynyl substituents are introduced in fused aromatic quinone backbones, followed by reductive aromatization of the diol intermediates yielding the trialkylsilyl ethynyl substituted target molecules **1a-c** and **2a-c**. Additionally, considering the lack of commercially available selenium-based compounds and limited availability of published procedures toward benzoselenophenes, synthetic approaches to obtain suitably substituted precursor will be evaluated.

The target compounds **1a-c** are expected to exhibit semiconducting behavior with good solubility in organic solvents, rendering them well-suited for OFET applications. By incorporation of selenium, a high-Z atom, into these materials, an increase in the radiation capture cross section compared to sulfur-based materials is expected. This improvement is expected to enhance the ionizing radiation absorption while maintaining the favorable characteristics of TIPS-pentacene including solution-processability, crystallization behavior and charge transport properties of deposited thin films.

3 Specific Part

3.1 Retrosynthetic Analysis

The retrosynthetic analysis of the target compounds **1a-c** is given in Figure 9. Retrosynthetic disconnection of the target compounds **1a-c** reveals two promising synthetic routes: **Route 1** is envisioned to yield bishalogenated **IIIa** and **IIIb** in an intramolecular cyclisation of substituted selenoethers **4a**, **IVb**, **IVc** and **IVd**. A subsequent C-C coupling reaction is planned to yield target compounds **1a-c**. Thus, the first part of this thesis focuses on the synthesis of symmetrically halogenated selenoethers **4a**, **IVb**, **IVc** and **IVd** as well as the subsequent ring-closure strategy. Here, the choice of the halogens and their positions is essential for the selected synthetic approach. Reactions such as nucleophilic aromatic substitution (S_NAr), transition-metal-catalyzed C-H activation, and alumina C-F activation were identified as promising synthetic approaches.

As an alternative, in **Route 2** a multistep reaction will be evaluated: a lithium-assisted dimerization reaction of amide **VIIb** toward quinone **VIb** will be used. Further nucleophilic substitution of quinone **VIb** with trialkylsilyl ethynyl substituents and subsequent reductive aromatization of the formed diols **Va-c** will be used to realize target compounds **1a-c**.

Both routes are planned to ensure the regioselective formation of the target compounds.

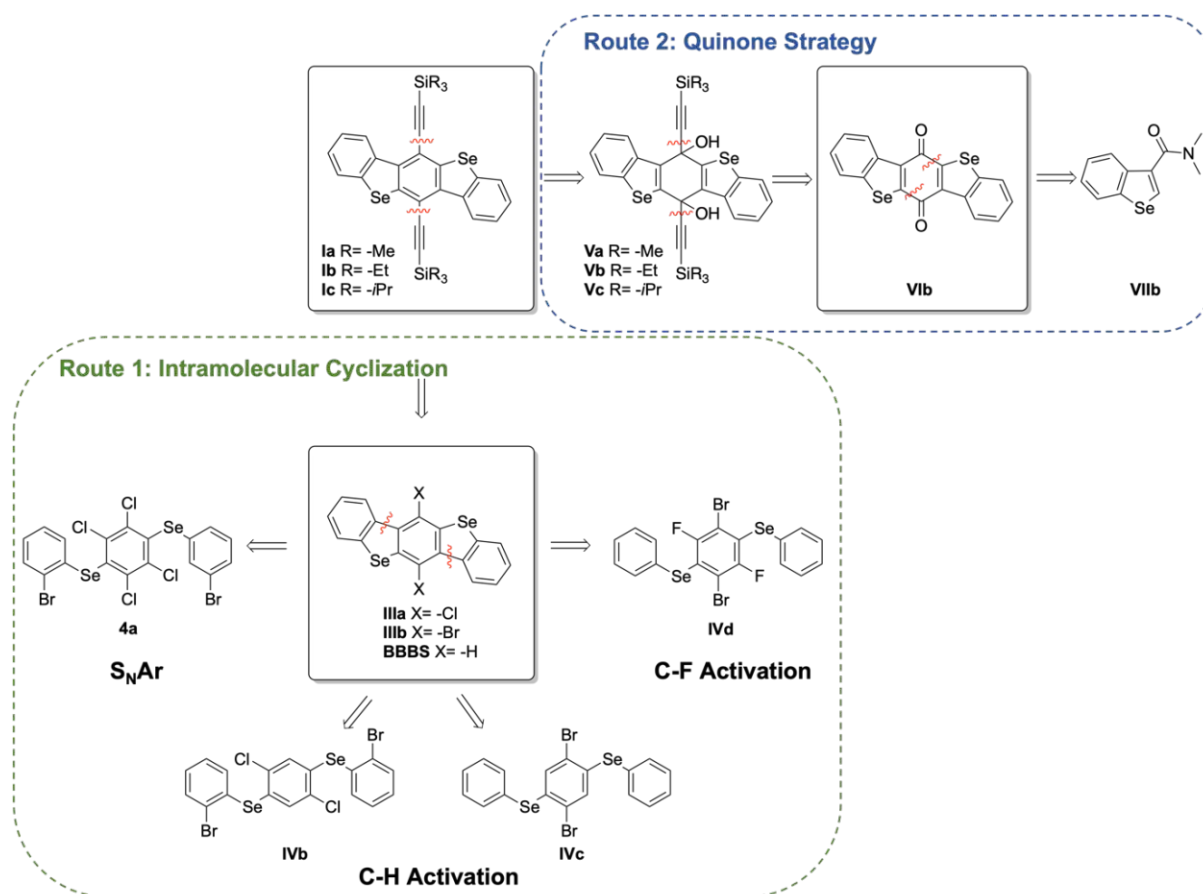


Figure 9: Retrosynthetic analysis of target compounds via two synthetic routes.

3.2 Intramolecular Cyclization Approach toward 6,12-Disubstituted Benzo[1,2-*b*:4,5-*b'*]bis[1]benzoselenophenes

In order to obtain the target compounds **1a-c**, different cyclisation protocols were taken under consideration. As outlined in the retrosynthetic analysis (Chapter 3.1), nucleophilic aromatic substitution (S_NAr), C-H as well as C-F activations were identified as potential intramolecular cyclization reactions. The starting materials for all three strategies (Figure 10) were designed to meet the following objectives: (i) facilitate regioselective ring closure of substituted bis(phenylseleno)benzenes **4a**, **IVb**, **IVc** and **IVd** and (ii) enable the introduction of a halide substituent **Y** (chloride or bromide) in the 6- and 12-position of the benzo[1,2-*b*:4,5-*b'*]bis[1]benzoselenophene backbone. The halide substituent **Y** can then be used in a subsequent Sonogashira coupling reaction to incorporate the trialkynyl substituents at the specific positions.

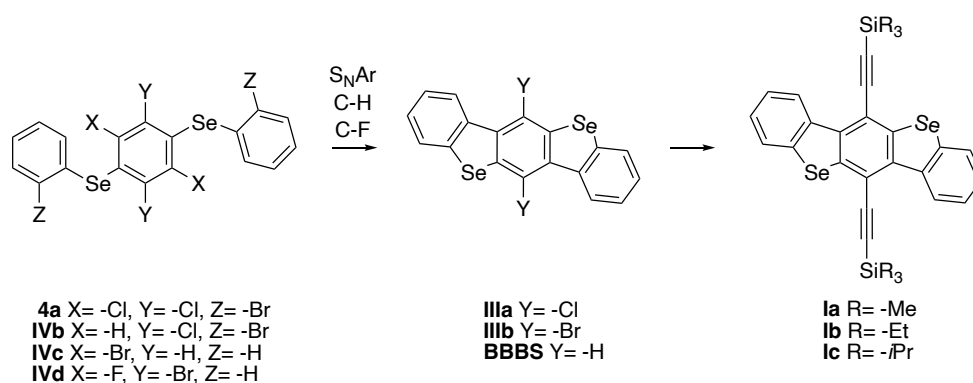


Figure 10: Cyclisation reactions toward halogen substituted compounds **IIIa** as well as **IIIb** and subsequent Sonogashira reaction toward target molecules **1a-c**.

For this purpose, the precursors bis(phenylseleno)benzenes **4a** and **IVb-d** had to be prepared. Here, a copper catalyzed coupling reaction of diselenide derivatives **9a** and **9b** with a properly substituted benzene **10** was chosen (Figure 11).

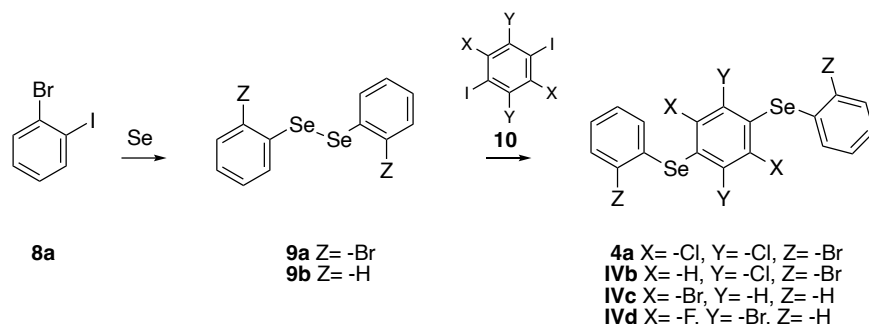
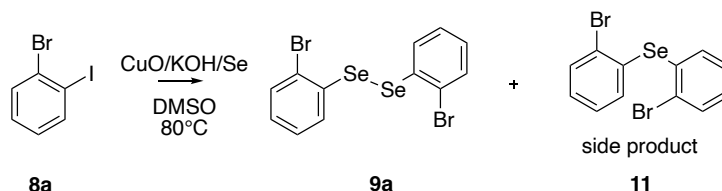


Figure 11: Synthetic route toward bis(phenylseleno)benzenes **4a** and **IVb-d**.

In the following, the synthesis of diselenide **9a**, bis(phenylseleno)benzenes **4a**, **IVb** and **IVc**, and the further ring closure strategies toward **IIIa** and **IIIb** are presented in detail.

3.2.1 Synthesis of Bis(phenylseleno)benzenes

The synthetic strategy toward substituted diselenide **9a** was planned using a synthetic procedure according to Singh et al.^[48] Commercially available 1-bromo-2-iodobenzene **8a** was treated with CuO and selenium under basic conditions yielding **9a** in 50% yield (Scheme 1). Bis(2-bromophenyl)selenane **11** was obtained as a side product.



Scheme 1. Synthetic route toward diselenide **9a**.

Singh et al. proposed a plausible reaction mechanism for this CuO-catalyzed cross-coupling of halides with selenium nucleophiles resulting in the formation of diselenides such as **9a**.^[48] In the presence of a strong base, selenium can be oxidized to form selenolate or diselenolate anions. In the catalytic cycle, the oxidative addition of an organohalide RX to copper oxide nanoparticles **a** yields complex **b** (Figure 12). It is suggested that a subsequent ligand-exchange with the formed diselenolate anion gives complex **c**. Through a reductive elimination step, the coupling product **d** is obtained as well as regenerated CuO. Further conversion of complex **d** with an additional equivalent of complex **b** results in the formation of complex **e**. In a second reductive elimination step, the desired diselenide as well as a reduced CuO are obtained.^[48]

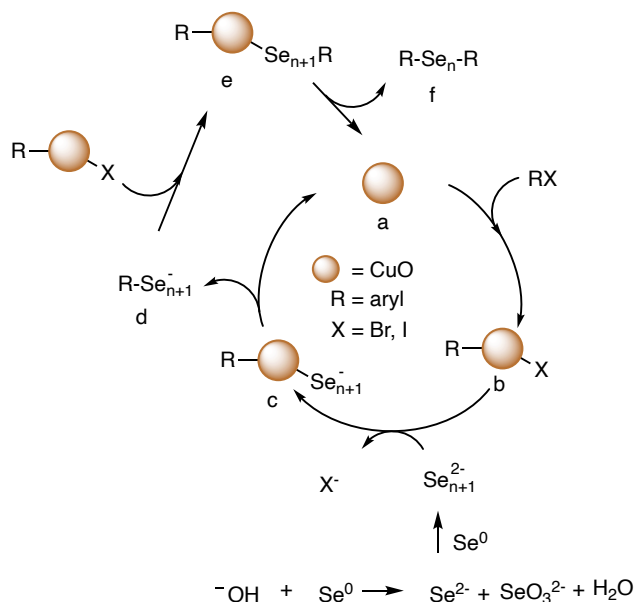


Figure 12. Proposed reaction mechanism toward organo diselenides according to Singh et al.^[48]

According to the planned subsequent intramolecular cyclisation approach (S_NAr , C-H or C-F activation), the installation of a defined halogen substitution pattern is essential to ensure the regioselectivity. In Figure 13, the respective reactive groups for each synthetic approach are highlighted

in color. For the C-H activation approach, two different strategies were pursued, one that ensures regioselectivity (a) and a second that is electronically favored (b).

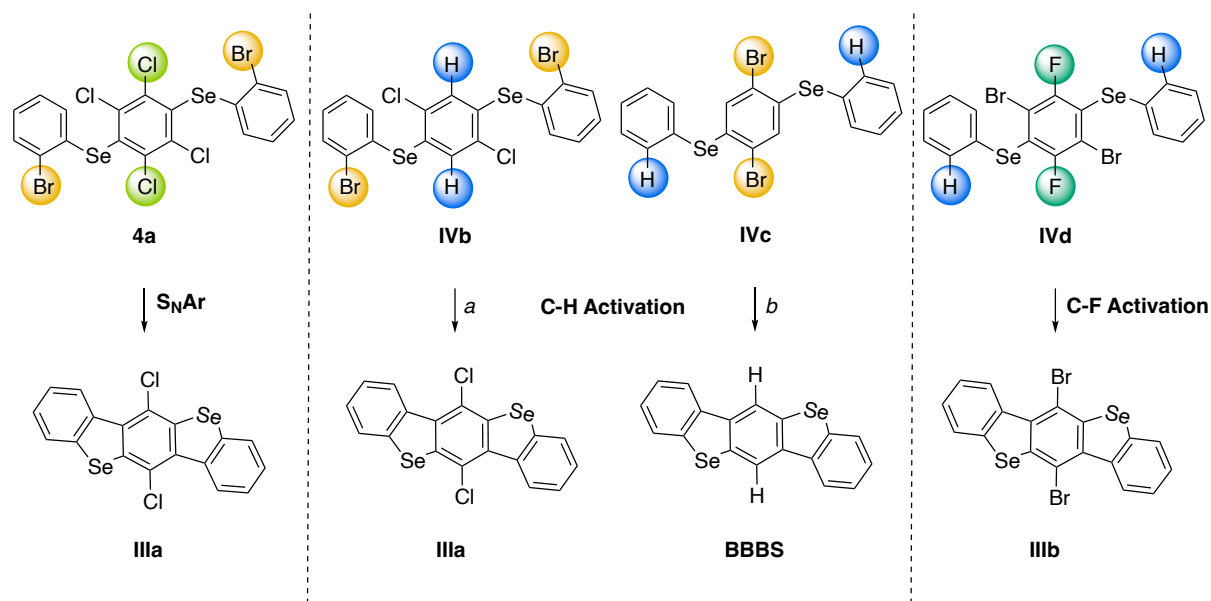
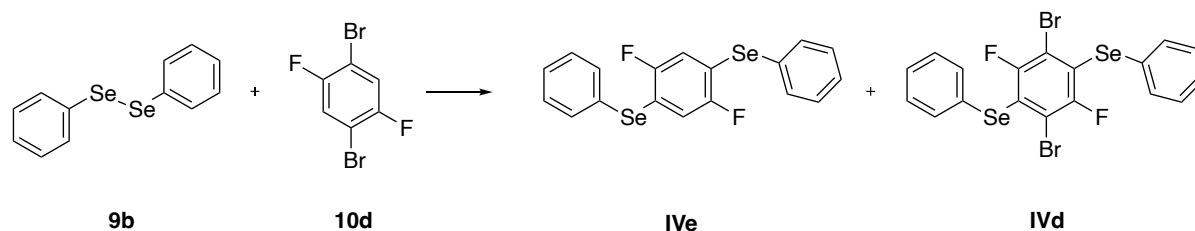


Figure 13. Intramolecular cyclization reactions.

The synthesis of the properly substituted bis(phenylseleno)benzenes **4a** as well as **IVb-c** was pursued using an adapted published transition-metal free protocol by Varala et al.^[49] for the cross-coupling reaction of selenides with aryl halogenides. It is important to note at this point, considering this reaction a S_NAr , first experiments toward bis(phenylseleno)benzenes showed an inverse order of reactivity of the halides in the utilized benzenes **10**. While fluoride is typically the preferred substituent in S_NAr reactions due to the acceleration of the first rate-determining step, iodine and bromine demonstrated higher reactivity -in the given order- when diselenides were used as nucleophiles. Therefore, the desired substitution patterns on the bis(phenylseleno)benzenes were achieved by using iodobenzenes in these reactions, while retaining any other halide present in the formed product, as outlined in Figure 13. Although the synthesis of **4a** as well as **IVb-c** yielded some dehalogenated side product, all bis(phenylseleno)benzenes could be obtained in low yields (Table 1).

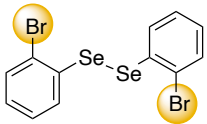
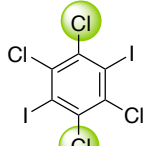
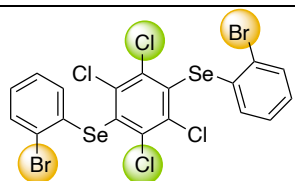
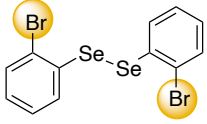
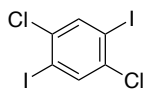
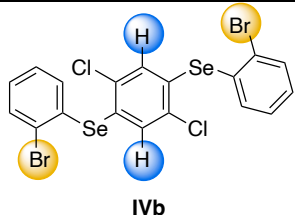
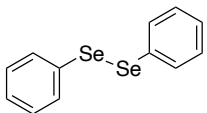
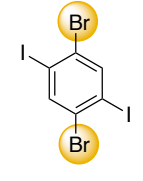
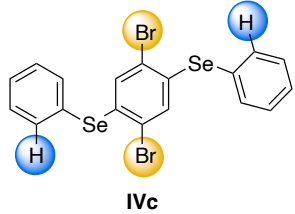
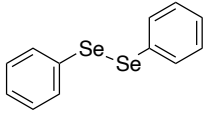
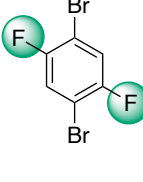
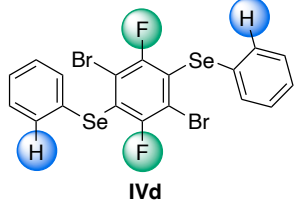
Interestingly, in a GC-MS screening reaction toward compound **IVe** using the same conditions as described above, it was observed, that besides the desired product also disubstituted compound **IVd** was obtained (Scheme 2). The reaction was conducted on a bigger scale and indeed 16% of **IVd** could be isolated (Table 1). The structure of **IVd** was confirmed by X-ray diffraction (Figure 14).



Scheme 2. Synthesis of **IVd**.

The formation of **IVd** may be explained by an aryne mechanism. Due to the vicinity of the fluoride, both protons in **10d** are more acidic than those in **10a-c**. Deprotonation may result in elimination of bromide and the formation of an aryne. The eliminated hydrogen bromide may then react with **9b** forming in-situ phenylselenenyl halogenide as a highly reactive intermediate, which may add to the aryne to yield **IVd**.

Table 1: Synthesis of bis(phenylseleno)benzenes.

	Diselenide	Halogen Derivative	Product	Yield
1	 9a	 10a	 4a	37%
2	 9a	 10b	 IVb	16%
3	 9b	 10c	 IVc	27%
4	 9b	 10d	 IVd	16%

Single crystals of **4a** and **IVd** were obtained by slow evaporation of a solution of the respective compound in 1,2-dichloroethane confirming the molecular structure as shown in Figure 14. While **4a** was obtained in the space group *Pbca*, **IVd** crystallized in the space group *C 2/c*.

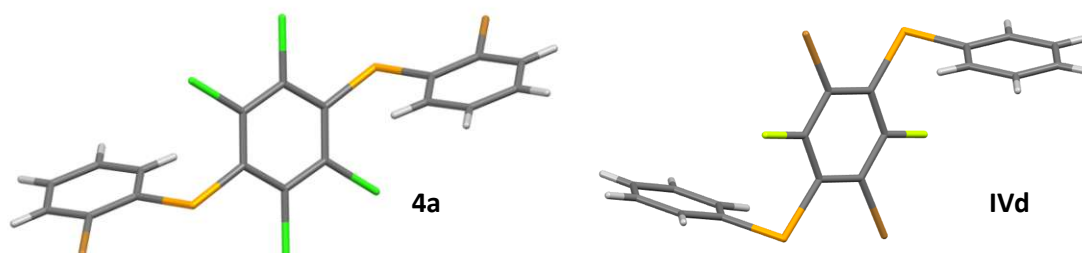
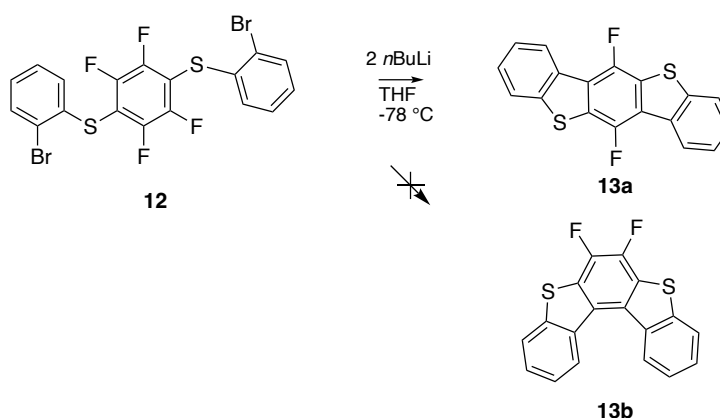


Figure 14. Molecular structures of **4a** and **IVd**.

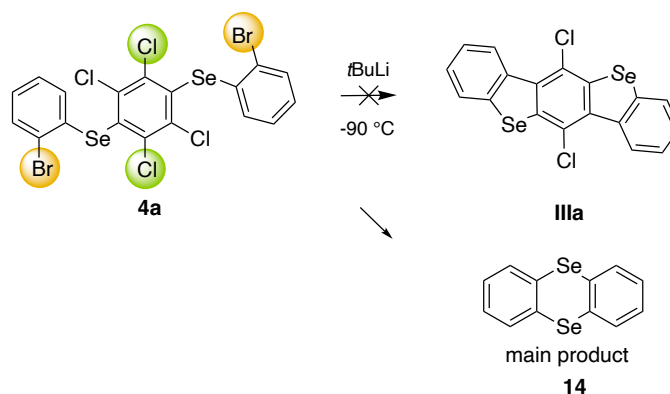
3.2.2 Intramolecular Cyclization *via* Nucleophilic Aromatic Substitution

The first intramolecular cyclization was carried out based on a study by Ponce Gonzalez et al., which showed that treatment of bis(phenylthieno)benzenes **12** (Scheme 3) with two equivalents of *n*-butyllithium induces cyclisation to yield the pentacyclic 6,12-difluorobenzo[1,2-*b*:4,5-*b'*]bis[1]benzothiophene **13a**, an analogue of **III**, in high yield of 95%.^[50] This reaction proceeds regioselectively; lithiation of the peripheral rings by metal-halogen exchange and subsequent S_NAr selectively yield the desired compound, as confirmed by X-ray crystallography. Importantly, no traces of the second regioisomer **13b** were observed.



Scheme 3. Synthetic strategy toward benzothiophene analogue **13a**.

Since the reactivity of fluoride species is limited for further coupling reactions to introduce the trialksilylethynyl side chains as planned for target compounds **Ia-c**, the reaction toward **IIIa**, the chlorine analogue of **13a**, was pursued starting from the precursor **4a** (Scheme 4). However, metal-halogen exchange using two equivalents of *n*-butyllithium according to Ponce Gonzalez et al.^[50] did not result in the formation of product **IIIa**, but in butylation of the *in situ* formed aryllithium.



Scheme 4. Intramolecular ring closure approach via S_NAr and the formed side product selanthrene **14**.

To circumvent this problem, *t*-butyllithium was used at $-90^\circ C$. Applying GC-MS analysis, traces of the product as well as a main side product could be detected. This side product could be characterized as selanthrene **14** (Scheme 4) via GC-MS and NMR analysis. The formation of this side product

may be explained based by a lithium/selenium exchange mechanism (Figure 15) according to similar systems described in literature.^[51]

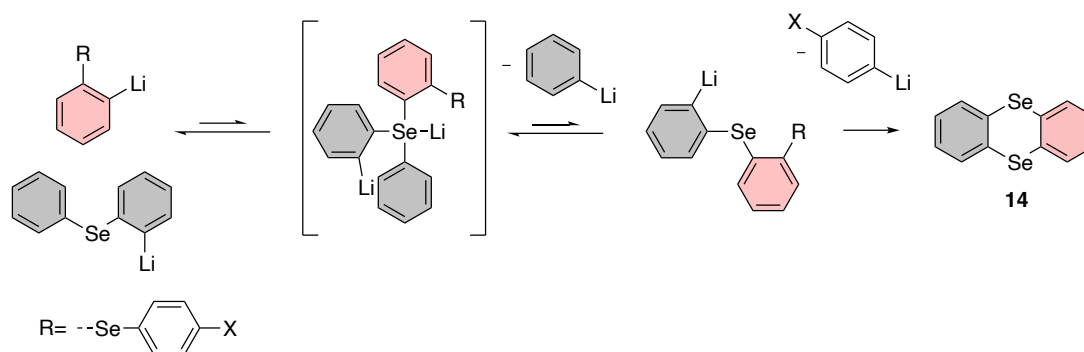


Figure 15: Possible mechanism of selanthrene formation.

3.2.3 Intramolecular Cyclization *via* C-H Activation

Transition metal-catalyzed C-H bond activation offers an efficient approach for C-C bond formation, providing improved atom efficiency by eliminating the need for organometallic reagents used in other coupling reactions such as Stille or Suzuki couplings. Furthermore, C-H activation can be performed under milder conditions utilizing less toxic or expensive reactants, while exhibiting higher functional group tolerance.^[52] Palladium-catalyzed C-H bond activations have shown to be a valuable synthetic method in intramolecular cyclisation reactions. Although limited reports exist on the ring annulation of selenophenes using palladium catalyzed C-H activation, the synthesis of its thiophene analogue has been successfully demonstrated from diaryl thioethers in good yields.^[53] C-H activation was demonstrated by Chen et al. to be applicable for unactivated 2-iodinated diaryl thioethers **15** yielding 82% of the ring-closure product dibenzo[*b,d*]thiophene **16** (Figure 16,a).^[54]

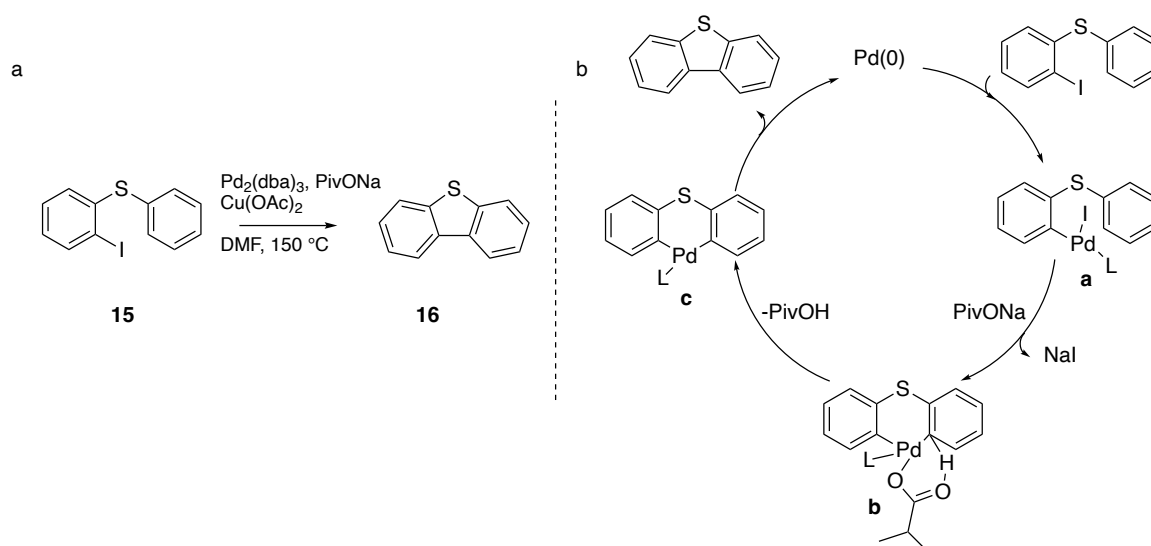


Figure 16. Synthetic route toward dibenzothiophene (a) and reaction mechanism of Pd-catalyzed synthesis of dibenzothiophenes (b).

A plausible reaction mechanism of this intramolecular cyclization is given in Figure 16,b. In the catalytic cycle, the addition of **15** to a Pd(0) species gave intermediate **a**. A subsequent ligand exchange

with the pivaloyl anion and C-H bond activation gives complex **b**. Subsequent reductive elimination gives the dibenzothiophene **16** as well as regenerated Pd(0).

Similar protocols have been used for the synthesis of 5-membered ring heterocycles: Lv et al. described a facile synthesis of indolo[3,2,1-*jk*]carbazoles **18** *via* palladium-catalyzed intramolecular cyclization in 83% yield (Figure 17,a).^[55] This protocol has been recently employed in our group toward the synthesis of planarized indolo[3,2,1-*jk*]carbazole derivatives **20** using a catalytic system of Pd(OAc)₂ and (1,3-bis(2,6-diisopropylphenyl)-1*H*-imidazol-3-ium chloride in DMA at 130 °C (Figure 17,b).^[56]

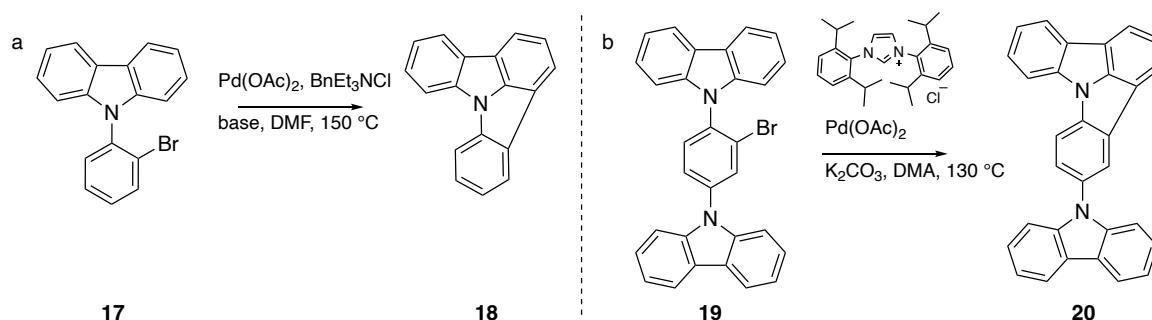
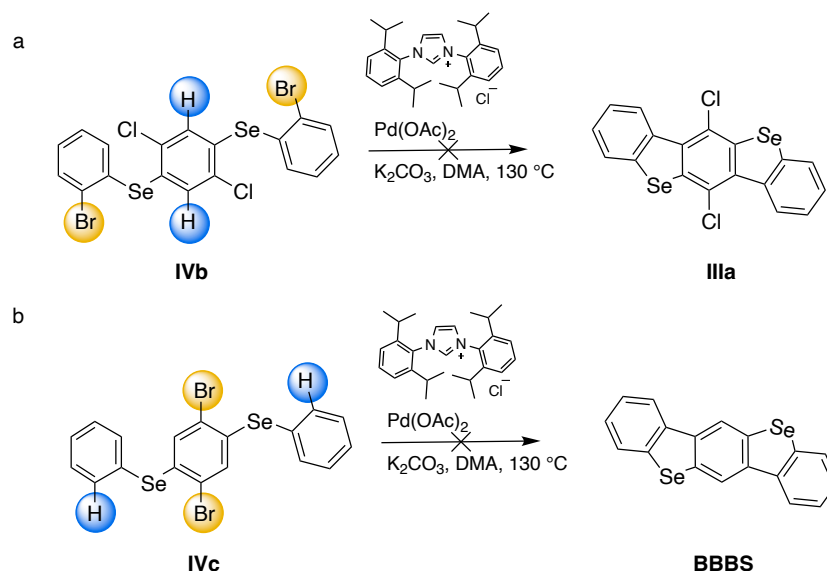


Figure 17. Synthetic approach toward indolo[3,2,1-*jk*]carbazole derivatives.

Given the broad range of applications of C-H activation in the synthesis of 5-membered heterocycles, within this work, this procedure was adapted for the C-H activation of **IVb** toward **IIIa** (Scheme 5). The palladium catalyst, ligand, K₂CO₃ and the starting material **IVb** were stirred in dimethylacetamide at 130 °C. However, no conversion could be observed after several days *via* TLC; also, GC-MS analysis showed no formation of the desired product **IIIa**. Similar results were observed for the reaction of **IVc** to **BBBS**.



Scheme 5. Intramolecular ring closure approach via C-H activation.

Since there are no reports in literature on the ring closure using C-H activation of selenoethers toward dibenzoselenophenes, this reaction may be hampered by the complexation of the catalyst by

selenium. Therefore, no further attempts were made to realize the target compounds *via* the C-H activation approach.

3.2.4 Intramolecular Cyclization *via* C-F Activation

In a last intramolecular cyclization approach starting from diselenides, a C-F activation reaction was chosen to obtain the substituted BBBS derivatives. Due to its low atomic weight and small size, fluorine atoms can be rather easily introduced also in sterically demanding molecules. Furthermore, C-F bonds exhibit high chemical stability, enabling the compatibility with a broad range of reactions and excellent functional group tolerance. However, as the reactivity of C-F bonds is low, harsh reaction conditions are necessary to use them as functional groups resulting in a low functional group tolerance and numerous side reactions. While the palladium(0)-catalyzed C-C bond formation utilizing bromo and chloro derivatives or aryl triflates is an effective intramolecular cyclisation method, this method can hardly be extended to fluorinated precursors, which are significantly less reactive compared to chlorinated and brominated analogues.

To circumvent these problems, the group of Siegel successfully applied C-F bond activation in transition-metal-free conditions utilizing silylium carborane catalysis for intramolecular aryl-aryl coupling.^[57] While remarkable yields up to 99% were reported for single C-F condensation, this approach has limited applicability for multifold reactions. In a different approach, Amsharov et al. describe solid-state catalysis for intramolecular C-C bond formation between two aromatic systems in highly insoluble fullerene precursors.^[58] As a model system, the cyclization of 1-fluorobenzo[*c*]phenanthrene (**F-Phen**) was investigated (Figure 18a) : quantitative conversion to benzo[*ghi*]fluoranthene could be achieved using activated γ -Al₂O₃ at 150 °C after 20h. Activated γ -Al₂O₃ could be obtained by annealing at 500 °C for 15 min at 10⁻³ mbar pressure. The cyclisation reaction is very site specific; if the fluorine is not in the 1-position no reaction is observed. Also, it has also been shown that an additional bromine is retained in the molecule under these reaction conditions (Figure 18b).

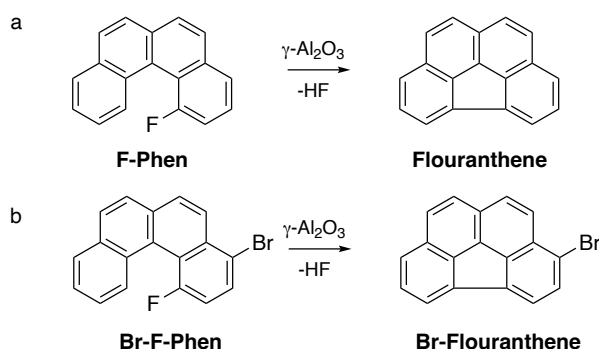


Figure 18. Intramolecular ring closure mediated by Al₂O₃ demonstrating high chemoselectivity.^[58]

The authors attribute the driving force of the reaction to the formation of an Al-F bond with high bond strength. The selectivity of this reaction was ascribed to a ring closure process, that exclusively proceeds *via* a cyclic transition state in a concerted reaction mechanism. As bond breaking and bond formation takes place simultaneously, no reactive intermediates are formed that could lead to

undesired side reactions. The involvement of an aromatic six-electron transition state may explain the low activation barrier allowing the reaction to proceed under mild conditions.^[58]

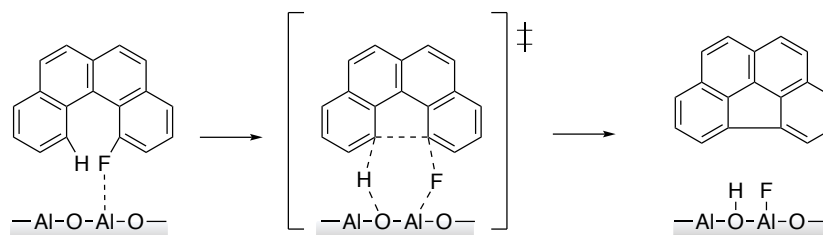
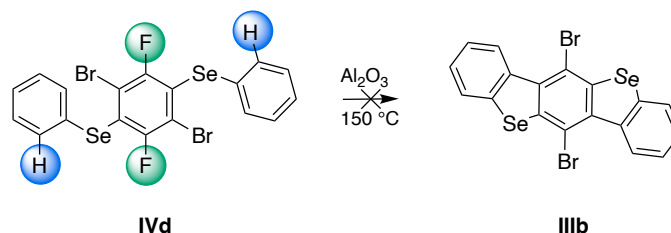


Figure 19. Mechanism of C-F activation according to Amsharov et al.^[58]

This protocol was adapted for the synthesis of **IIIb**. Al₂O₃ was converted to its cubic γ -modification under vacuum in a furnace at 500°C. After cooling, diselenide **IVd** was added in an argon counterflow, and the mixture was heated at 150°C for six days.



Scheme 6. Intramolecular ring closure approach via C-F activation.

The substance obtained was extracted by DCM and then purified by liquid chromatography. However, subsequent GC/MS and NMR analyzes could not identify the desired product. Even after a renewed attempt at a reaction temperature of 200-260 °C, the product **IIIb** could not be detected but a manifold of decomposition products.

Although nucleophilic aromatic substitution, transition-metal-catalyzed C-H activation, and alumina C-F activation were identified as promising reactions for intramolecular cyclisation, compounds **IIIa** and **IIIb** could not be isolated. Therefore, a different synthetic strategy toward the target compounds was pursued.

3.3 Synthesis via Quinones

According to the retrosynthetic analysis in Figure 9, a different approach toward the target compounds **1a-c** was followed. The synthesis of benzoselenophene based target compounds **1a-c** was pursued by the dimerization of the respective amides, nucleophilic attack on the resulting quinones using lithiated trialkylsilylalkynes and a last reductive aromatization step of the resulting diols **5a-c** to give the final products (Figure 20). To investigate the influence of selenium on the properties of this semiconductor class, also benzothiophene analogues **2a-c** were synthesized according to literature.

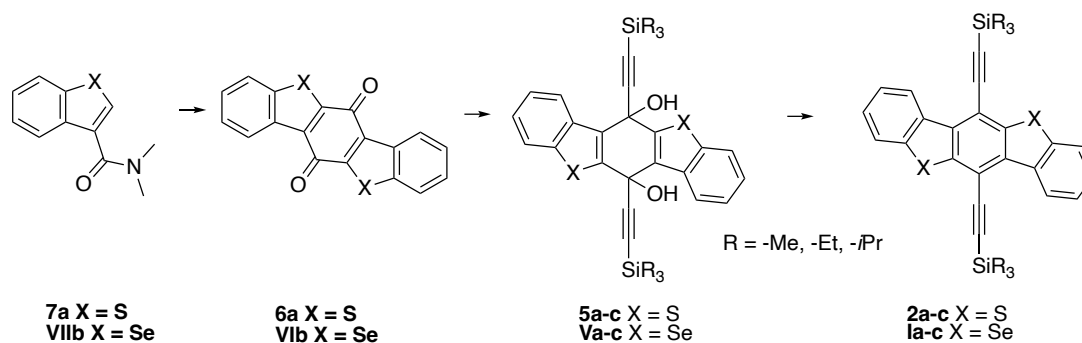


Figure 20: Synthetic approach toward target compounds **1a-c** and **2a-c**.

In the following the synthetic steps toward quinones **6a** and **VIb**, their precursors as well as the synthesis of target compounds **1a-c** and **2a-c** are presented.

3.3.1 Synthesis of Fused Aromatic Quinones

For the synthesis of benzothiophene and benzoselenophene based fused aromatic quinones, amide substituted precursors **7a** and **VIIb** had to be synthesized (Figure 21).

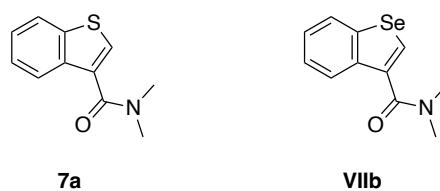
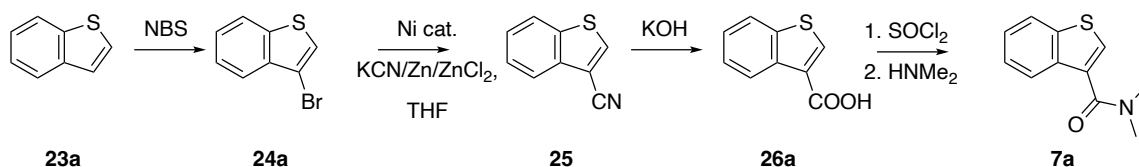


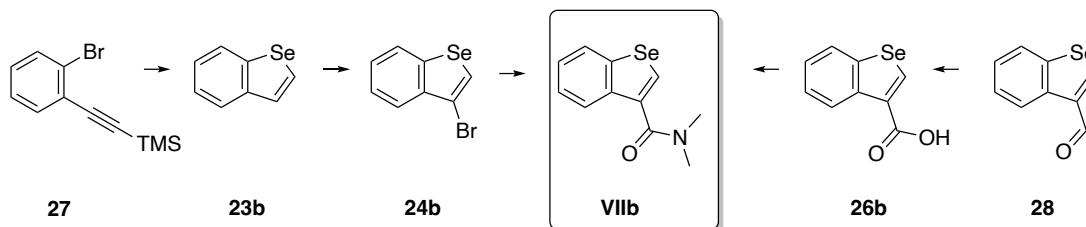
Figure 21: Amide precursors **7a** and **VIIb** for quinones.

The synthesis of **7a** was realized in a multistep reaction (Scheme 7). Commercially available benzo[*b*]thiophene **23a** was brominated in the 3-position using NBS. Subsequent introduction of the nitrile was realized by a zinc-catalyzed using potassium cyanide in 60% yield according to a procedure developed earlier in the group.^[59] Hydrolysis of the nitrile **25** yielded carboxylic acid **26a** quantitatively. Further conversion to **7a** was realized by *in situ* generation of an acid chloride and further reaction with aqueous dimethylamine in a yield of 79%.



Scheme 7. Synthetic approach toward amide **7a**.

For the synthesis of **VIIb** two different strategies were pursued. The synthesis of unsubstituted benzoselenophene was realized using a protocol by Kashiki et al.^[60] which was further converted to bromide **23b**. Since the cyanation of **24b** did not work applying the protocol used for the synthesis of **25**, a different approach was used. The direct formation of **VIIb** from **24b** using lithiation and subsequent quenching with dimethylcarbamoyl chloride could only be achieved in low yields (44%). Therefore, a second strategy was used: carbaldehyde **28** was synthesized by a previously published procedure.^[61] After conversion of **28** to the carboxylic acid **26b**, a similar protocol as toward **7a** was used: *in situ* formation of an acid chloride and further reaction with aqueous dimethylamine yielded compound **VIIb** in 88%.



Scheme 8. Synthetic approaches toward amide **VIIb**.

In a next step, the synthesis of fused aromatic quinones **6a** and **VIIb** was evaluated. The basis for this synthetic approach has been described by the group of Heeney for the synthesis of bisalkylsilyl-ethynylated benzo[1,2-*b*:4,5-*b'*]bis[*b*]benzothiophenes (BBBT).^[47] Treatment of benzo[*b*]thiophene-3-carboxylic acid dimethylamide **7a** with a strong base results in deprotonation of the compound at the 2-position at low temperature generating a reactive organolithium reagent. Upon heating of this intermediate an intermolecular condensation reaction with another carboxylic acid dimethylamide is promoted resulting in a fused aromatic diaryl ketone. A second intramolecular reaction between the aryllithium and the carboxylic acid dimethylamide of the resulting ketone yields a quinone as shown in Figure 22.

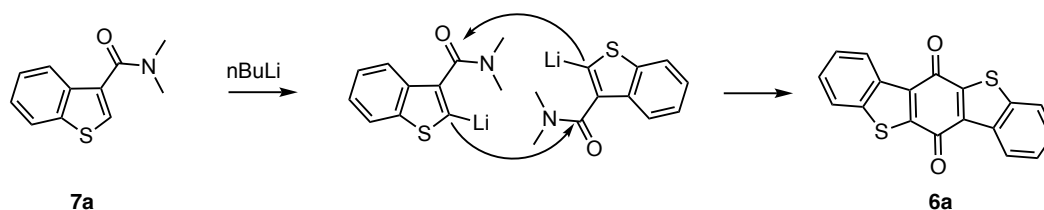


Figure 22: Mechanism for the synthesis of quinones **6a** described by the group of Heeney.^[47]

This synthetic procedure is in analogy to an earlier study by Slocum and Gierer, which describes the exclusive lithiation in 2-position observed for thiophene-3-carboxylic acid dimethylamide

21 in diethylether (Figure 23).^[62] The formed lithiated intermediate condensed with itself giving benzo[1,2-*b*:4,5-*b'*]dithiophene-4,8-dione **22** in 41% yield.

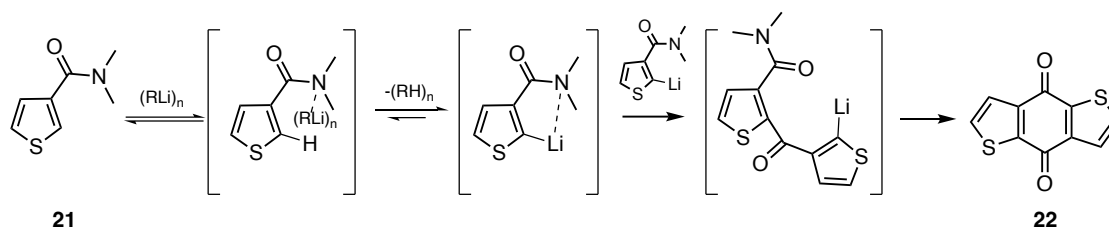


Figure 23: Mechanism for the synthesis of quinone **22** described by Slocum and Gierer.^[62]

The regioselectivity of this reaction is attributed to the directing effect of the substituent in the 3-position. For a successful deprotonation to occur in the 2-position, the directing metalation group has to fulfill two criteria: (i) serve as a good coordinating site for alkyllithium and (ii) have a poor electrophilic site for attack by this strong base.^[63] The directed ortho metalation proceeds in a three-step sequence (Figure 23): (1) coordination of the (RLi)_n aggregate to the heteroatom-containing directing metalation group (amide), (2) deprotonation leading to formation of the coordinated ortho-lithium species, and (3) reaction with an electrophile.^[63] In analogy to Slocum and Gierer,^[62] the complex in step 1 is formed by the coordination of the butyllithium tetramer and **21** in diethylether (formed in step 1) and consists of a pseudo-six-membered chelated ring, which facilitates the transfer of the hydrogen at the 2-position of **21** to a coordinated *n*-butyl group in step 2 (Figure 24).

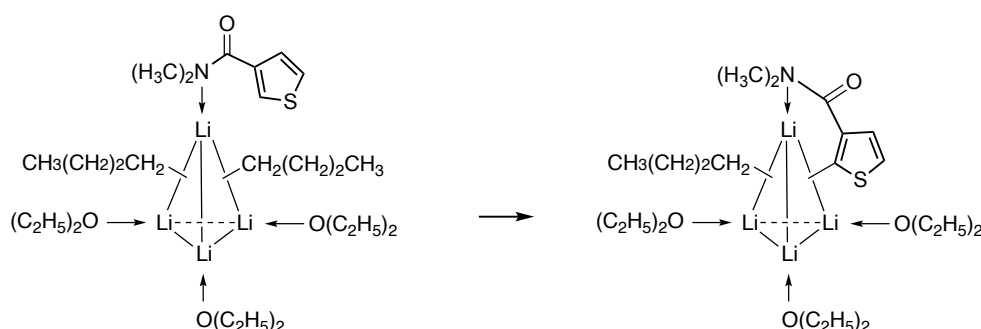
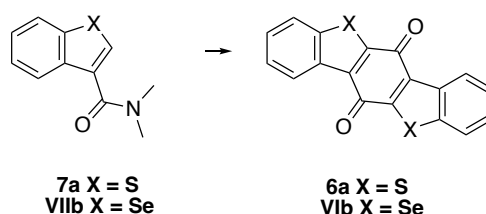


Figure 24: Coordination of butyllithium to amide **21** as a direct metalation group in diethylether according to ^[62].

As mentioned above, a procedure toward **6a** has already been described in literature^[47] and therefore used for both target quinones in this work (Scheme 9). While the synthesis of quinone **6a** could be successfully realized by lithiation of amide **7a** using *n*BuLi in anhydrous ether in 43% yield, this procedure did not work toward quinone **Vlb**.



Scheme 9. Synthetic approaches toward quinones **6a** and **Vlb**.

Using the same reaction conditions nucleophilic substitution of the amide by butyllithium as well as further side-products, that suggest a benzoselenophene ring opening, could be observed. To avoid the nucleophilic properties of *n*BuLi, a non-nucleophilic base, lithium diisopropylamide was prepared in THF resulting in successful deprotonation of the amide in the 2-position and further dimerizing of the lithiated species according to Figure 22. Quinone **Vlb** was obtained in 60% yield. The structure of **Vlb** was confirmed by NMR spectroscopy as well as X-ray diffraction (Figure 25).

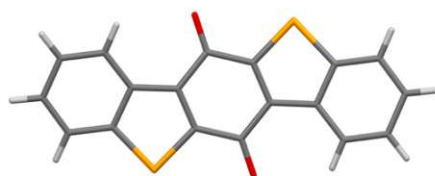
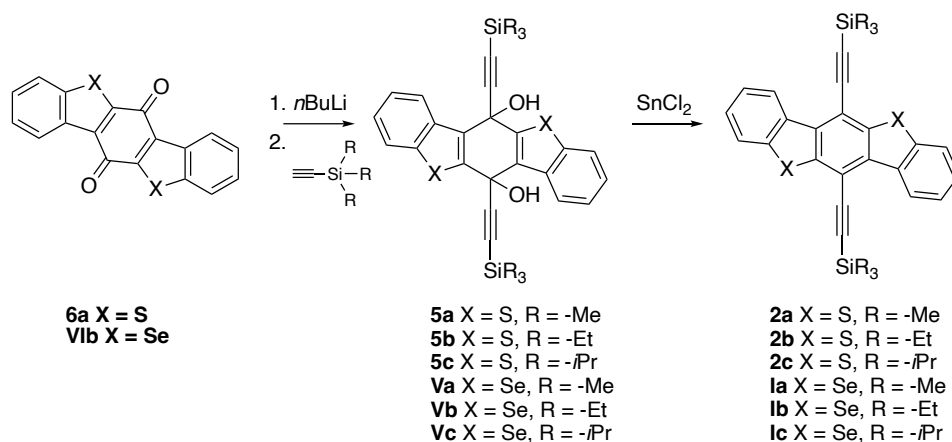


Figure 25: Molecular structure of quinone **Vlb**.

3.3.2 Synthesis of Trialkylsilyl-ethynyl-substituted Target Compounds

Subsequently, the synthesis of target compounds **la-c** and **2a-c** was pursued. For this purpose, the addition of an excess of a nucleophilic ethynyl species to the fused aromatic quinone resulting in a diol intermediate was evaluated. While in earlier reports on the synthesis of benzothiophene based target compounds **2a-c**, the isolation of the diols has not been reported, in this study all intermediates were isolated and characterized.



Scheme 10. Synthetic approaches toward target compounds **la-c** and **2a-c**.

While the synthesis of diols **5a-c** could be accomplished by addition of lithiated trialkylsilyl-ethyne to the fused aromatic quinone **6a** at -78 °C in anhydrous THF, only mono-substitution of the quinone **Vlb** could be observed using these conditions. This may be explained by the more polarizable properties of selenium compared to sulfur, which induces a push-pull system (chalcogen-ketone) hampering the addition of a second equivalent of nucleophile. While a change of solvent to THF did not give diols **Va-c**, rising the temperature after addition of the nucleophile to 30 °C resulted in double substitution of quinone **Vlb** and the formation of **Va-c** (Table 2).

Reductive aromatization using tin (II) chloride as a reducing agent -similarly as described for pentacene derivatives by Anthony and co-workers^[14]- results in the formation of the target compounds **1a-c** and **2a-c** (Table 2).

Table 2: Yields of diols **Va-c** and **5a-c** as well as target compounds **1a-c** and **2a-c**.

Diol	Yield	Target compound	Yield
5a	85%	2a	56%
5b	72%	2b	57%
5c	41%	2c	75%
Va	60%	1a	83%
Vb	54%	1b	80%
Vc	49%	1c	69%

3.4 Analysis of Target Compounds

3.4.1 Single Crystal Structures

The efficiency of charge-transport processes plays a crucial role in the performance of semi-conduction materials in OFET devices. The solid-state packing arrangement of organic molecules critically impacts their materials properties such as charge transport.^[64] At the microscopic level, one of the key factors influencing the transport properties is the amplitude of the electronic transfer integrals between adjacent molecules, which are depending on the molecular packing.^[65] Therefore, the structural properties of conjugated molecules such as planarity, high symmetry and specific π -electronic delocalization, play an important role in designing tightly packed molecular arrangements, as they contribute to a more efficient charge carrier transfer in the crystal. The intermolecular transfer electron or hole in such systems mainly occurs through π - π orbital overlap. Therefore, even slight alterations or imperfections in the crystal packing significantly impact the efficiency of electronic coupling leading to variations in the charge transport parameters.^[66]

Therefore, within this work, the effect of molecular conformation and packing properties in single crystals of the target compounds **1a-c** was investigated. Single crystals of **1a-c** and **2b** were grown by slow evaporation from CHCl_3 , **2a** and **2c** from acetone (Figure 26 and Figure 27). Structural comparison of the obtained polymorphs of the target compounds with benzothiophene based materials shows a remarkable resemblance in packing arrangement. While compounds **2a**, **2b**, **1a** and **1b** crystallize in the space group P21/c, **2c** and its selenium analogue crystallize in the space group P1. However, a closer look at the packing arrangements of benzothiophene and benzoselenophene derivatives reveals the presence of intermolecular short contacts between neighboring molecules predominantly in the selenium compounds (Table 3). Contacts are classified as short ones when the distance between two adjacent atoms is less than the sum of the Bondi van der Waals radii.

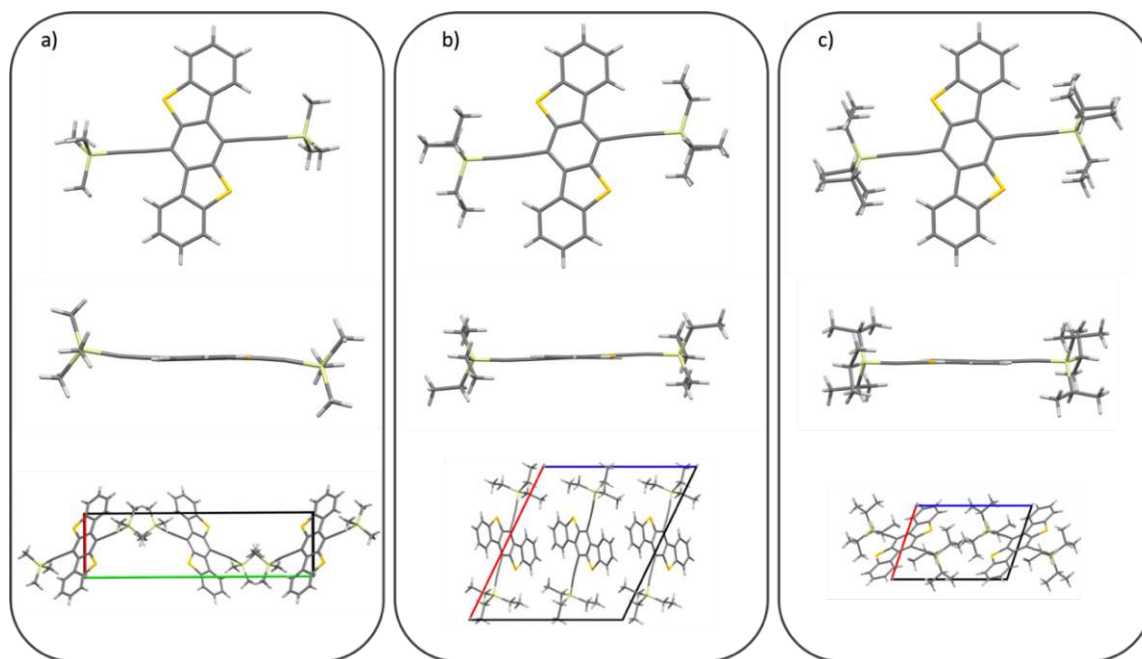


Figure 26: Molecular structures and packing of target compounds **2a-c**.

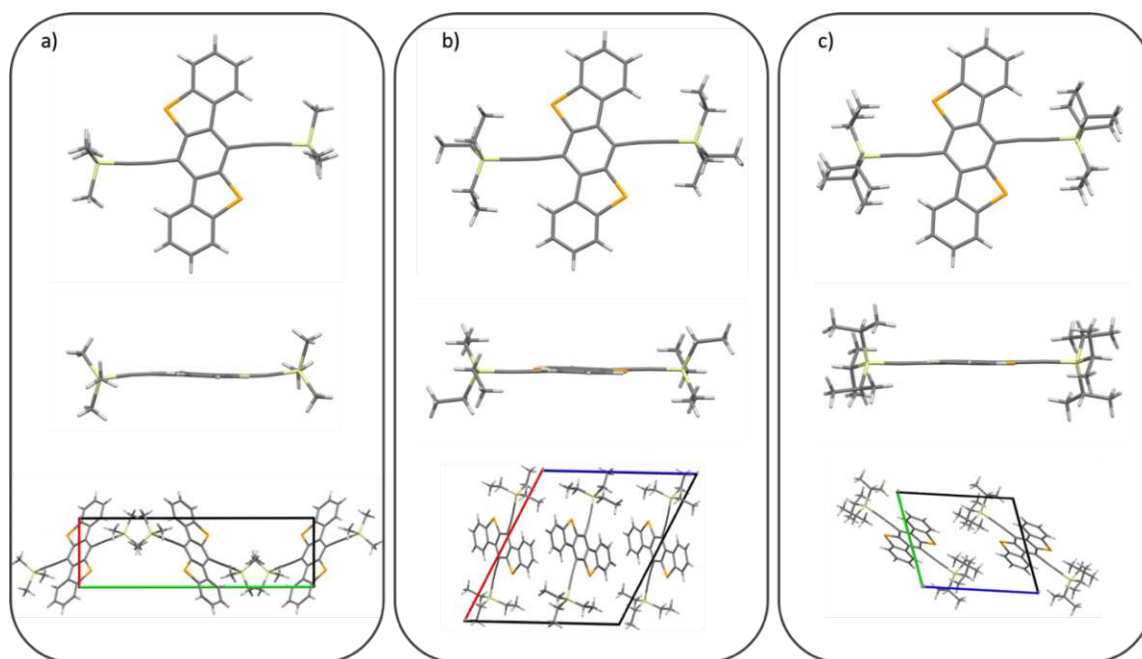


Figure 27: Molecular structures and packing of target compounds **1a-c**.

Table 3: Short intermolecular distances (less than the sum of the van der Waal radii) in target compounds.

Compound	Space group	Short Contacts	[Å]
2a	P21/c	-	-
2b	P21/c	H-H	2.173
		H-H	2.347
2c	P1	-	-
1a	P21/c	H-H	2.235
1b	P21/c	C-p	2.850
		C-C	2.341
		H-H	2.187
1c	P1	C-Se	3.506

While compounds **2a** and **2c** do not exhibit any short contacts in this polymorph, **2b** shows intermolecular short contacts, which are located at adjacent ethyl groups of the silyl group. Therefore, in the benzothiophene compounds no direct interactions can be observed, that facilitate charge carrier transport between adjacent molecules such as π - π or S-S interactions. Heeney et al. reported on the semiconducting properties of **2a-c**.^[47] The fabricated OFET devices showed charge carrier mobilities as given in Table 4. Interestingly, compound **2b** exhibiting H-H interactions showed the highest charge carrier mobility.

Table 4: Average saturated charge carrier mobility of **2a-c** reported in literature.^[47]

Compound	Mobility ($\text{cm}^2 \text{V}^{-1} \text{s}^{-1}$)
2a	0.05
2b	0.53
2c	0.00003

Given the increased number of short contacts in the selenium-based materials, a better transfer of charges between adjacent molecules beneficial for device performance may be expected.

3.4.2 Assessment of the HOMO-LUMO energy gap

Photophysical and electrochemical analysis of the synthesized target compounds were conducted to gain insight into the electronic properties such as HOMO and LUMO energy level as well as HOMO-LUMO energy gap.

Photophysical Properties

The absorbance process measures the energy difference between the ground state and the excited state as electromagnetic radiation is absorbed. Here, the onset wavelength (λ_{onset}) represents an estimate for determining underlying physical properties of a compound based solely on optical spectral data. The onset wavelength λ_{onset} is an approximation of the optical energy gap and can be determined by x-intercept of a tangent line on the inflection point of the lowest energy absorption transition of a compound.^[67]

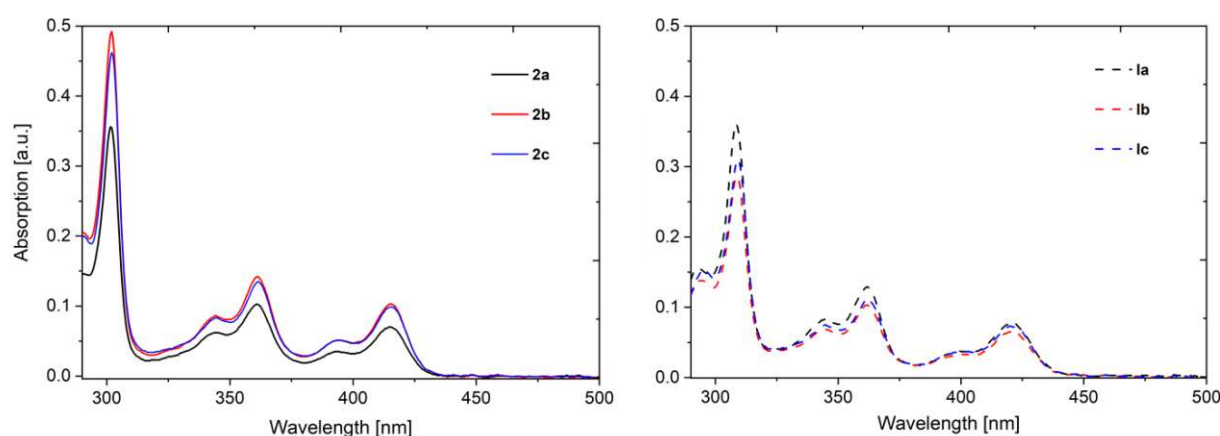


Figure 28: Absorption spectra of target compounds **1a-c** and **2a-c** in dichloromethane solution.

The photophysical properties of **1a-c** were analyzed in 5 μM CH_2Cl_2 solution by UV-Vis spectroscopy (Figure 28) and compared to the sulfur-based compounds **2a-c**. The absorption spectra of both sulfur- and selenium-based materials exhibit similar absorption characteristics, indicating similar band structures. Within the sulfur and selenium series, the absorption maxima are nearly at the same position. However, the selenium-based compounds showed a redshift of approximately 8-9 nm compared to the sulfur-based materials, which can be attributed to the higher electron density induced by the selenium heteroatom. The HOMO–LUMO gaps were determined from the onset of the UV-Vis absorption and are given in Table 5. The selenium compounds **1a-c** exhibit a slightly smaller HOMO-LUMO energy gap compared to the sulfur-based materials **2a-c**. Furthermore, both series were compared to BBBT and BBBS data taken from literature (Table 5). Here, the influence of the introduced trialkylsilyl ethynyl group is evident, a reduction of 0.4 eV for both systems could be observed, suggesting a facilitated charge transport in the substituted materials.

Table 5: Experimental data and physical characterization of compounds **1a–c** and **2a–c**.

	E_{ox}^a [V]	λ_{max}^b [nm]	E_g^b [eV]	HOMO ^c [eV]	LUMO ^d [eV]
TIPS-pentacene	-	-	1.81	-5.16 ^f	-3.35 ^f
BBBT	-	-	3.3 ^e	-5.8 ^e	-2.5 ^e
BBBS	-	-	3.2 ^e	-5.6 ^e	-2.4 ^e
2a	0.96	429	2.89	-5.76	-2.87
2b	1.02	429	2.89	-5.82	-2.93
2c	1.02	429	2.89	-5.82	-2.93
1a	0.95	437	2.83	-5.75	-2.92
1b	0.97	438	2.83	-5.77	-2.94
1c	0.97	437	2.83	-5.77	-2.94

^aanodic onset versus Fc/Fc⁺; ^bEnergy gap estimated from the absorption onset; ^cEstimated from the onset of the oxidation peak. ^dLUMO levels were determined from the optical bandgap and the HOMO energy level according to the following equation: $E_{LUMO}=E_{HOMO}+E_{eg}$. ^eData taken from Ref.^[17] ^fData taken from Ref.^[68]

Electrochemical Properties

The electrochemical characteristics of compounds **1a–c** and **2a–c** were investigated by cyclic voltammetry (CV) methods (Figure 29). Using cyclic voltammograms, the peak oxidation potential, V_{ox} , and the peak reduction potential, V_{red} , of organic compounds can be determined in solution. To determine the HOMO and LUMO from these measurements, the assumption is made that when a molecule is oxidized, this process removes one electron from the HOMO (or valence band), contrary reduction which occurs when an electron is transferred into the LUMO (or conductance band). The energy gap (in electronvolts) can be concluded as the difference between the two potentials (in volts) multiplied by the charge on the electron $e=-1$ eV/V.

As can be seen in Figure 29, cyclic voltammetry of target compounds **1a–b**, **2a**, and **2b** show irreversible oxidation, while **2c** also shows a reduction peak. The HOMO energy levels were determined from the onset of the oxidation potential assuming the ferrocene/ferrocenium reference to be 4.8 eV^[69] below the vacuum level.

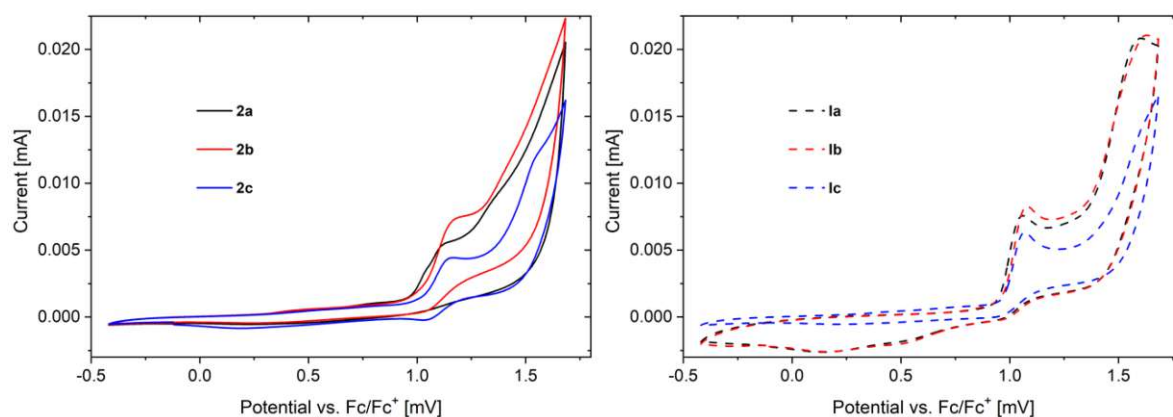


Figure 29: Cyclic voltammograms of target compounds **1a–c** and **2a–c** in dichloromethane solution.

The HOMO levels of selenium-based compounds **1a-c** are slightly increased (ranging from -5.75 to -5.77 eV) compared to **2a-c** (ranging from -5.76 to -5.82 eV). The LUMO energy levels were determined from the optical energy gaps and the HOMO levels obtained from CV data. These are in a relatively small range between -2.87 to -2.93 eV for sulfur-based materials and from -2.92 to -2.94 eV for selenium-based materials. When comparing the HOMO level of the target compounds with those of the benchmark semiconductor TIPS-pentacene (-5.15 eV), it becomes clear, that those are lower by about 0.6 eV being indicative for a more stable p-type material.

The stability of p-type organic semiconductors is crucial for their application under oxygen-rich conditions. Oxygen significantly impacts the effective lifetime and the on/off currents in OFETs by the introduction of bulk charge carriers through oxygen doping resulting in an increased conductivity of the organic semiconductor when the gate voltage is off.^[21] Electrochemical reactions with oxygen from the surrounding environment typically induce electron loss from the HOMO, particularly if the HOMO energy level is above -4.97 eV. Therefore, it is essential to adjust the HOMO level in π -conjugated materials by rational design strategies leading to a HOMO energy level to below this value. In this context, the obtained results within this thesis strengthen the potential application of the synthesized materials as stable p-channel organic semiconductors.

3.5 Summary & Outlook

Within this thesis, trialkylsilylethynyl substituted selenium-based analogues of TIPS-pentacene were designed and synthesized. The novel potential semiconductors were planned to incorporate (i) trialkylsilylethynyl groups facilitating the solubility of the target compounds rendering these compounds solution-processable and (ii) selenium heteroatoms ensuring a large radiation capture cross section beneficial for application in ionizing radiation detectors. Additionally, benzothiophene-based analogues were investigated to evaluate the influence of the heteroatom in this series.

To realize these materials, two different synthetic approaches were assessed. On the one hand intramolecular ring closure reactions starting from biseleno ethers were considered. On the other hand, the applicability of nucleophilic addition of the trialkylsilylethynyl group to suitable aromatic quinones and subsequent reduction of the resulting diols to the target molecules was evaluated.

In the first approach, reliable synthetic protocols to biseleno ethers were developed and the structures of representative compounds were confirmed by X-ray diffraction. As a further step, different intramolecular ring closure reactions were assessed: nucleophilic substitution, C-H and C-F activation. While nucleophilic substitution led to the formation of selanthrene as the main product, C-H activation did not show any traces of product. Using C-F activation, only degradation products could be observed. Unfortunately, all intramolecular ring closure procedures turned out to be not feasible to realize the desired target compounds.

Therefore, a second approach using fused aromatic quinones as precursors was pursued. For this purpose, optimized procedures toward amide substituted benzothiophene and benzoselenophene were developed. Subsequently, the synthesized amides were regioselectively lithiated using the amide group as an ortho directing group in the 2-position and further converted to both benzothiophene and benzoselenophene-based fused aromatic quinones. The structure of the benzoselenophene-based quinone was confirmed by X-ray diffraction. Further conversion toward the target compounds was realized by nucleophilic substitution of the keto group using lithiated trialkylsilylethyne. In a final step, a reductive aromatization, the target compounds were successfully obtained.

Crystallization of all target compounds as well as the benzothiophene-based analogues from solution gave single crystals. Structural comparison of the obtained polymorphs of the obtained structures shows a remarkable similarity in packing arrangement of both benzothiophene- and benzoselenophene derivatives. A closer look at the packing arrangements revealed the presence of an increased number of intermolecular short contacts between neighboring molecules predominantly in the selenium compounds. While these interactions are not present in benzothiophene based compounds, it is expected that especially they may be crucial for facilitating charge carrier transport in organic semiconductors.

Furthermore, the photophysical and electrochemical properties of all target compounds as well as their benzothiophene analogues were evaluated. The absorption spectra of both sulfur- and selenium-based materials exhibit similar absorption characteristics, indicating similar band structures. Within the sulfur and selenium series, the absorption maxima are nearly at the same position.

However, the selenium-based compounds showed a slight redshift compared to the sulfur-based materials, which can be attributed to the higher electron density induced by the selenium heteroatom. The selenium compounds exhibit a slightly smaller HOMO-LUMO energy gap compared to the sulfur-based materials, which may be beneficial for charge carrier transport. Furthermore, both series were compared to BBBT and BBBS data taken from literature. Here, the influence of the introduced trialkylsilylethynyl group is evident, a reduction of the HOMO-LUMO energy gap of 0.4 eV for both systems could be observed also suggesting facilitated charge transport in the target compounds. Cyclic voltammetry of the target compounds showed that the HOMO energy levels of the selenium-based target compounds are slightly increased compared to thiophene-based materials. As the stability of organic semiconductors is essential for their application in OFET devices, π -conjugated materials must exhibit HOMO energy levels below -4.97 eV.^[21] The synthesized compounds are well above this value and therefore may be suitable materials for the application in organic electronics. In summary, the obtained characteristics of these materials strengthen the potential application of the synthesized materials as stable p-channel organic semiconductors.

Further, these promising new compounds will be processed as semiconductors in OFET devices. Here, the device performance will be characterized. It is expected that the incorporation of selenium increases the radiation capture cross section compared to sulfur based materials and improves ionization radiation absorption. Therefore, these materials will be further investigated toward their applicability in ionizing radiation detectors.

4 Experimental Part

4.1 Materials and Methods

4.1.1 Reactants and Solvents

Unless noted otherwise, all reagents were purchased from commercial suppliers and used without further purification. Dichloromethane, diethyl ether, methanol, tetrahydrofuran and toluene intended for water-free reactions were purified on PURESOLV-columns (Innovative Technology Inc.).

Chemicals were commercially purchased and used without any purification unless otherwise stated.

4.1.2 Chromatographic Methods

Thin layer chromatography was performed on TLC plates on aluminum support (Merck, TLC Silica gel 60, fluorescence indicator F₂₅₄). Column Chromatography was performed on the following system:

Preparative MPLC: Büchi Sepacore TM Flash System (2 x Büchi Pump Module C-605, Büchi Pump Manager C-615, Büchi UV Photometer C-635, Büchi Fraction Collector C-660).

The appropriate PP-cartridges were packed with silica gel from Merck (40-63 µm). Further details (el-uents, amount of stationary phase) are given in the respective experimental procedures.

4.2 Analytic Methods

4.2.1 Mass Spectrometers

GCMS measurements were conducted *via* a GCMS interface from Thermo Finnigan TRACETM 1300 Gas Chromatograph on a Restek® Rxi® -5Sil MS column (l=30 m, d_i=0,25 mm, 0.25 µm coating thickness) coupled to a ISQTM LT Single Quadrupole Mass Spectrometer (electron ionization EI).

4.2.2 NMR Spectroscopy

NMR spectra were recorded on a Bruker DPX-200 (200 MHz for ¹H; 50 MHz for ¹³C), Bruker Avance UltraShield 400 (400 MHz for ¹H 100 MHz for ¹³C) and a Bruker Avance III HD 600 (600 MHz for ¹H; 150 MHz for ¹³C) Fourier transform spectrometer. Chemical shifts are reported in parts per million (ppm) referenced to the according solvent (¹H: CDCl₃ δ = 7.26 ppm, DMSO-d₆ δ = 2.50 ppm; ¹³C: CDCl₃ δ = 77.0 ppm, DMSO-d₆ δ = 39.5 ppm) with tetramethylsilane at δ = 0 ppm as internal standard. The following abbreviations were used for the multiplicities of the signals in ¹H: s = singlet, d = doublet, dd = doublets of doublets, t = triplet, q = quartet, quin = quintet, hept = heptet, m = multiplet and bs = broad signal.

4.2.3 UV-Vis Spectroscopy

Absorption measurements were conducted on a UV-Vis absorption spectrometer in DCM solutions (5 µM) with a NanoDrop One® UV-Vis Spectrophotometer from Thermo Fisher Scientific.

4.2.4 Cyclic Voltammetry

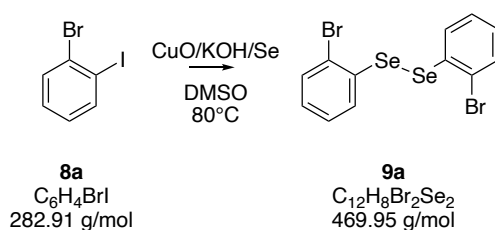
Cyclic voltammetry was performed using a three-electrode configuration consisting of a Pt working electrode, a Pt counter electrode and an Ag/AgCl reference electrode connected to a Metrohm Autolab PGSTAT204 potentiostat with NOVA software. Measurements were carried out in a 0.5 mM solution in anhydrous DCM (oxidation scan) with Bu₄NBF₄ (0.1 M) as the supporting electrolyte. The

solutions were purged with nitrogen for 15 minutes prior to measurement. HOMO energy levels were calculated from the onset of oxidation. The onset potential was determined by the intersection of two tangents drawn at the background and the rising of oxidation peaks.

4.3 Synthesis and Characterization of all Compounds

4.3.1 Synthetic Intermediates for Ring-Closure Strategy

4.3.1.1 1,2-bis(2-bromophenyl)diselane **9a**

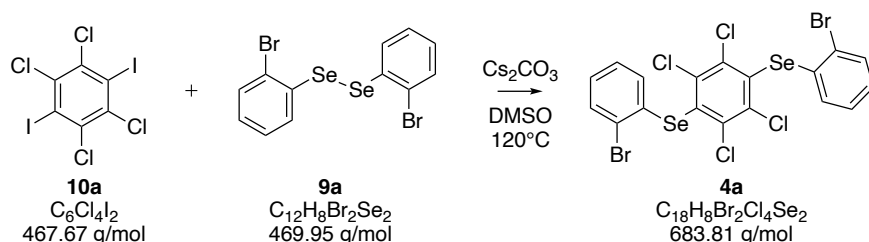


The reaction toward **9a** was conducted on the basis of a procedure published by Singh et. al^[48]. In a three-neck round bottom flask selenium (2.79 g, 35.3 mmol, 2 eq) was placed under inert atmosphere. Then **8a** (5.05 g, 17.9 mmol, 1 eq) was added as a solution in 40 mL degassed DMSO. Subsequently, CuO (144 mg, 1.81 mmol, 0.1 eq) and KOH (1.98 g, 35.3 mmol, 2 eq) were added in an argon counter-flow. The reaction was stirred at $80^\circ C$ for six hours. The reaction was monitored using GC/MS. Excess selenium was filtered through Celite® and washed with DCM. The solvent was removed in vacuo and 3.50 g crude product were obtained. The product was purified by column chromatography (90 g silica gel, 100% PE) and 2.10 g (50%) of **9a** could be obtained.

1H NMR (200 MHz, $CDCl_3$, TSC032/30): δ = 7.59 (dd, J = 1.6, 7.7 Hz, 1H), 7.50 (dd, J = 1.5, 7.7 Hz, 1H), 7.21 (dt, J = 1.5, 7.7 Hz, 1H), 7.08 (dt, J = 1.6, 7.6, 1H) ppm.

^{13}C NMR (50 MHz, $CDCl_3$, TSC032/33): δ = 132.7 (d), 131.5 (s), 130.6 (d), 128.7 (d), 128.6 (d), 123.0 (s) ppm.

4.3.1.2 (2,3,5,6-tetrachloro-1,4-phenylene)bis((2-bromophenyl)selane) **4a**

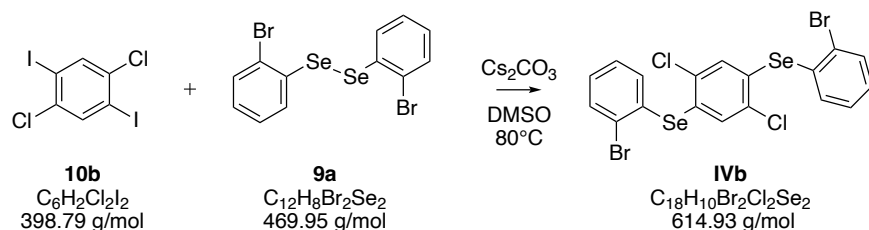


In a vial, **10a** (468 mg, 1 mmol, 1 eq), **9a** (470 mg, 1 mmol, 1 eq) and Cs_2CO_3 (652 mg, 2 mmol, 2 eq) were dissolved in 4 mL DMSO and stirred at $80^\circ C$ overnight. The reaction was monitored by GC/MS. After 24 h complete conversion was observed. The reaction mixture was poured into 50 mL water and the aqueous layer was extracted repeatedly with chloroform. The organic layers were dried over Na_2SO_4 and the solvent was removed in vacuo. The product was purified by column chromatography

(40 g silica gel, PE:DCM) yielding 763 mg (37%) **4a** as a colorless solid. Single crystals were obtained from a solution in DCE.

^1H NMR (200 MHz, CD_2Cl_2 , TSC063/20): δ = 7.62 - 7.53 (m, 2H), 7.23 - 7.09 (m, 4H), 6.88 - 6.79 (m, 2H) ppm.

4.3.1.3 (2,5-dichloro-1,4-phenylene)bis((2-bromophenyl)selane) IVb

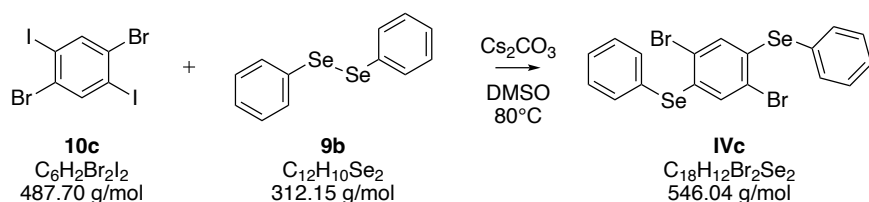


In a vial, **10b** (400 mg, 1 mmol, 1 eq), **9a** (472 mg, 1 mmol, 1 eq) and Cs_2CO_3 (326 mg, 1 mmol, 1 eq) were dissolved in 4 mL DMSO and stirred at 70 °C. The reaction was monitored by GC/MS. After 6 h no reaction conversion was detectable. The temperature was raised to 100 °C yielding only intermediate product. Additional Cs_2CO_3 (652 mg, 2 mmol, 1 eq) was added and the reaction mixture was heated to 120 °C. After further 96 h full conversion was observed. The reaction mixture was poured into 50 mL water and the aqueous layer was extracted repeatedly with chloroform. The organic layers were dried over Na_2SO_4 and the solvent was removed in vacuo. The product was purified by column chromatography (40 g silica gel, 100% PE) yielding 100 mg (16%) **IVb** as a colorless solid.

^1H NMR (200 MHz, CD_2Cl_2 , TSC038/10): δ = 7.73-7.65 (m, 2H), 7.41-7.33 (m, 2H), 7.33-7.23 (m, 4H), 7.20 (s, 2H) ppm.

^{13}C NMR (50 MHz, CD_2Cl_2 , TSC038/33): δ = 135.4 (d), 135.1 (s), 133.8 (d), 133.7 (d), 132.4 (s), 130.4 (d), 129.0 (d), 127.9 (s) ppm, singulett was not detected.

4.3.1.4 (2,5-dibromo-1,4-phenylene)bis(phenylselane) IVc

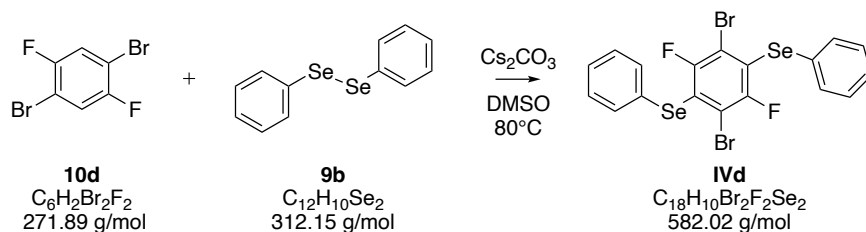


In a vial, **10c** (244 mg, 0.5 mmol, 1 eq), **9b** (235 mg, 0.75 mmol, 1.5 eq) and Cs_2CO_3 (163 mg, 0.5 mmol, 1 eq) were dissolved in 2 mL DMSO and stirred at 80°C. The reaction was monitored by GC/MS and TLC. After 24 h no reaction conversion was detectable. The temperature was raised to 115°C yielding only intermediate product. Additional Cs_2CO_3 (163 mg, 0.5 mmol, 1 eq) was added and after further 78 h full conversion was observed. The reaction mixture was poured into 40 mL water and the aqueous layer was extracted repeatedly with chloroform. The organic layers were dried over Na_2SO_4 and the

solvent was removed in vacuo. The product was purified by column chromatography (40 g silica gel, 100% PE) yielding 150 mg (27%) **IVc** as a colorless solid.

^1H NMR (200 MHz, CDCl_3 , TSC055/20): δ = 7.64-7.57 (m, 4H), 7.46-7.38 (m, 6H), 6.95 (s, 2H) ppm.

4.3.1.5 (2,5-Dibromo-3,6-fluoro-1,4-phenylene)bis(phenylselane) **IVd**



In a three-neck bottom round flask, **10d** (872 mg, 4 mmol, 1 eq), **9b** (1.87 g, 6 mmol, 1.5 eq) and Cs_2CO_3 (2.60 g, 8 mmol, 2 eq) were dissolved in 20 mL DMSO and stirred at 80°C . The reaction was monitored by GC/MS. After 7 h full conversion was observed. The reaction mixture was poured into 40 mL water and the aqueous layer was extracted repeatedly with chloroform. The organic layers were dried over Na_2SO_4 and the solvent was removed in vacuo. The product was purified by column chromatography (40 g silica gel, 100% PE) yielding 362 mg (16%) **IVd** as a colorless solid. Single crystals were obtained by slow evaporation of a solution of **IVd** in DCE.

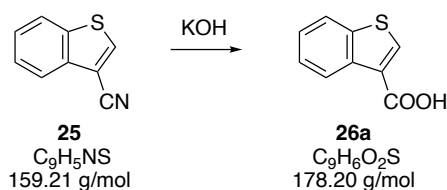
^1H NMR (400 MHz, CDCl_3 , FID TSC020#F/50): δ = 7.50-7.45 (m, 4H), 7.29-7.19 (m, 6H) ppm.

^{13}C NMR (100 MHz, CDCl_3 , FID TSC020#F/51): δ = 133.1 (d), 129.5 (d), 128.3 (d) ppm; singulets not detected.

4.3.2 Synthetic Strategy Toward Target Compounds *via* Quinone

4.3.2.1 Synthesis of Benzo[*b*]thiophene Precursor

4.3.2.1.1 Benzo[*b*]thiophene-3-carboxylic acid **26a**

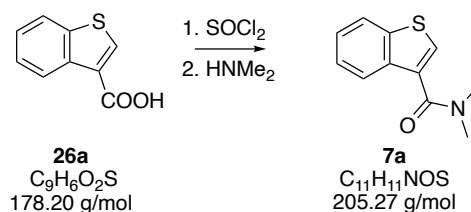


In a three-neck round-bottom flask with condenser, thermometer, and magnetic stir bar, **25** (4.20 g, 26 mmol, 1eq.) and KOH (5.00 g, 88 mmol, 3.34 eq.) were added to 100 mL ethylene glycol. The reaction mixture was heated to 200°C overnight under an argon atmosphere. The solution was cooled to room temperature and 150 mL water added. The reaction solution was extracted with diethyl ether. The aqueous phase was acidified with 6 N HCl and repeatedly extracted with diethyl ether. The combined organic solutions were washed with water as well as brine and dried over Na_2SO_4 . The solvent was removed under vacuo. **26a** was obtained quantitatively (4.20 g) as a yellow solid.

^1H NMR (600 MHz, DMSO, HBR459/10): δ = 12.96 (s, 1H), 8.64 (s, 1H), 8.50 (d, J = 8.2 Hz, 1H), 8.08 (d, J = 8.2 Hz, 1H), 7.50 (dt, J = 7.2, 1.1 Hz, 1H), 7.44 (dt, J = 7.2, 1.1 Hz, 1H) ppm.

^{13}C NMR (150 MHz, DMSO, HBR459/11): δ = 163.8, 139.8, 138.0, 136.6, 127.2, 125.3, 125.0, 124.2, 123.1 ppm.

4.3.2.1.2 *N,N*-Dimethylbenzo[*b*]thiophene-3-carboxamide **7a**



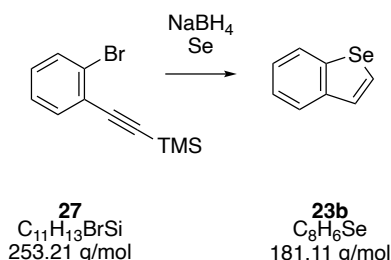
In a three-neck round-bottom flask with condenser, thermometer, and magnetic stir bar, to **26a** (4.20 g, 23.7 mmol, 1eq.) was added thionyl chloride (7.92 g, 40 mmol, 1.7 eq.) and catalytic amounts of DMF (three drops). The reaction mixture was heated to reflux overnight. Excess thionyl chloride was removed by distillation. The crude acid chloride was used without further purification, dissolved in anhydrous dioxane to which 20 mL of an aqueous dimethylamine solution (40 wt.%) was added dropwise at 0°C. The reaction solution was stirred for one hour and subsequently quenched with 200 mL ice water and acidified with 2 N HCl. The solution was extracted repeatedly with chloroform and the organic layer was dried over Na_2SO_4 . The solvent was removed in vacuo. Amide **7a** was obtained in 79% (4.64 g) as a brownish liquid.

^1H NMR (600 MHz, CDCl_3 , HBR459/20): δ = 7.89-7.86 (m, 1H), 7.83-7.81 (m, 1H), 7.56 (s, 1H), 7.43-7.37 (m, 2H), 3.10 (bs, 6H) ppm.

^{13}C NMR (150 MHz, CDCl_3 , HBR459/21): δ = 166.7, 139.6, 136.9, 132.0, 126.5, 124.9, 124.8, 123.2, 122.5, 38.9, 35.3 ppm.

4.3.2.2 Synthesis of Benzo[*b*]selenophene Precursor

4.3.2.2.1 Benzo[*b*]selenophene **23b**



The reaction was carried out according to Kashiki et al.^[60] To a suspension of selenium powder (6.20 g, 45 mmol, 1.75 eq.) in ethanol (120 mL) was added sodium borohydride (2.98 g, 79 mmol, 1.75 eq.) at ice-bath temperature. After the mixture was stirred for 40 min, NMP (250 mL) and 1-bromo-2-(trimethylsilyl)ethynylbenzene **27** (11.39 mg, 45 mmol) were added. After stirring at 150 °C for overnight, the mixture was poured into saturated aqueous ammonium chloride solution (500 mL), and the

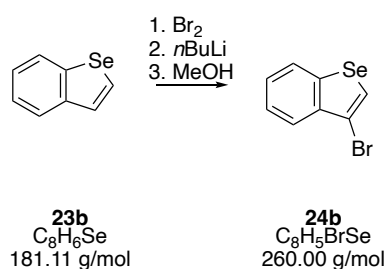
resulting precipitate was extracted with pentane. The combined organic layers were washed with brine, dried over Na₂SO₄ and concentrated in vacuo. The residue was purified by column chromatography in pentane yielding benzo[*b*]selenophene in 37% yield (3.01 g).

¹H NMR (600 MHz, CDCl₃, TSC003/10): δ = 8.00 (d, *J* = 5.9 Hz, 1H), 7.97 (d, *J* = 7.9 Hz, 1H), 7.86 (d, *J* = 7.9 Hz, 1H), 7.60 (d, *J* = 5.9 Hz, 1H), 7.41 (dt, *J* = 1.5, 7.7 Hz, 1H), 7.31 (dt, *J* = 1.5, 7.7 Hz, 1H) ppm.

¹³C NMR (150 MHz, CDCl₃, TSC003/11): δ = 142.0, 141.2, 128.6, 127.7, 125.6, 125.3, 124.4, 124.3 ppm.

⁷⁷Se NMR (114 MHz, CDCl₃, TSC003/13): δ = 524 ppm.

4.3.2.2.2 3-Bromobenzo[*b*]selenophene **24b**

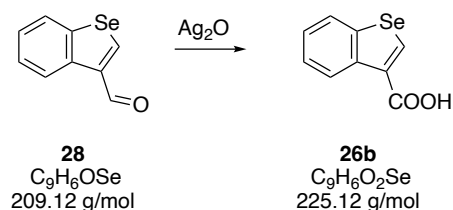


The bromination of benzo[*b*]selenophene was carried out according to Murphy et al.^[70] **23b** (1.01 g, 7.5 mmol, 1 eq.) was dissolved in 250 mL chloroform. At 0°C bromine (2.64 g, 16.5 mmol, 2.2 eq.) was added dropwise within one hour. The reaction mixture was stirred overnight and quenched with a NaHSO₃ solution, the aqueous phase was repeatedly extracted with chloroform. The combined organic layers were washed with brine, dried over Na₂SO₄ and concentrated in vacuo. The residue was flashed through a silica pad and concentrated. Crude 2,3-dibromobenzo[*b*]selenophene was obtained in 93% yield (2.03 g) and used without further purification.

In the next step, 2,3-dibromobenzo[*b*]selenophene was dissolved in 50 mL anhydrous diethylether under argon atmosphere. *n*BuLi (2.4 mL, 6 mmol, 1 eq.) was added at -40 °C. GC-MS analysis showed full conversion after 15 min. The reaction was quenched with 1 mL methanol. A solution of NH₄Cl was added and the aqueous phase was repeatedly extracted with diethylether. The combined organic layers were washed with brine, dried over Na₂SO₄ and concentrated in vacuo. **24b** was obtained in 58% yield (1.13 g).

¹H NMR (200 MHz, CDCl₃, HBR281/10): δ = 7.97 (s, 1H), 7.94-7.88 (m, 2H), 7.52-7.46 (m, 1H), 7.40-7.34 (m, 1H). The NMR is in accordance to literature.^[71]

4.3.2.2.3 Benzo[*b*]selenophene-3-carboxylic acid **26b**



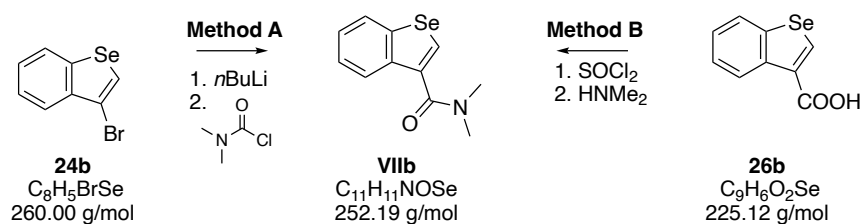
In a three-neck round-bottom flask, Ag₂O (5.98 g, 25.82 mmol, 2.0 eq.) was dissolved in 25 mL water. NaOH (2.07 g, 51.65 mmol, 4.0 eq) was dissolved in 25 mL and added to the Ag₂O solution. Aldehyde **28** (2.70 g, 12.91 mmol, 1 eq.) was added and the reaction solution was stirred for one hour at room temperature. Subsequently the solution was heated to 50 °C and stirred for 16 hours. The suspension was filtered over Celite® and filtrate was extracted twice with 40 mL ethyl acetate. The combined organic layers were washed with 20 mL water and added to the aqueous phase. The combined aqueous solutions were acidified with 2 N HCl. The obtained precipitate was filtered, washed with cold water and dried in vacuo. Carboxylic acid **26b** was obtained in 66% yield (1.92 g) as a white solid.

¹H NMR (600 MHz, DMSO, FAS007/30): δ = 12.83 (s, 1H), 9.20 (s, 1H), 8.57 (d, *J* = 7.9 Hz, 1H), 8.14 (d, *J* = 7.8 Hz, 1H), 7.53-7.28 (m, 2H) ppm.

¹³C NMR (150 MHz, DMSO, FAS007/31): δ = 164.1, 143.6, 141.8, 138.6, 130.2, 126.2, 126.0, 125.1, 124.8 ppm.

⁷⁷Se NMR (114 MHz, DMSO, FAS007/32): δ = 529 ppm.

4.3.2.2.4 *N,N*-Dimethylbenzo[*b*]selenophene-3-carboxamide **VIIb**



Method A:

Benzoselenophene **24b** (260 mg, 1 mmol, 1 eq.) was dissolved in 3 mL anhydrous diethylether under argon atmosphere. *n*BuLi (440 μL, 1.1 mmol, 1.1 eq.) was added at -78°C. At this temperature dimethylcarbamoyl chloride was added after 30 min. The solution was stirred overnight and quenched with 5 mL water. After extraction with diethylether, the organic layer was washed with a NaHCO₃ solution and dried over Na₂SO₄. The solvent was removed in vacuo. Amide **VIIb** was obtained 44 % yield (110 mg) as a brownish liquid.

Method B:

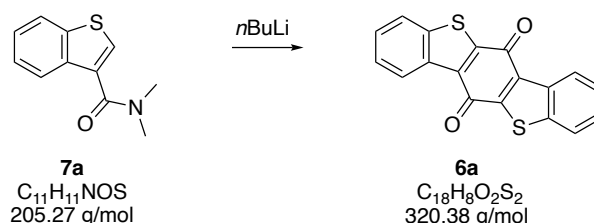
In a three-neck round-bottom flask with condenser, thermometer, and magnetic stir bar, to **26b** (1.91 g, 8.50 mmol, 1 eq.) was added thionyl chloride (1.72 g, 14.5 mmol, 1.7 eq.) and catalytic amounts of DMF (three drops). The reaction mixture was heated to reflux overnight. Excess thionyl chloride was removed by distillation. The crude acid chloride was used without further purification, dissolved in 50 mL anhydrous dioxane to which 15 mL of an aqueous dimethylamine solution (40 wt.%) was added dropwise at 0°C. The reaction solution was stirred for one hour and subsequently quenched with 200 mL ice water and neutralized with 2 N HCl. The solution was extracted repeatedly with chloroform and the organic layer was dried over Na₂SO₄. The solvent was removed in vacuo. Amide **VIIb** was obtained 88 % yield (1.88 g) as a brownish liquid.

^1H NMR (200 MHz, CDCl_3 , HBR294/50): δ = 8.01 (s, 1H), 7.90-7.86 (m, 1H), 7.77-7.72 (m, 1H), 7.42-7.24 (m, 2H), 3.14 (bs, 3H), 2.90 (bs, 3H) ppm.

^{13}C NMR (50 MHz, CDCl_3 , HBR294/53): δ = 167.5 (s), 141.4 (s), 139.2 (s), 135.7 (s), 128.4 (d), 125.5 (d), 124.8 (d), 124.8 (d), 124.7 (d), 38.7 (q), 34.9 (q) ppm.

4.3.2.3 Synthesis of Benzo[1,2-*b*:4,5-*b'*]bis[1]benzochalcogenophene-6,12-dione

4.3.2.3.1 Benzo[1,2-*b*:4,5-*b'*]bis[1]benzothiophene-6,12-dione



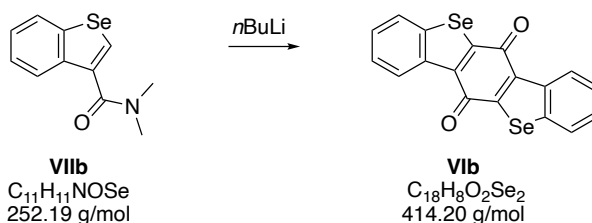
Amide **7a** (3.08 g, 15.0 mmol, 1.0 eq.) was dissolved in 110 mL anhydrous diethyl ether and cooled to -70°C under argon atmosphere. Subsequently $n\text{BuLi}$ (6.3 mL, 2.5 M in hexanes, 15.75 mmol, 1.05 eq.) was added slowly. After complete addition, the reaction mixture was allowed to warm to room temperature. The reaction progress was monitored by GC-MS analysis. After completion of the reaction, the solution was poured into 300 mL of water. The orange-red precipitate was filtered and washed with 40 mL water and 30 mL diethyl ether. The obtained solid was dried in vacuo. Dione **6a** was obtained in 43% yield (1.05 g).

TLC: 0.38 (PE/EA 19:1)

^1H NMR (600 MHz, CDCl_3 , MIS019/10): δ = 8.82-8.81 (m, 2H), 7.96-7.95 (m, 2H), 7.61-7.54 (m, 4H) ppm.

^{13}C NMR (150 MHz, CDCl_3 , MIS019/11): δ = 176.9, 148.5, 141.6, 136.0, 133.9, 128.0, 127.3, 126.5, 123.1 ppm.

4.3.2.3.2 Benzo[1,2-*b*:4,5-*b'*]bis[1]benzoselenophene-6,12-dione



DIPA (5.01 g, 49.5 mmol, 4.4 eq.) was dissolved in 50 mL anhydrous THF and cooled to -65°C under argon atmosphere. Subsequently $n\text{BuLi}$ (18 mL, 2.5 M in hexanes, 45.0 mmol, 4.0 eq.) was added and the solution was stirred 15 min at -60°C . The solution was allowed to warm to room temperature and stirred for one hour. Subsequently, the solution was cooled to -65°C again and amide **VIIb** (2.84 mg, 11.2 mmol, 1.0 eq.) dissolved in 5 mL anhydrous THF was added. The reaction mixture was allowed to warm to room temperature and stirred overnight. The reaction was heated to reflux for 5 hours. The reaction progress was monitored by GC-MS analysis as well as TLC (PE:EE 95:5). After completion of

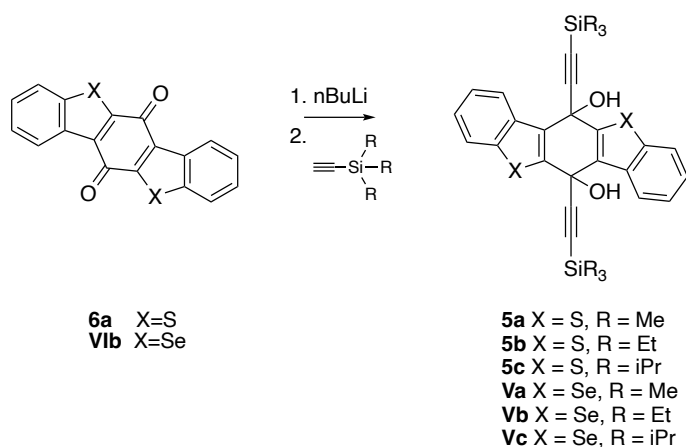
the reaction, the solution was poured into 300 mL of water. The aqueous phase was repeatedly extracted with chloroform and the organic layer was dried over Na₂SO₄. The solvent was removed in vacuo. Dione **Vlb** was obtained in 60% yield (1.39 g).

¹H NMR (600 MHz, CDCl₃, HBR456/30): δ = 8.94 (d, *J* = 8.2 Hz, 2H), 7.98 (d, *J* = 8.2 Hz, 2H), 7.58-7.56 (m, 2H), 7.50-7.47 (m, 2H) ppm.

¹³C NMR (150 MHz, CDCl₃, HBR456/31): δ = 178.0, 155.6, 143.7, 138.7, 136.4, 128.7, 127.8, 127.0, 125.9 ppm.

⁷⁷Se NMR (114 MHz, CDCl₃, HBR456/32): δ = 535 ppm.

4.3.2.4 Substituted Benzo[1,2-*b*:4,5-*b'*]bis[1]benzochalcogenophene-6,12-diols



General procedure toward diols **5a-c**

To a solution of trialkylsilylacetylene (2.9 eq.) in anhydrous THF (2 mL/mmol) *n*BuLi (2.5 M in hexanes, 2.5 eq.) was added dropwise at -50°C under inert atmosphere. The solution was stirred for one hour, followed by the addition of dione **6a** (1eq.) as a solid. The resulting mixture was allowed to warm to room temperature and stirred overnight. The reaction was quenched with NH₄Cl solution and extracted repeatedly with chloroform. The combined organic layers were dried over Na₂SO₄ and the solvent was removed in vacuo. Diols **5a-c** were purified by column chromatography.

6,12-Dihydro-6,12-bis[2-(trimethylsilyl)ethynyl]benzo[1,2-*b*:4,5-*b'*]bis[1]benzothiophene-6,12-diol **5a**

To trimethylsilylacetylene (417 mg, 4.25 mmol, 2.5 eq.) in 9 mL anhydrous THF, *n*BuLi (1.70 mL, 4.25 mmol 2.5 eq.) was added at -50°C. After one hour dione **6a** (535 mg, 1.7 mmol) was added. After work-up according to the general procedure and column chromatography (PE:EE), **5a** could be obtained in 85% yield (733 mg) as an orange solid.

¹H NMR (600 MHz, CDCl₃, HBR400/140): δ = 8.46-8.45 (m, 2H), 7.92-7.91 (m, 2H), 7.50-7.43 (m, 4H), 2.99 (s, 2H), 0.14 (s, 18H) ppm.

¹³C NMR (150 MHz, CDCl₃, HBR400/141): δ = 143.6, 140.1, 135.7, 130.4, 125.6, 125.0, 124.4, 122.7, 104.1, 92.8, 64.0, -0.5 ppm.

6,12-Dihydro-6,12-bis[2-(triethylsilyl)ethynyl]benzo[1,2-*b*:4,5-*b'*]bis[1]benzothiophene-6,12-diol **5b**

To triethylsilylacetylene (350 mg, 2.5 mmol, 2.5 eq.) in 5 mL anhydrous THF, *n*BuLi (1 mL, 2.5 mmol, 2.5 eq.) was added at -50°C. After one hour dione **6a** (350 mg, 1 mmol) was added. After work-up according to the general procedure and column chromatography (9 g silica gel, PE:EE 0 → 15%), **5b** could be obtained in 72% yield (432 mg) as a yellow solid.

¹H NMR (600 MHz, CDCl₃, HBR400/40): δ = 8.51-8.49 (m, 2H), 7.93-7.88 (m, 2H), 7.48-7.41 (m, 4H), 2.93 (s, 2H), 0.94 (t, *J* = 7.8 Hz, 18H), 0.58 (q, *J* = 7.8 Hz, 12H) ppm.

¹³C NMR (150 MHz, CDCl₃, HBR400/43): δ = 143.8 (s), 140.3 (s), 135.9 (s), 130.6 (s), 125.5 (d), 125.2 (d), 124.3 (d), 122.7 (d), 105.6 (s), 90.7 (s), 64.3 (s), 4.4 (q), 4.15 (t) ppm.

6,12-Dihydro-6,12-bis[2-(triisopropylsilyl)ethynyl]benzo[1,2-*b*:4,5-*b'*]bis[1]benzothiophene-6,12-diol **5c**

To triisopropylsilylacetylene (192 mg, 1.05 mmol, 2.5 eq.) in 2.5 mL anhydrous THF, *n*BuLi (420 μL, 2.5 mmol, 2.5 eq.) was added at -50°C. After one hour dione **6a** (135 mg, 0.42 mmol) was added. After work-up according to the general procedure and column chromatography (9 g silica gel, PE:EE 0 → 15%), **5c** could be obtained in 41% yield (118 mg) as a yellow solid.

¹H NMR (600 MHz, CDCl₃, HBR400/170): δ = 8.56-8.51 (m, 2H), 7.93-7.90 (m, 2H), 7.46-7.42 (m, 4H), 2.93 (s, 2H), 1.09-1.01 (m, 42H) ppm.

¹³C NMR (150 MHz, CDCl₃, HBR400/171): δ = 143.8, 140.1, 135.7, 130.4, 125.5, 125.1, 124.3, 122.7, 106.3, 89.6, 64.0, 18.6, 11.1 ppm.

General procedure toward diols **Va-c**

To a solution of trialkylsilylacetylene (4 eq.) in anhydrous THF (1 mL/mmol) *n*BuLi (2.5 M in hexanes, 3.9 eq.) was added dropwise at -50°C under inert atmosphere. The solution was stirred for one hour, followed by the addition of dione **Vib** (1eq.) as a solid. The resulting mixture was allowed to warm to room temperature and further stirred at 50 °C for 16 hours. The reaction conversion was monitored by TLC PE:EE 5%. The reaction was quenched with NH₄Cl solution and extracted repeatedly with chloroform. The combined organic layers were dried over Na₂SO₄, and the solvent was removed in vacuo. Diols **Va-c** were purified by column chromatography.

6,12-Dihydro-6,12-bis[2-(trimethylsilyl)ethynyl]benzo[1,2-*b*:4,5-*b'*]bis[1]benzoselenophene-6,12-diol **Va**

To trimethylsilylacetylene (391 mg, 4 mmol, 4 eq.) in 4 mL anhydrous THF, *n*BuLi (1.56 mL, 3.9 mmol, 3.9 eq.) was added at -50°C. After one hour dione **Vib** (414 mg, 1 mmol) was added. After work-up according to the general procedure and column chromatography (40 g silica gel, PE:EE 0 → 25%), **Va** could be obtained in 60% yield (369 mg) as a yellow solid.

¹H NMR (600 MHz, CDCl₃, HBR457/20): δ = 8.51 (dd, *J* = 7.8 Hz, 0.9 Hz, 2H), 7.93 (d, *J* = 7.8 Hz, 2H), 7.49-7.46 (m, 2H), 7.39-7.36 (m, 2H), 3.00 (s, 2H), 0.14 (m, 18H) ppm.

^{13}C NMR (150 MHz, CDCl_3 , HBR457/21): δ = 148.6, 141.3, 138.3, 132.7, 127.3, 125.7, 125.6, 124.5, 105.0, 93.0, 66.1, -0.5 ppm.

^{77}Se NMR (114 MHz, CDCl_3 , HBR457/22): δ = 502 ppm.

6,12-Dihydro-6,12-bis[2-(triethylsilyl)ethynyl]benzo[1,2-*b*:4,5-*b'*]bis[1]benzoselenophene-6,12-diol **Vb**

To triethylsilylacetylene (561 mg, 4 mmol, 4 eq.) in 4 mL anhydrous THF, *n*BuLi (1.56 μL , 3.9 mmol, 3.9 eq.) was added at -50°C . After one hour dione **Vib** (414 mg, 1 mmol) was added. After work-up according to the general procedure and column chromatography (40 g silica gel, PE:EE 0 \rightarrow 25%), **Vb** could be obtained in 54% yield (373 mg) as a yellow solid.

^1H NMR (600 MHz, CDCl_3 , LMK115/20): δ = 8.56 (dd, J = 8.1, 0.8 Hz, 2H), 7.93 (d, J = 8.1 Hz, 2H), 7.46-7.43 (m, 2H), 7.38-7.35 (m, 2H), 2.94 (s, 2H), 0.93 (t, J = 7.9 Hz, 18H), 0.57 (q, J = 7.9 Hz, 12H) ppm.

^{13}C NMR (150 MHz, CDCl_3 , HBR451/31): δ = 148.6, 141.3, 138.3, 132.7, 127.4, 125.7, 125.6, 124.4, 106.2, 90.8, 66.1, 7.4, 4.1 ppm.

^{77}Se NMR (114 MHz, CDCl_3 , HBR452/32): δ = 501 ppm.

6,12-Dihydro-6,12-bis[2-(triisopropylsilyl)ethynyl]benzo[1,2-*b*:4,5-*b'*]bis[1]benzoselenophene-6,12-diol **Vc**

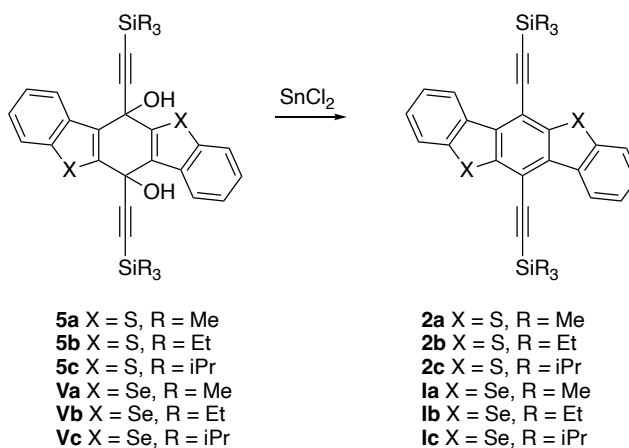
To triisopropylsilylacetylene (730 mg, 4 mmol, 4 eq.) in 4 mL anhydrous THF, *n*BuLi (1.56 μL , 3.9 mmol, 3.9 eq.) was added at -50°C . After one hour dione **Vib** (414 mg, 1 mmol) was added. After work-up according to the general procedure and column chromatography (40 g silica gel, PE:EE 0 \rightarrow 25%), **Vc** could be obtained in 49% yield (384 mg) as a yellow solid.

^1H NMR (600 MHz, CDCl_3 , HBR452/30): δ = 8.60 (dd, J = 7.8, 1.1 Hz, 2H), 7.93 (d, J = 7.8 Hz, 2H), 7.45-7.42 (m, 2H), 7.37-7.35 (m, 2H), 2.89 (s, 2H), 1.06-1.00 (m, 42H) ppm.

^{13}C NMR (150 MHz, CDCl_3 , HBR452/31): δ = 148.7, 141.2, 138.3, 132.7, 127.5, 125.6, 125.6, 124.4, 107.1, 89.8, 66.2, 18.6, 11.2 ppm.

^{77}Se NMR (114 MHz, CDCl_3 , HBR452/32): δ = 500 ppm.

4.3.2.4.1 Synthesis of Trialkylsilylethynyl-substituted Benzo[1,2-*b*:4,5-*b'*]bis[1]benzochalcogenophenes



General procedure toward **2a-c** and **la-c**

Anhydrous SnCl_2 (4 eq.) was added to a dispersion of the substituted diols **5a-c** and **Va-c** (1 eq.) in acetonitrile (~ 0.05 M) and the mixture was stirred under argon atmosphere overnight at room temperature. The reaction mixture was quenched with water, extracted with chloroform, dried over Na_2SO_4 and concentrated in vacuo. The obtained residues were purified by column chromatography to obtain pure products **2a-c** and **la-c**. Further purification for device fabrication was done by sublimation (250°C , 0.1 mbar).

6,12-bis[2-(trimethylsilyl)ethynyl]benzo[1,2-*b*:4,5-*b'*]bis[1]benzothiophene 2a

According to the general procedure **2a** was synthesized starting from **5a** (367 mg, 0.7 mmol) and SnCl_2 (534 mg, 2.8 mmol) in 11 mL ACN under argon atmosphere. After work-up the crude product was purified by column chromatography (40 g silica gel, light petroleum) and product **2a** isolated as yellow solid in 56% yield (190 mg).

^1H NMR (600 MHz, CDCl_3 , LMK095/70): δ = 9.21 (dd, J = 7.7, 1.3 Hz, 2H), 7.92 (dd, J = 7.7, 1.3 Hz, 2H), 7.55-7.50 (m, 4H), 0.47 (s, 18H) ppm.

^{13}C NMR (150 MHz, CDCl_3 , LMK095/71): δ = 142.7, 140.3, 135.2, 132.5, 127.3, 124.7, 124.3, 122.5, 112.1, 109.1, 101.3, 0.1 ppm.

6,12-bis[2-(triethylsilyl)ethynyl]benzo[1,2-*b*:4,5-*b'*]bis[1]benzothiophene 2b

According to the general procedure **2b** was synthesized starting from **5b** (300 mg, 0.5 mmol) and SnCl_2 (379 mg, 2.0 mmol) in 5 mL ACN under argon atmosphere. After work-up the crude product was purified by column chromatography (40 g silica gel, light petroleum) and product **2b** isolated as yellow solid in 57% yield (162 mg).

^1H NMR (400 MHz, CDCl_3 , LMK104/20): δ = 9.32-9.28 (m, 2H), 7.94-7.90 (m, 2H), 7.56-7.46 (m, 4H), 1.23 (t, J = 7.8 Hz, 18H), 0.90 (q, J = 7.8 Hz, 12H) ppm.

^{13}C NMR (150 MHz, CDCl_3 , LMK104/51): δ = 141.8, 139.3, 134.3, 131.5, 126.3, 123.8, 123.2, 121.5, 111.2, 106.0, 101.4, 6.66, 3.44 ppm.

6,12-bis[2-(triisopropylsilyl)ethynyl]benzo[1,2-*b*:4,5-*b'*]bis[1]benzothiophene 2c

According to the general procedure **2c** was synthesized starting from **5c** (189 mg, 0.28 mmol) and SnCl_2 (215 mg, 1.13 mmol) in 3 mL ACN under argon atmosphere. After work-up the crude product was purified by column chromatography (40 g silica gel, light petroleum) and product **2c** isolated as yellow solid in 75% yield (142 mg).

TLC: 0.43 (PE)

^1H NMR (600 MHz, CDCl_3 , MMA044/20): δ = 9.40-9.36 (m, 2H), 7.95-7.91 (m, 2H), 7.55-7.46 (m, 4H), 1.37-1.29 (m, 42H) ppm.

^{13}C NMR (150 MHz, CDCl_3 , MMA044/21): δ = 143.1, 140.2, 135.3, 132.5, 127.2, 124.9, 124.1, 122.6, 112.3, 106.1, 103.1, 18.8, 11.5 ppm.

6,12-bis[2-(trimethylsilyl)ethynyl]benzo[1,2-*b*:4,5-*b'*]bis[1]benzoselenophene **1a**

According to the general procedure **1a** was synthesized starting from **Va** (305 mg, 0.5 mmol) and SnCl₂ (379 mg, 2 mmol) in 8 mL ACN under argon atmosphere. After work-up the crude product was purified by column chromatography (40 g silica gel, light petroleum) and product **1a** isolated as yellow solid in 83% yield (238 mg).

¹H NMR (600 MHz, CDCl₃, HBR457/20): δ = 9.32 (dd, *J* = 7.8, 1.2 Hz, 2H), 7.93 (dd, *J* = 7.8, 1.2 Hz, 2H), 7.53-7.44 (m, 4H), 0.45 (m, 18H) ppm.

¹³C NMR (150 MHz, CDCl₃, HBR457/41): δ = 144.9, 140.1, 138.2, 134.3, 127.4, 126.3, 125.6, 124.6, 116.1, 108.4, 103.1, 0.1 ppm.

⁷⁷Se NMR (114 MHz, CDCl₃, HBR457/42): δ = 461 ppm.

6,12-bis[2-(triethylsilyl)ethynyl]benzo[1,2-*b*:4,5-*b'*]bis[1]benzoselenophene **1b**

According to the general procedure **1b** was synthesized starting from **Vb** (373 mg, 0.54 mmol) and SnCl₂ (407 mg, 2.1 mmol) in 8 mL ACN under argon atmosphere. After work-up the crude product was purified by column chromatography (40 g silica gel, light petroleum) and product **1b** isolated as yellow solid in 80% yield (285 mg).

¹H NMR (600 MHz, CDCl₃, HBR451/70): δ = 9.42 (dd, *J* = 7.6, 1.5 Hz, 2H), 7.94 (dd, *J* = 7.6, 1.5 Hz, 2H), 7.49-7.44 (m, 4H), 1.21 (q, *J* = 8.3 Hz, 18H), 0.88 (t, *J* = 8.3 Hz, 12H) ppm.

¹³C NMR (150 MHz, CDCl₃, HBR451/61): δ = 145.0, 140.1, 138.2, 134.4, 127.3, 126.4, 125.6, 124.5, 116.2, 106.3, 104.2, 7.7, 4.5 ppm.

⁷⁷Se NMR (114 MHz, CDCl₃, HBR451/62): δ = 461 ppm.

6,12-bis[2-(triisopropylsilyl)ethynyl]benzo[1,2-*b*:4,5-*b'*]bis[1]benzoselenophene **1c**

According to the general procedure **1c** was synthesized starting from **Vc** (384 mg, 0.7 mmol) and SnCl₂ (374 mg, 2.8 mmol) in 11 mL ACN under argon atmosphere. After work-up the crude product was purified by column chromatography (40 g silica gel, light petroleum) and product **1c** isolated as yellow solid in 69% yield (254 mg).

¹H NMR (600 MHz, CDCl₃, HBR453/20): δ = 9.51-9.49 (m, 2H), 7.96-7.93 (m, 2H), 7.47-7.45 (m, 4H), 1.37-1.26 (m, 42H) ppm.

¹³C NMR (150 MHz, CDCl₃, HBR453/20): δ = 145.1, 140.0, 138.2, 134.5, 127.3, 126.6, 125.5, 124.5, 116.3, 105.4, 105.0, 18.8, 11.5 ppm.

⁷⁷Se NMR (114 MHz, CDCl₃, HBR457/42): δ = 452 ppm.

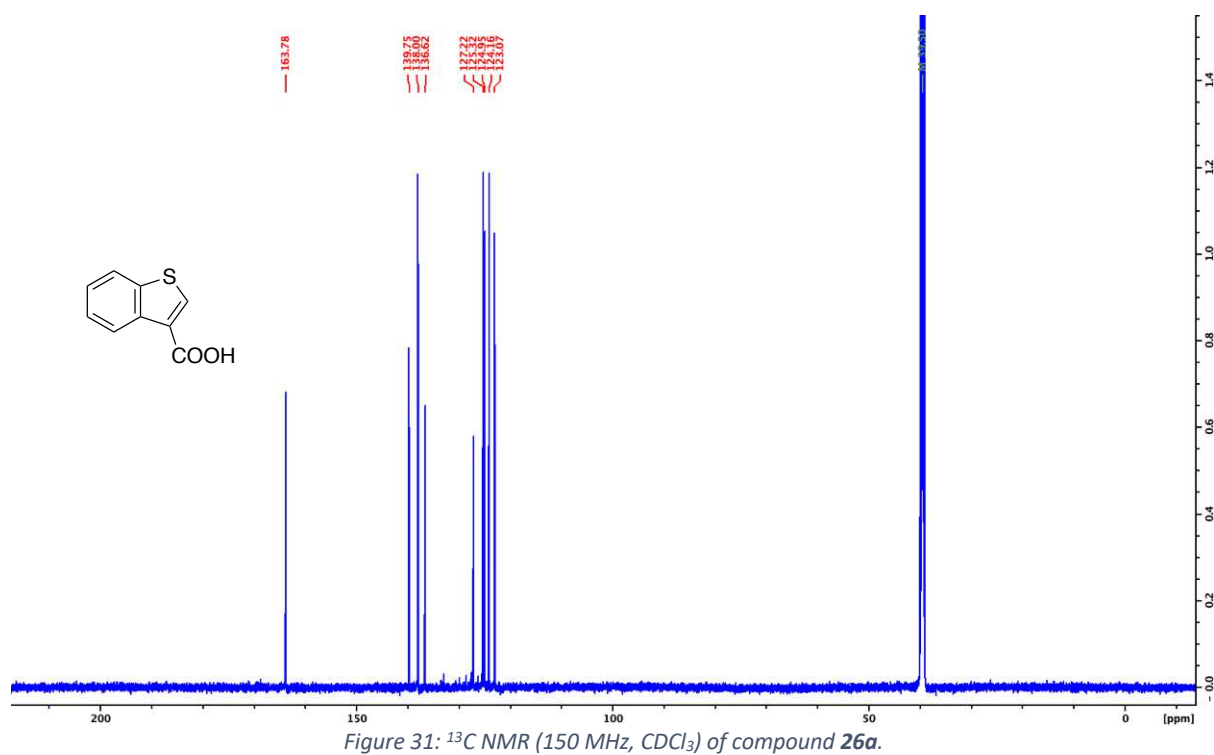
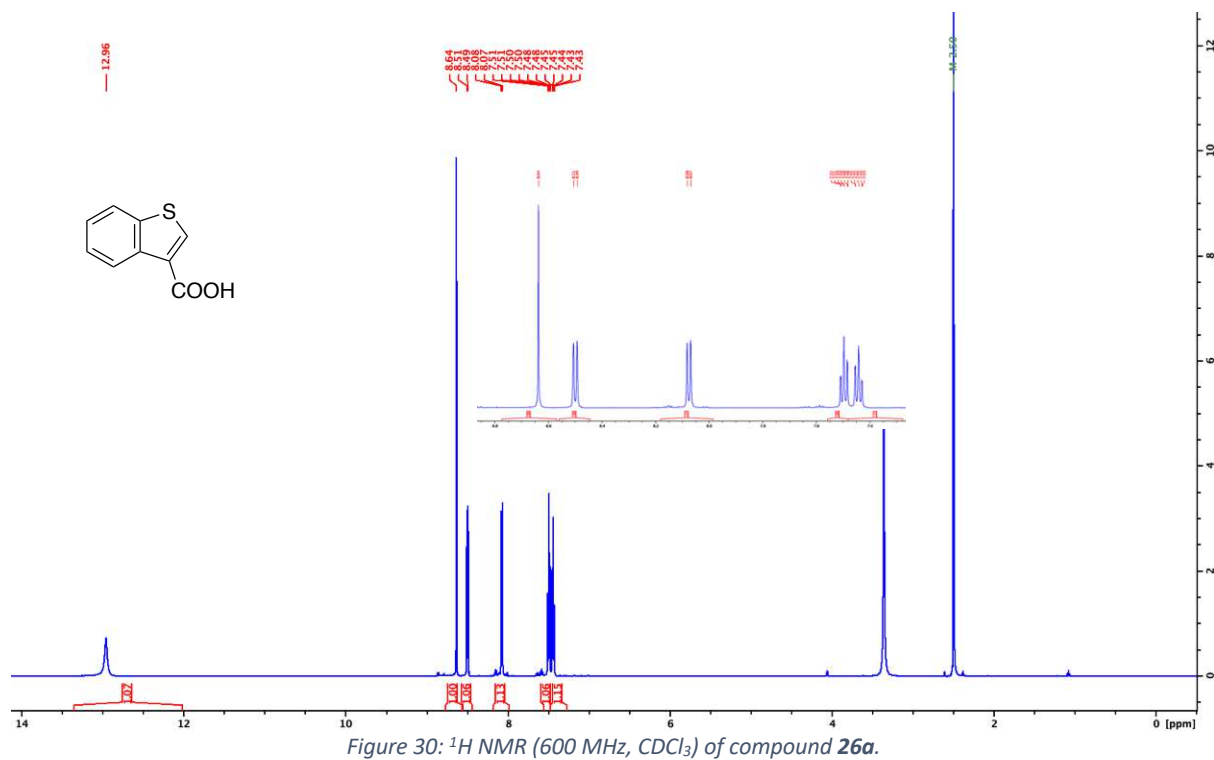
4.1 References

- [1] K. Liu, B. Ouyang, X. Guo, Y. Guo, Y. Liu, *npj Flex. Electron.* **2022**, 6, 1.
- [2] H. Letheby, *J. Chem. Soc.* **1862**, 15, 161.
- [3] H. Akamatu, H. Inokuchi, Y. Matsunaga, *Nature* **1954**, 173, 168.
- [4] C. K. Chiang, M. A. Druy, S. C. Gau, A. J. Heeger, E. J. Louis, A. G. MacDiarmid, Y. W. Park, H. Shirakawa, *J. Am. Chem. Soc.* **1978**, 100, 1013.
- [5] <https://www.nobelprize.org/prizes/chemistry/2000/summary/>.
- [6] K. Takimiya, S. Shinamura, I. Osaka, E. Miyazaki, *Heterocycles* **2011**, 83, 1187.
- [7] H. Koezuka, A. Tsumura, T. Ando, *Synth. Met.* **1987**, 18, 699.
- [8] A. Dodabalapur, L. Torsi, H. E. Katz, *Science* **1995**, 268, 270.
- [9] Y.-Y. Lin, D. J. Gundlach, S. F. Nelson, T. N. Jackson, *IEEE Electron Device Lett.* **1997**, 18, 606.
- [10] C. J. Kousseff, R. Halaksa, Z. S. Parr, C. B. Nielsen, *Chem. Rev.* **2022**, 122, 4397.
- [11] O. D. Jurchescu, J. Baas, T. T. M. Palstra, *Appl. Phys. Lett.* **2004**, 84, 3061.
- [12] H. Yoshida, N. Sato, *Phys. Rev. B* **2008**, 77, 235205.
- [13] R. R. Tykwinski, *Acc. Chem. Res.* **2019**, 52, 2056.
- [14] M. M. Payne, S. R. Parkin, J. E. Anthony, C.-C. Kuo, T. N. Jackson, *J. Am. Chem. Soc.* **2005**, 127, 4986.
- [15] P. Coppo, S. G. Yeates, *Adv. Mater.* **2005**, 17, 3001.
- [16] J. Chen, J. Anthony, D. C. Martin, *J. Phys. Chem. B* **2006**, 110, 16397.
- [17] H. Ebata, E. Miyazaki, T. Yamamoto, K. Takimiya, *Org. Lett.* **2007**, 9, 4499.
- [18] D. Yuan, W. Liu, X. Zhu, *Chem.* **2021**, 7, 333.
- [19] M. J. Griffith, S. Cottam, J. Stamenkovic, J. A. Posar, M. Petasecca, *Front. Phys.* **2020**, 8, 22.
- [20] H. Bronstein, C. B. Nielsen, B. C. Schroeder, I. McCulloch, *Nat. Rev. Chem.* **2020**, 4, 66.
- [21] E. K. Lee, M. Y. Lee, C. H. Park, H. R. Lee, J. H. Oh, *Adv. Mater.* **2017**, 29, 1703638.
- [22] G. Schweicher, G. Garbay, R. Jouclas, F. Vibert, F. Devaux, Y. H. Geerts, *Adv. Mater.* **2020**, 32, 1905909.
- [23] J. E. Anthony, D. L. Eaton, S. R. Parkin, *Org. Lett.* **2002**, 4, 15.
- [24] I. Salzmann, A. Moser, M. Oehzelt, T. Breuer, X. Feng, Z.-Y. Juang, D. Nabok, R. G. Della Valle, S. Duhm, G. Heimel, A. Brillante, E. Venuti, I. Bilotti, C. Christodoulou, J. Frisch, P. Puschnig, C. Draxl, G. Witte, K. Müllen, N. Koch, *ACS Nano* **2012**, 6, 10874.
- [25] X. Shi, W. Bao, *Front. Chem.* **2021**, 9, 723718.
- [26] A. L. Briseno, S. C. B. Mannsfeld, S. A. Jenekhe, Z. Bao, Y. Xia, *Mater. Today* **2008**, 11, 38.
- [27] W. Wang, Z. He, C. Di, D. Zhu, *Mater. Today Electronics* **2023**, 3, 100028.
- [28] J. Kang, D. Son, G. N. Wang, Y. Liu, J. Lopez, Y. Kim, J. Y. Oh, T. Katsumata, J. Mun, Y. Lee, L. Jin, J. B. -H. Tok, Z. Bao, *Adv. Mater.* **2018**, 30, 1706846.
- [29] S. Wang, J. Xu, W. Wang, G.-J. N. Wang, R. Rastak, F. Molina-Lopez, J. W. Chung, S. Niu, V. R. Feig, J. Lopez, T. Lei, S.-K. Kwon, Y. Kim, A. M. Foudeh, A. Ehrlich, A. Gasperini, Y. Yun, B. Murmann, J. B.-H. Tok, Z. Bao, *Nature* **2018**, 555, 83.
- [30] S. Calvi, L. Basiricò, S. M. Carturan, I. Fratelli, A. Valletta, A. Aloisio, S. De Rosa, F. Pino, M. Campajola, A. Ciavatti, L. Tortora, M. Rapisarda, S. Moretto, M. Verdi, S. Bertoldo, O. Cesarini, P. Di Meo, M. Chiari, F. Tommasino, E. Sarnelli, L. Mariucci, P. Branchini, A. Quaranta, B. Fraboni, *npj Flex. Electron.* **2023**, 7, 5.
- [31] C. Baudin, B. Vacquier, G. Thin, L. Chenene, J. Guersen, I. Partarrieu, M. Louet, H. Ducou Le Pointe, S. Mora, C. Verdun-Esquer, J. Feuarent, F. Rousseau, H. Roy, L. Bensefa-Colas, L. Boyer, M.-O. Bernier, *Eu.r Radiol.* **2023**, DOI 10.1007/s00330-023-09541-z.
- [32] M. Kraus, M. Redies, P. Richter, *OP-Journal* **2015**, 30, 138.
- [33] G. Mastrangelo, U. Fedeli, E. Fadda, A. Giovanazzi, L. Scoizzato, B. Saia, *Occup. Med.* **2005**, 55, 498.
- [34] A. Ciavatti, L. Basiricò, I. Fratelli, S. Lai, P. Cosseddu, A. Bonfiglio, J. E. Anthony, B. Fraboni, *Adv. Funct. Mater.* **2019**, 29, 1806119.

- [35] M. I. Ahmad, M. H. Ab. Rahim, R. Nordin, F. Mohamed, A. Abu-Samah, N. F. Abdullah, *Sensors* **2021**, *21*, 7629.
- [36] S. Kasap, J. B. Frey, G. Belev, O. Tousignant, H. Mani, J. Greenspan, L. Laperriere, O. Bubon, A. Reznik, G. DeCrescenzo, K. S. Karim, J. A. Rowlands, *Sensors* **2011**, *11*, 5112.
- [37] L. Basiricò, A. Ciavatti, B. Fraboni, *Adv. Mater. Technol.* **2021**, *6*, 2000475.
- [38] S. Lai, P. Cosseddu, L. Basiricò, A. Ciavatti, B. Fraboni, A. Bonfiglio, *Adv. Electron. Mater.* **2017**, *3*, 1600409.
- [39] A. Tamayo, I. Fratelli, A. Ciavatti, C. Martínez-Domingo, P. Branchini, E. Colantoni, S. De Rosa, L. Tortora, A. Contillo, R. Santiago, S. T. Bromley, B. Fraboni, M. Mas-Torrent, L. Basiricò, *Adv. Elec.t Mater.* **2022**, *8*, 2200293.
- [40] I. Temiño, L. Basiricò, I. Fratelli, A. Tamayo, A. Ciavatti, M. Mas-Torrent, B. Fraboni, *Nat. Commun.* **2020**, *11*, 2136.
- [41] C. A. Mills, Y.-F. Chan, A. Intaniwet, M. Shkunov, A. Nisbet, J. L. Keddie, P. J. Sellin, *Phys. Med. Biol.* **2013**, *58*, 4471.
- [42] A. Ciavatti, E. Capria, A. Fraleoni-Morgera, G. Tromba, D. Dreossi, P. J. Sellin, P. Cosseddu, A. Bonfiglio, B. Fraboni, *Adv. Mater.* **2015**, *27*, 7213.
- [43] B. Fraboni, A. Fraleoni-Morgera, N. Zaitseva, *Adv. Funct. Mater.* **2016**, *26*, 2276.
- [44] L. Basiricò, A. Ciavatti, I. Fratelli, D. Dreossi, G. Tromba, S. Lai, P. Cosseddu, A. Bonfiglio, F. Mariotti, C. Dalla Val, V. Bellucci, J. E. Anthony, B. Fraboni, *Front. Phys.* **2020**, *8*, 13.
- [45] L. Basiricò, A. Ciavatti, T. Cramer, P. Cosseddu, A. Bonfiglio, B. Fraboni, *Nat. Commun.* **2016**, *7*, 13063.
- [46] J. C. Sorli, Q. Ai, D. B. Granger, K. Gu, S. Parkin, K. Jarolimek, N. Telesz, J. E. Anthony, C. Risko, Y.-L. Loo, *Chem. Mater.* **2019**, *31*, 6615.
- [47] M. Heeney, W. Zhang, I. McCulloch, *Organic Semiconductors*, **2008**, WO 2008/131835 A1.
- [48] D. Singh, A. M. Deobald, L. R. S. Camargo, G. Tabarelli, O. E. D. Rodrigues, A. L. Braga, *Org. Lett.* **2010**, *12*, 3288.
- [49] R. Varala, E. Ramu, S. R. Adapa, *Bull. Chem. Soc. Jpn.* **2006**, *79*, 140.
- [50] J. Ponce González, M. Edgar, M. R. J. Elsegood, G. W. Weaver, *Org. Biomol. Chem.* **2011**, *9*, 2294.
- [51] H. J. Reich, M. J. Bevan, B. Ö. Gudmundsson, C. L. Puckett, *Angew. Chem. Int. Ed.* **2002**, *41*, 3436.
- [52] B. H. Lipshutz, A. R. Abela, Ž. V. Bošković, T. Nishikata, C. Duplais, A. Krasovskiy, *Top Catal.* **2010**, *53*, 985.
- [53] P. Saravanan, P. Anbarasan, *Org. Lett.* **2014**, *16*, 848.
- [54] Z.-T. Du, T. Zhang, Y.-F. Chen, R.-Y. Ma, L.-N. Zhou, *Heterocycles* **2016**, *92*, 1874.
- [55] J. Lv, Q. Liu, J. Tang, F. Perdih, K. Kranjc, *Tetrahedron Lett.* **2012**, *53*, 5248.
- [56] C. Zhao, T. Schwartz, B. Stöger, F. J. White, J. Chen, D. Ma, J. Fröhlich, P. Kautny, *J. Mater. Chem. C* **2018**, *6*, 9914.
- [57] O. Allemann, S. Duttwyler, P. Romanato, K. K. Baldridge, J. S. Siegel, *Science* **2011**, *332*, 574.
- [58] K. Yu. Amsharov, M. A. Kabdulov, M. Jansen, *Angew. Chem. Int. Ed.* **2012**, *51*, 4594.
- [59] Horkel, Ernst, Synthese Neuer N,N'-Dialkenylthiophendicarboxamide Als Substrate Für Ringschlußmetathesereaktionen, Dissertation, TU Wien, **2007**.
- [60] T. Kashiki, S. Shinamura, M. Kohara, E. Miyazaki, K. Takimiya, M. Ikeda, H. Kuwabara, *Org. Lett.* **2009**, *11*, 2473.
- [61] B. Holzer, B. Dellago, A. Thamm, T. Mathis, B. Stöger, E. Horkel, C. Hametner, B. Batlogg, J. Fröhlich, D. Lumpi, *Chem. Eur. J.* **2020**, *26*, 2869.
- [62] D. W. Slocum, P. L. Gierer, *J. Org. Chem.* **1976**, *41*, 3668.
- [63] V. Snieckus, *Chem. Rev.* **1990**, *90*, 879.
- [64] G. E. Purdum, N. G. Telesz, K. Jarolimek, S. M. Ryno, T. Gessner, N. C. Davy, A. J. Petty, Y. Zhen, Y. Shu, A. Facchetti, G. E. Collis, W. Hu, C. Wu, J. E. Anthony, R. T. Weitz, C. Risko, Y.-L. Loo, *J. Am. Chem. Soc.* **2018**, *140*, 7519.
- [65] J. L. Bredas, J. P. Calbert, D. A. da Silva Filho, J. Cornil, *Proc. Natl. Acad. Sci. U.S.A.* **2002**, *99*, 5804.

- [66] N. N. Karaush-Karmazin, G. V. Baryshnikov, A. V. Kuklin, D. I. Saykova, H. Ågren, B. F. Minaev, *J. Mater. Chem. C* **2021**, *9*, 1451.
- [67] A. M. Wallace, C. Curiac, J. H. Delcamp, R. C. Fortenberry, *J. Quant. Spectrosc. Radiat. Transf.* **2021**, *265*, 107544.
- [68] Y.-F. Lim, Y. Shu, S. R. Parkin, J. E. Anthony, G. G. Malliaras, *J. Mater. Chem.* **2009**, *19*, 3049.
- [69] J. Pommerehne, H. Vestweber, W. Guss, R. F. Mahrt, H. Bässler, M. Porsch, J. Daub, *Adv. Mater.* **1995**, *7*, 551.
- [70] E. J. Thomas, Ed., *Science of Synthesis, 10: Category 2, Hetarenes and Related Ring Systems: Fused Five-Membered Hetarenes with One Heteroatom*, Georg Thieme Verlag, Stuttgart, **2000**.
- [71] E. Paegle, S. Belyakov, P. Arsenyan, *Eur. J. Org. Chem.* **2014**, *2014*, 3831.

4.2 Appendix





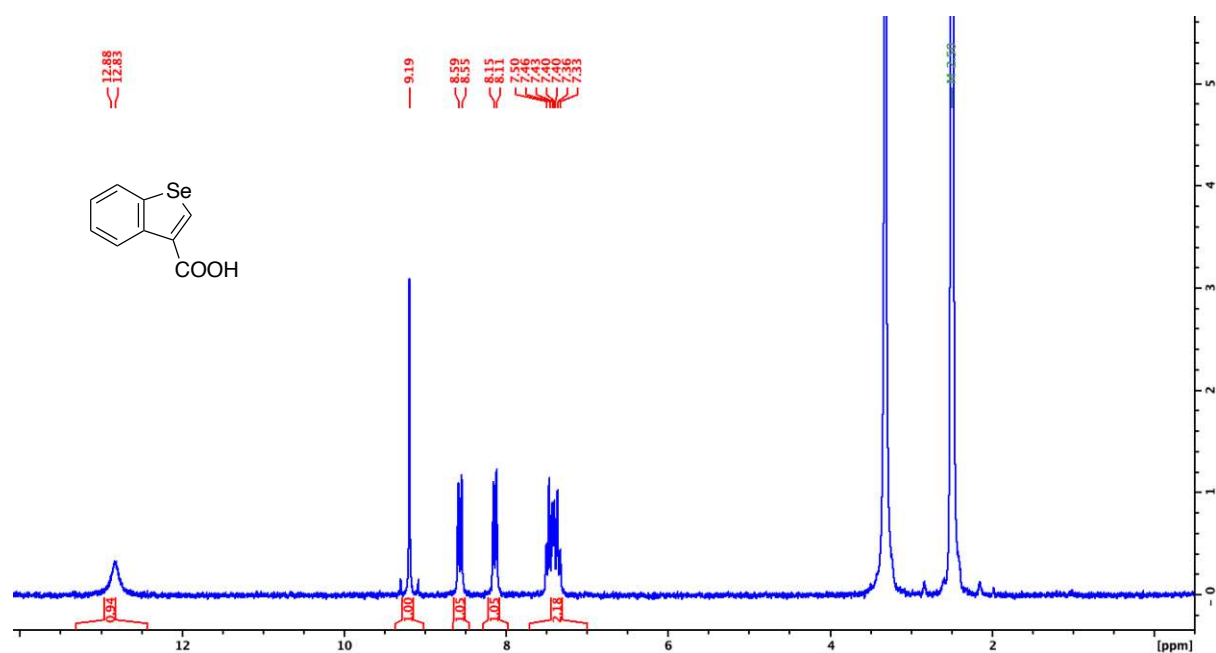


Figure 34: ¹H NMR (600 MHz, CDCl₃) of compound **26b**.

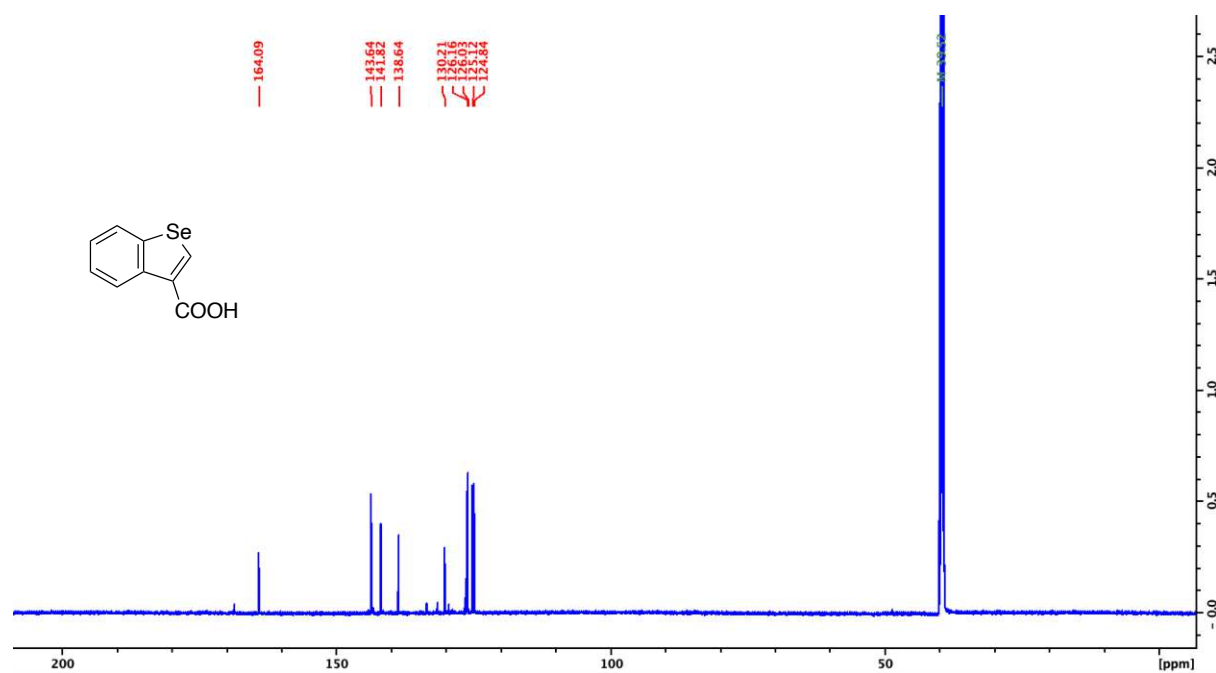


Figure 35: ¹³C NMR (150 MHz, CDCl₃) of compound **26b**.

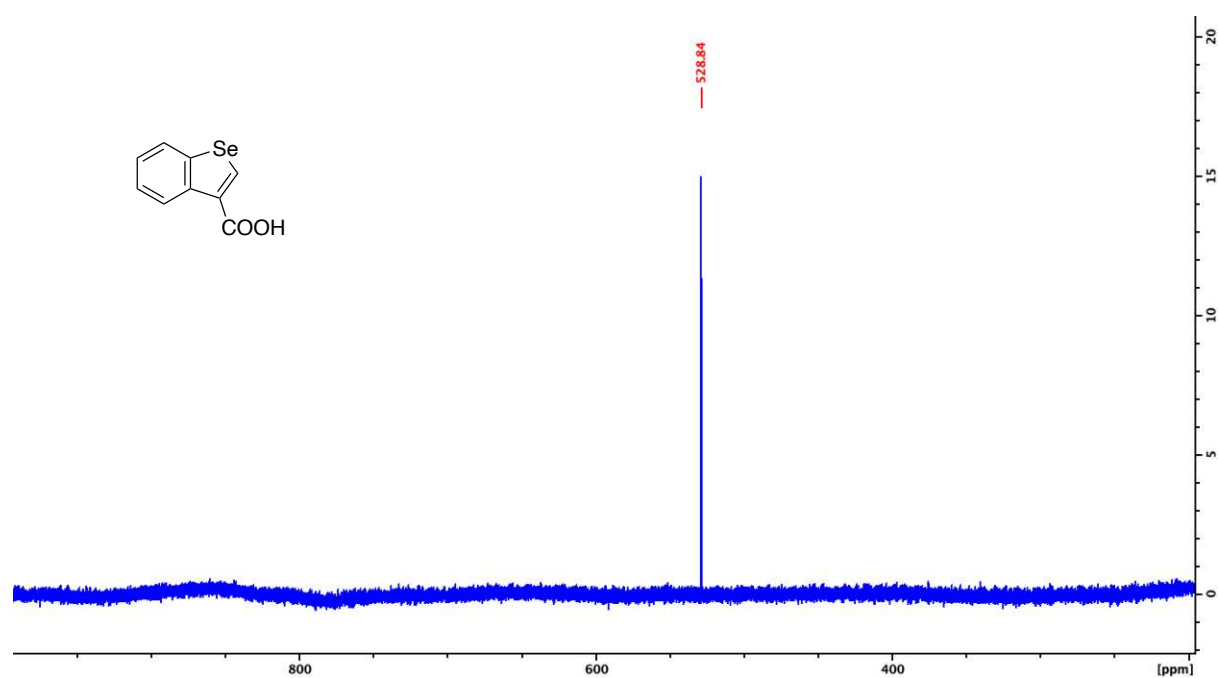
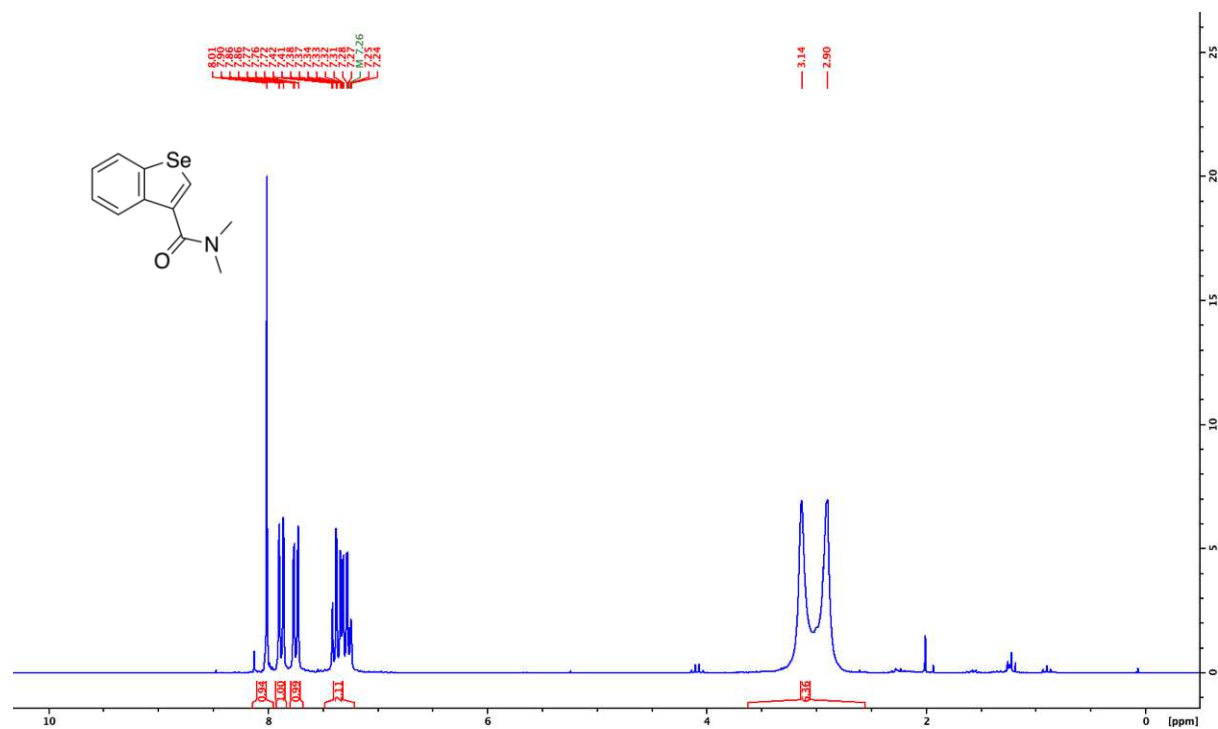


Figure 36: ^{77}Se NMR (114 MHz, CDCl_3) of compound **26b**.



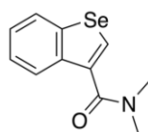


Figure 38: ^{13}C NMR (50 MHz, CDCl_3) of compound **VIIb**.

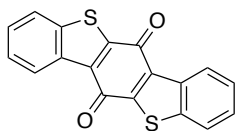


Figure 39: ^1H NMR (600 MHz, CDCl_3) of compound **6a**.

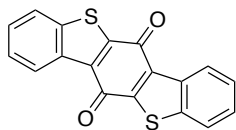
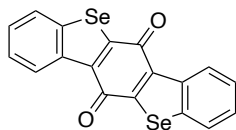


Figure 41: ^1H NMR (600 MHz, CDCl_3) of compound **Vlb**.



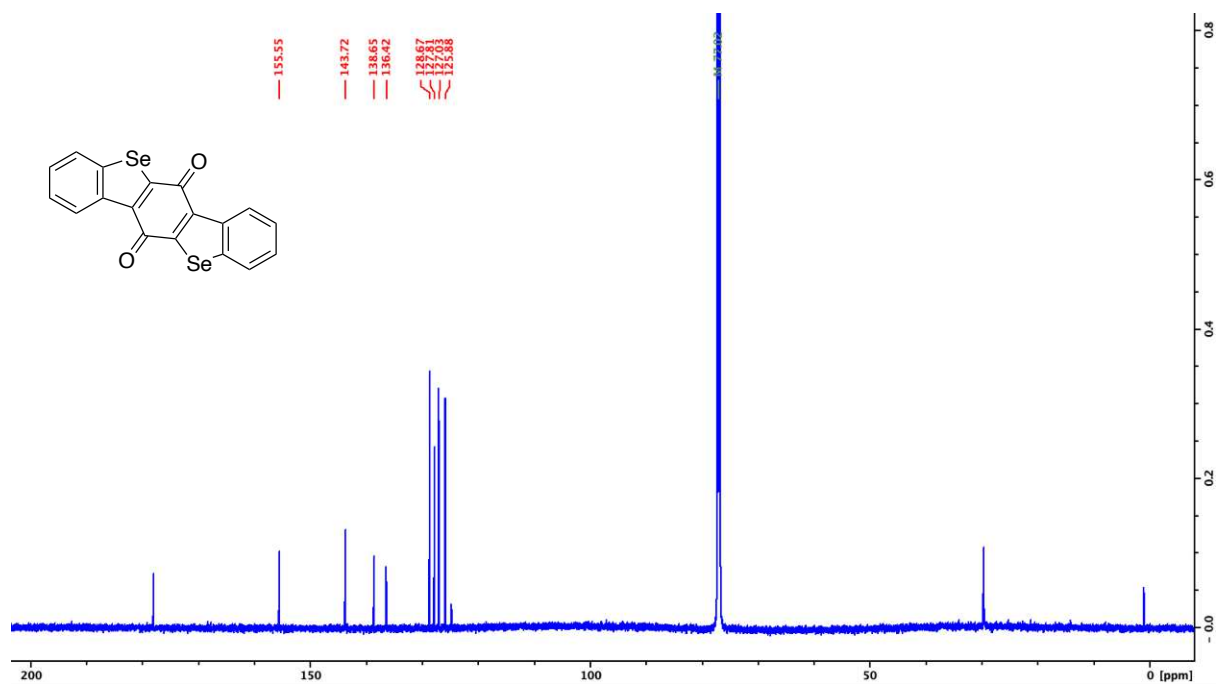


Figure 42: ¹³C NMR (150 MHz, CDCl₃) of compound VIb.

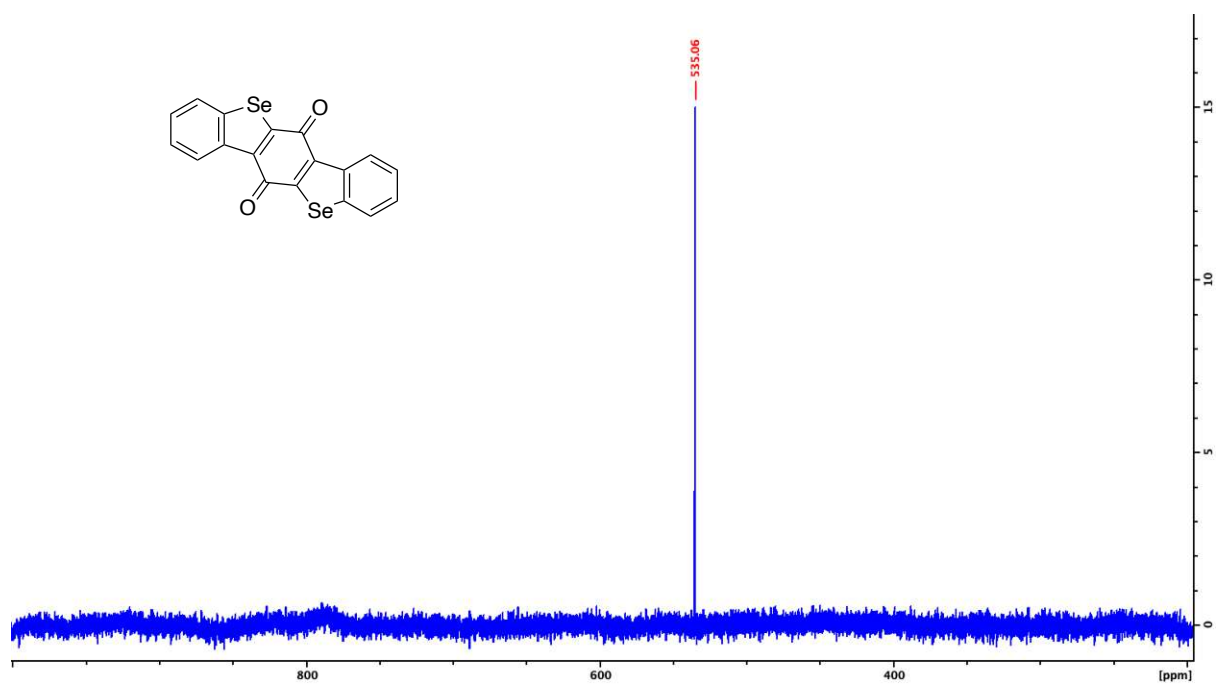
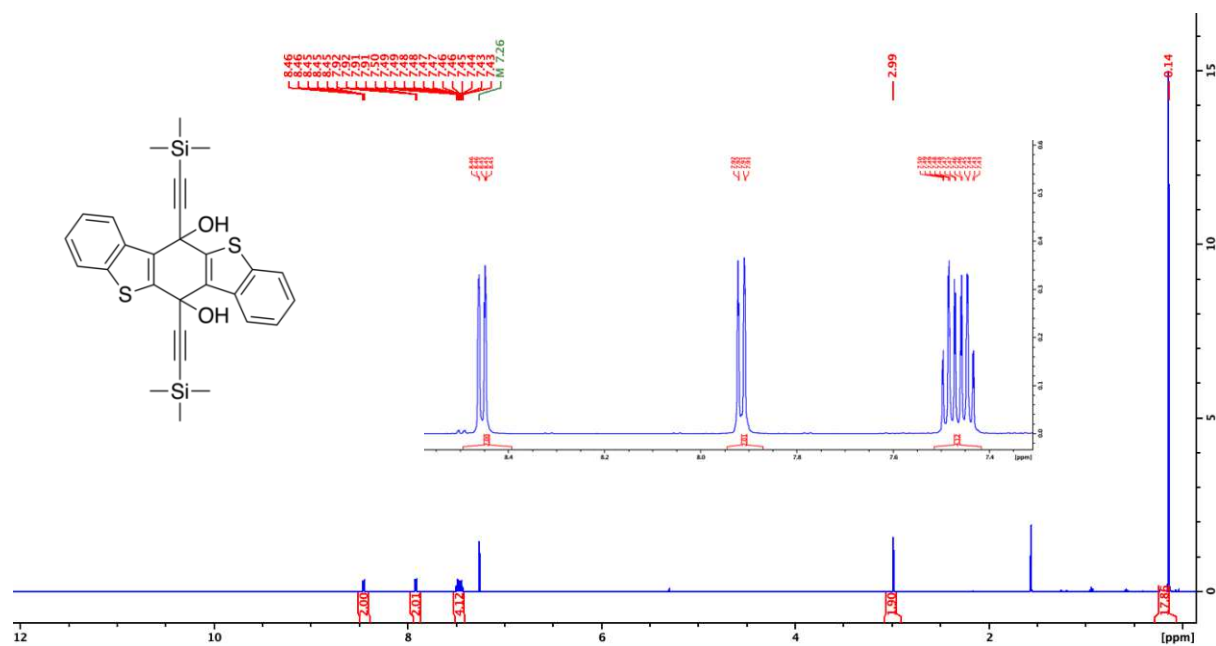
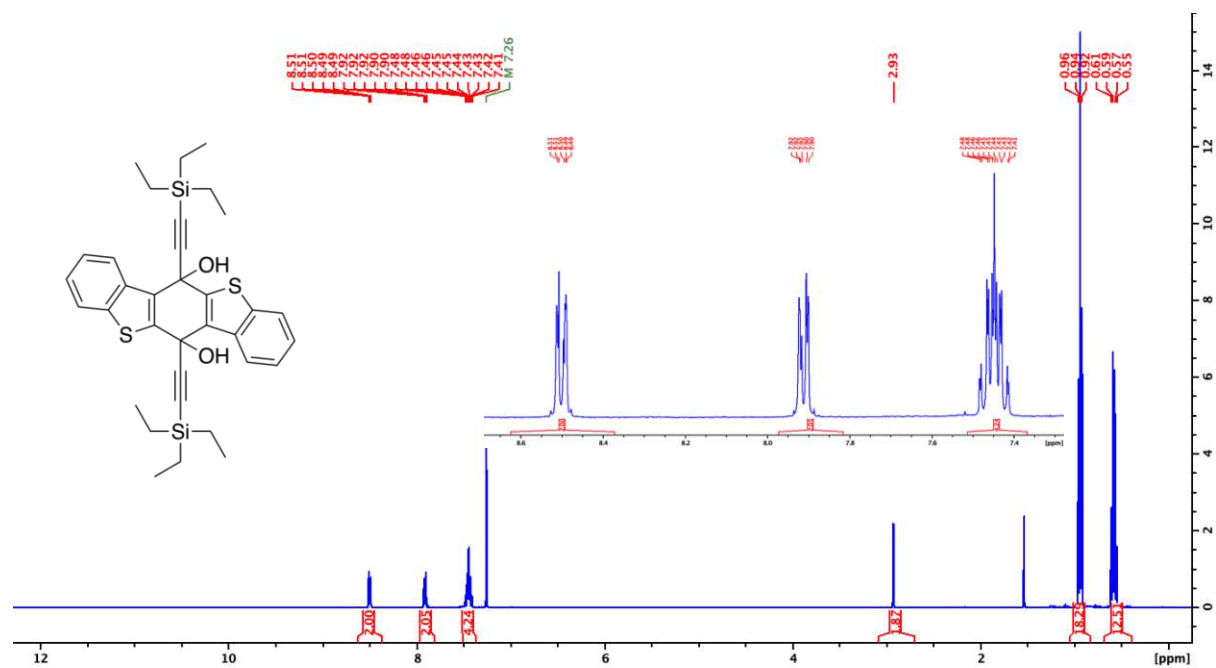


Figure 43: ⁷⁷Se NMR (114 MHz, CDCl₃) of compound VIb.





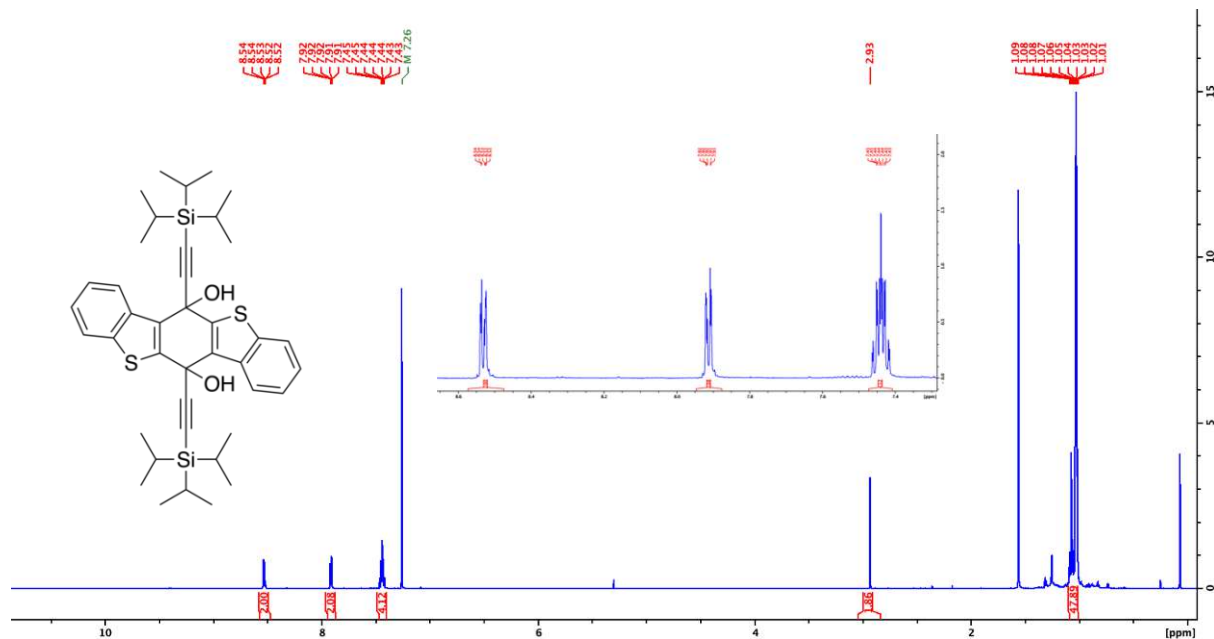


Figure 48: ^1H NMR (600 MHz, CDCl_3) of compound **5c**.

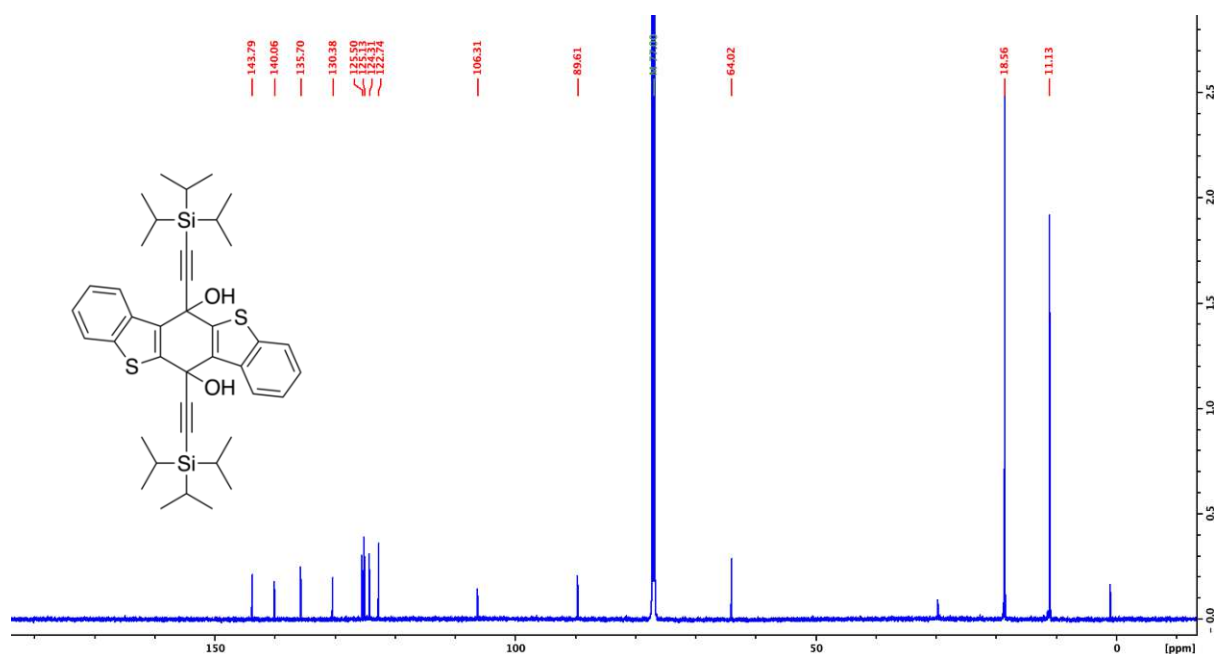


Figure 49: ^{13}C NMR (150 MHz, CDCl_3) of compound **5c**.

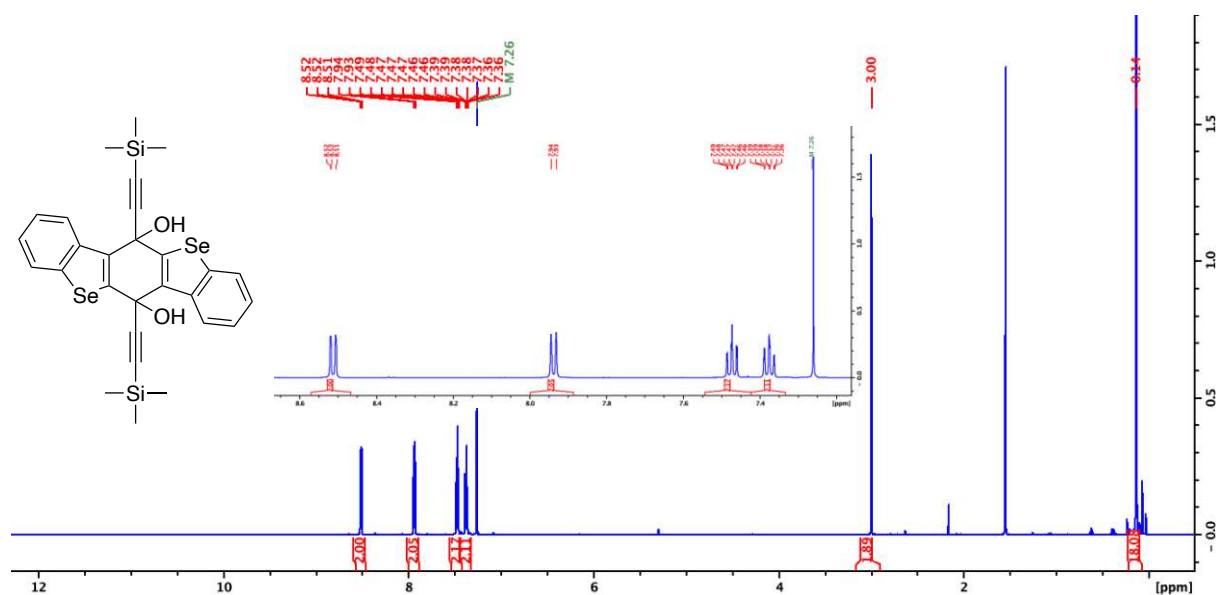


Figure 50: ^1H NMR (600 MHz, CDCl_3) of compound **Va**.

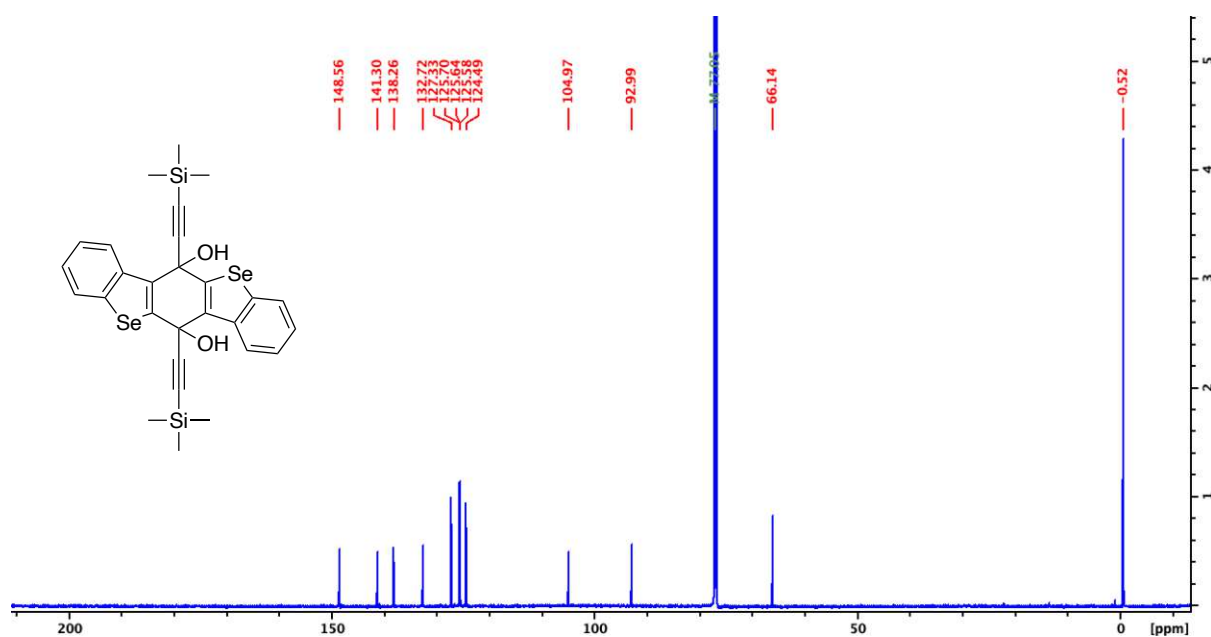


Figure 51: ^{13}C NMR (150 MHz, CDCl_3) of compound **Va**.

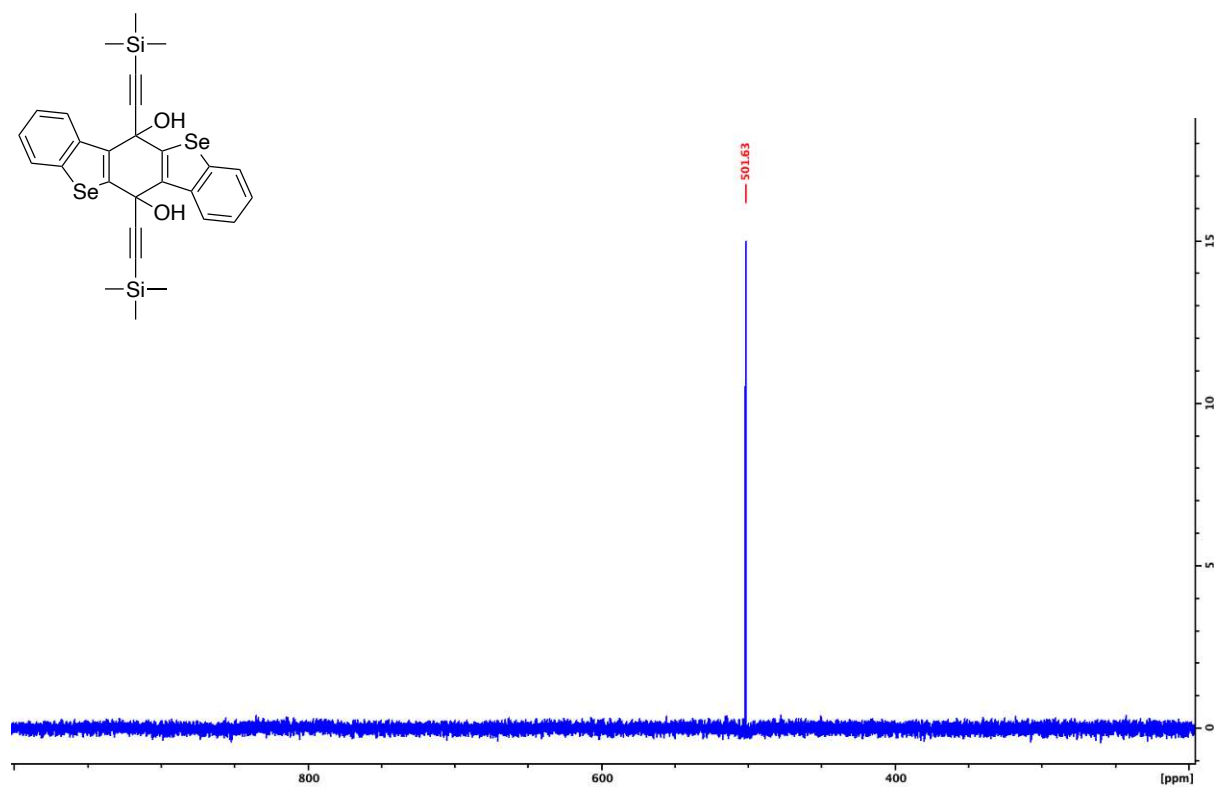


Figure 52: ^{77}Se NMR (114 MHz, CDCl_3) of compound **Va**.

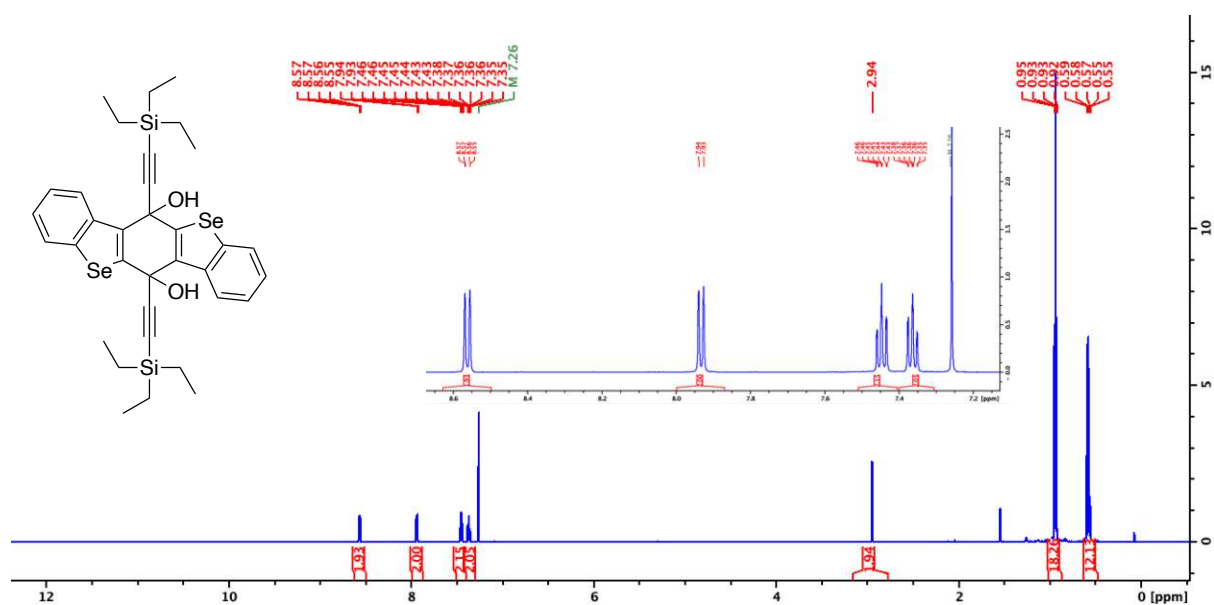


Figure 53: ^1H NMR (600 MHz, CDCl_3) of compound **Vb**.

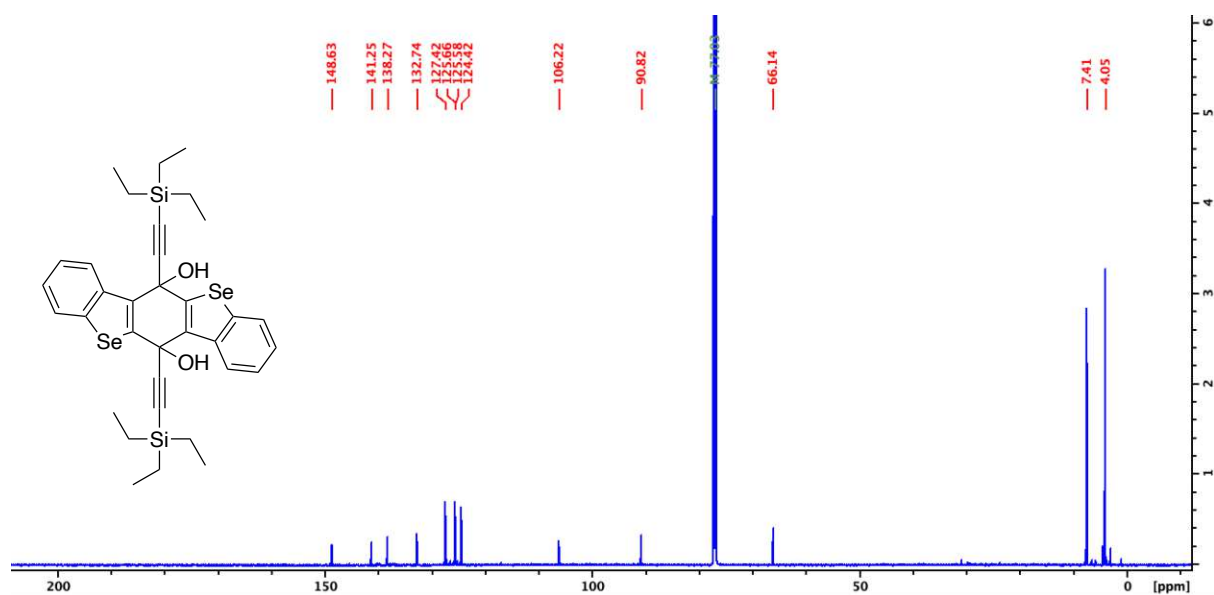


Figure 54: ¹³C NMR (150 MHz, CDCl₃) of compound Vb.

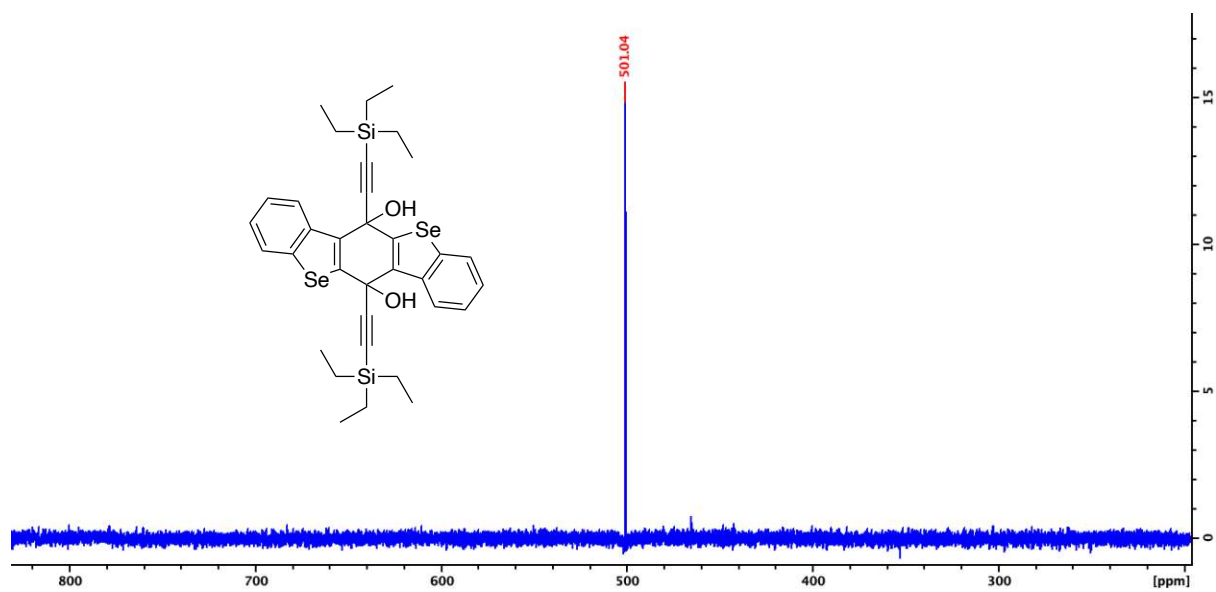
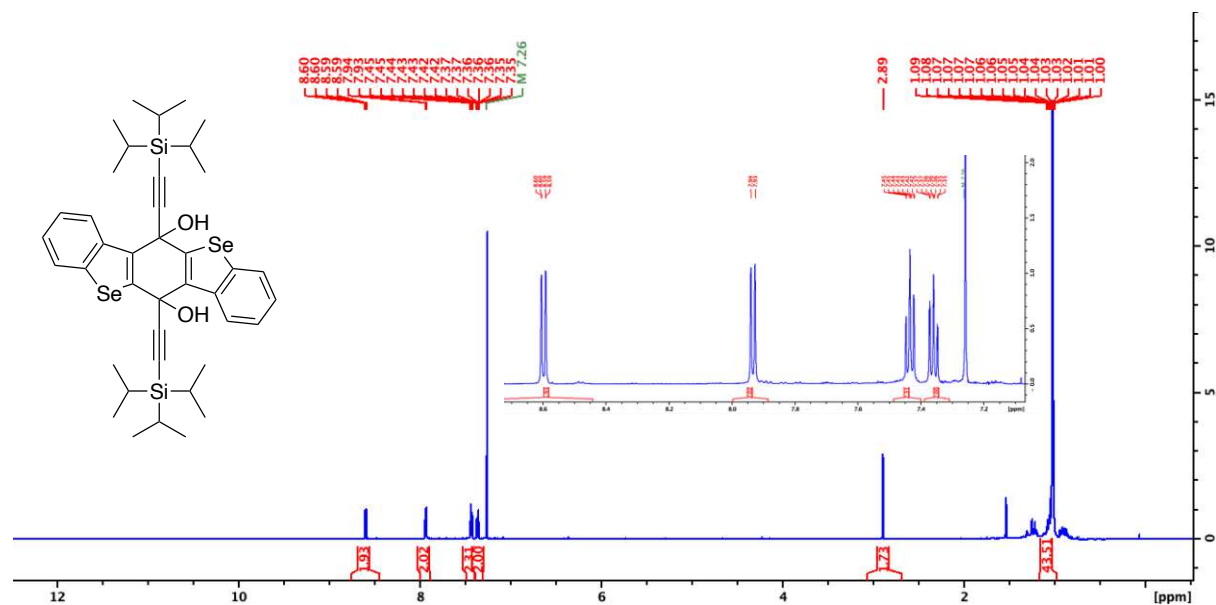


Figure 55: ⁷⁷Se NMR (114 MHz, CDCl₃) of compound Vb.







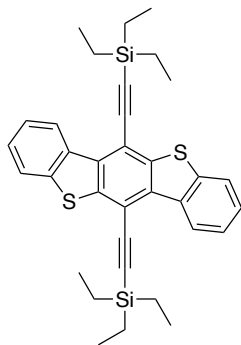


Figure 62: ^{13}C NMR (100 MHz, CDCl_3) of compound **2b**.

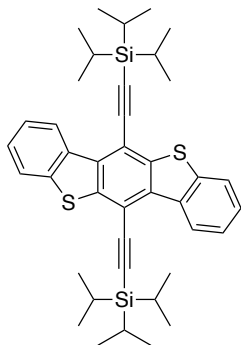


Figure 63: ^1H NMR (600 MHz, CDCl_3) of compound **2c**.

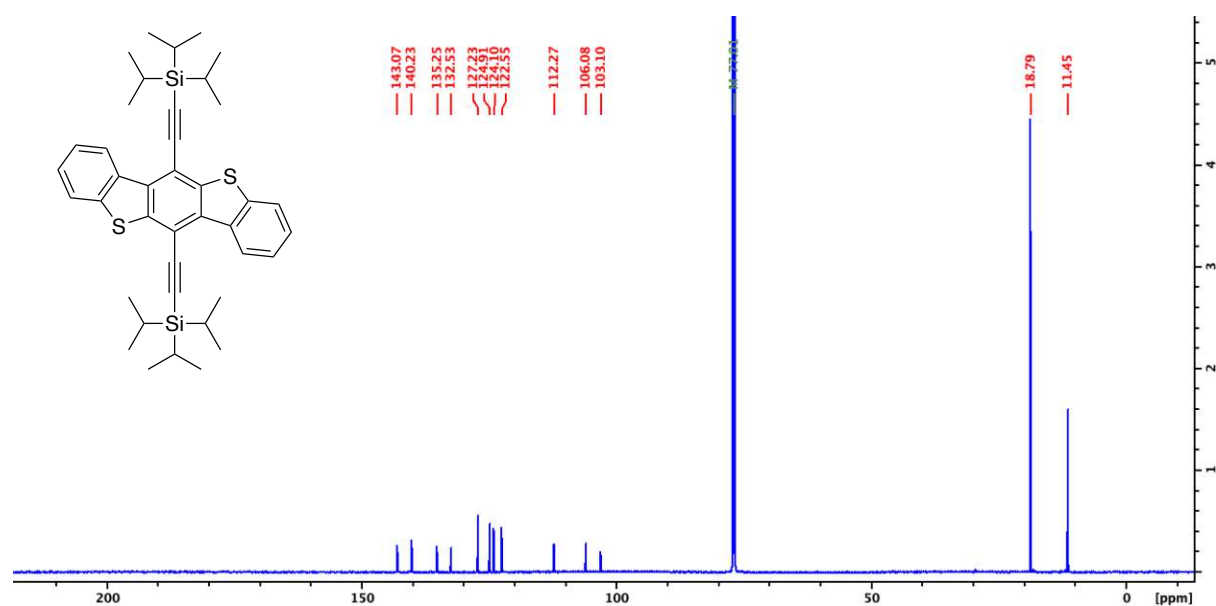


Figure 64: ^{13}C NMR (150 MHz, CDCl_3) of compound **2c**.

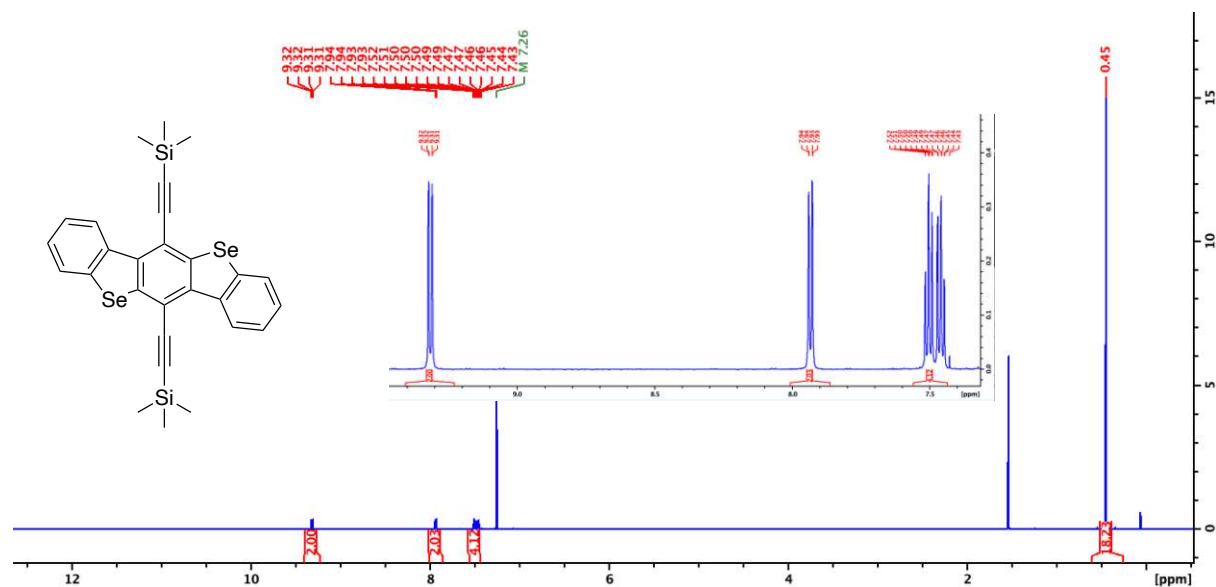


Figure 65: ^1H NMR (600 MHz, CDCl_3) of compound **1a**.

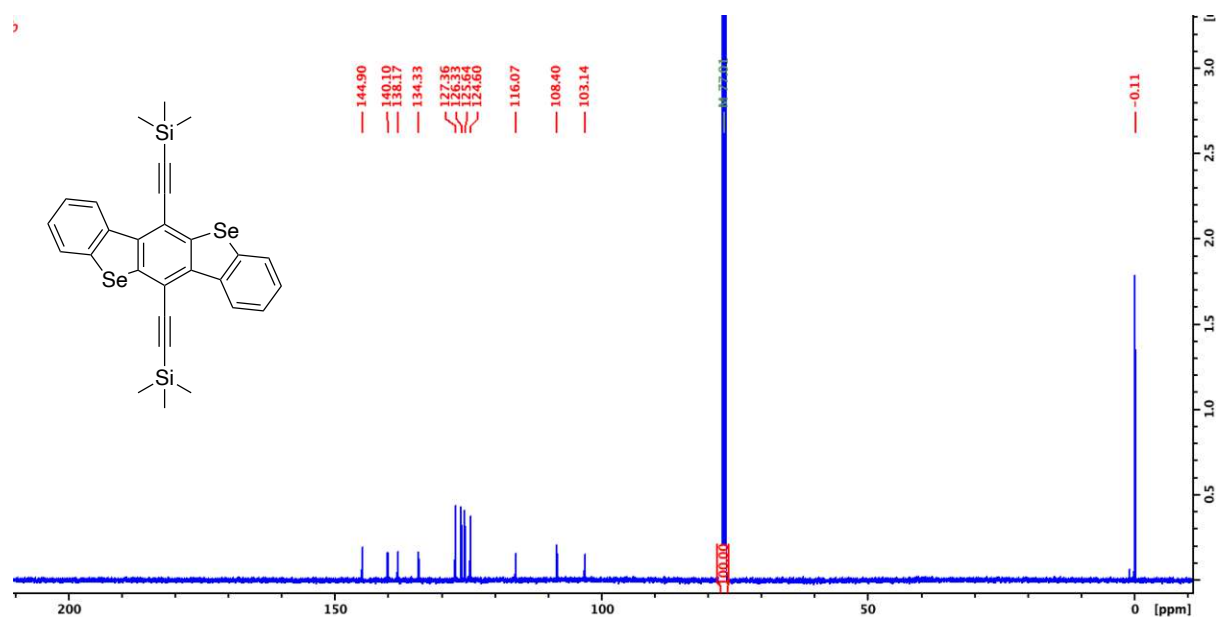


Figure 66: ^{13}C NMR (150 MHz, CDCl_3) of compound **1a**.

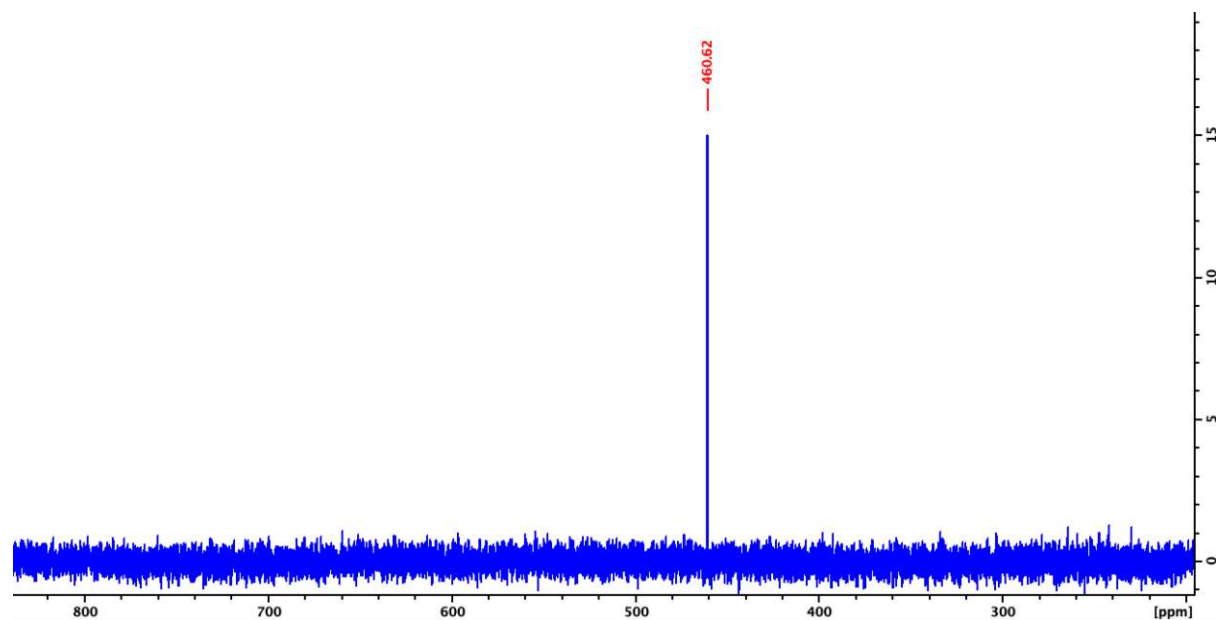


Figure 67: ^{77}Se NMR (114 MHz, CDCl_3) of compound **1a**.

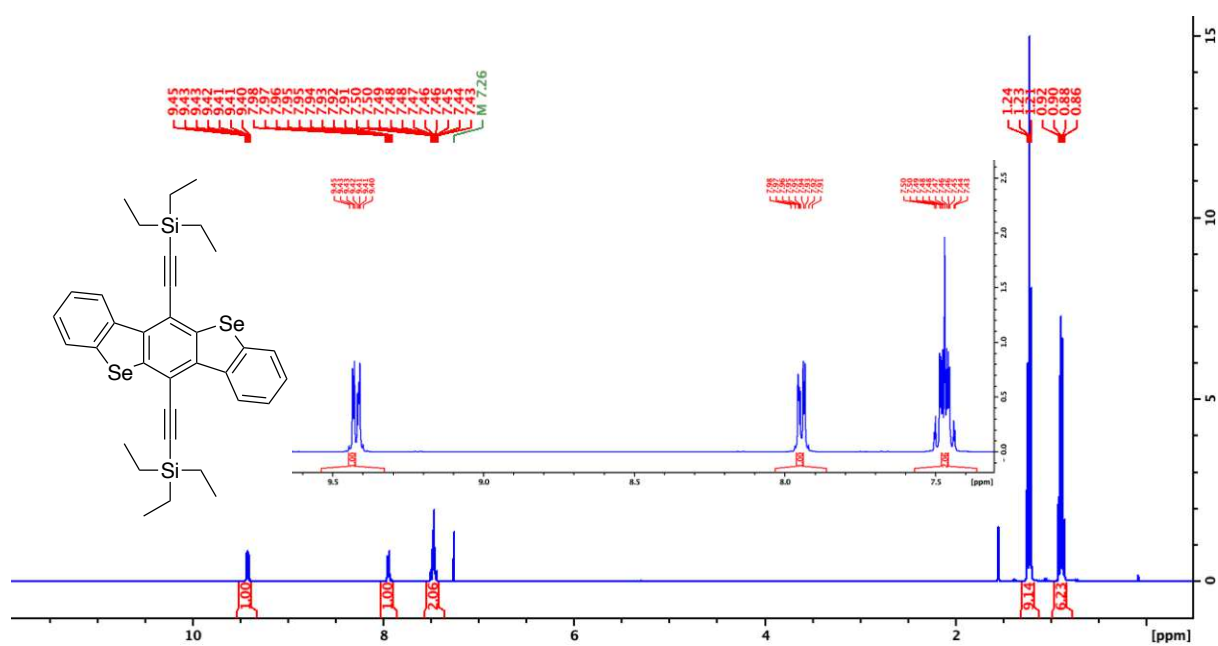


Figure 68: ¹H NMR (400 MHz, CDCl₃) of compound 1b.

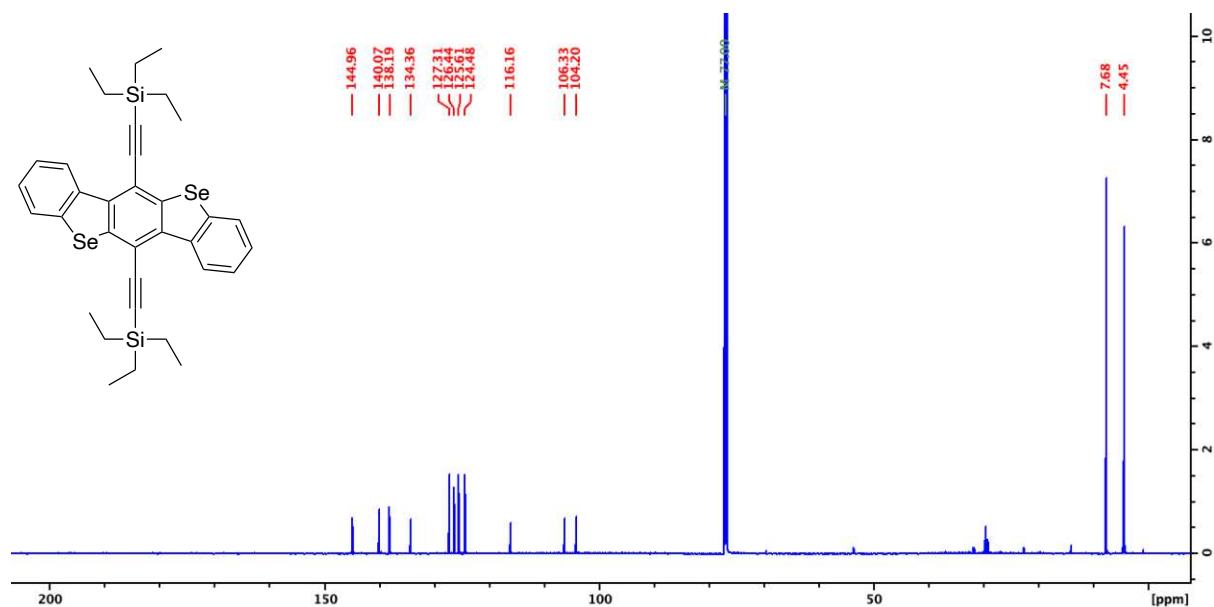
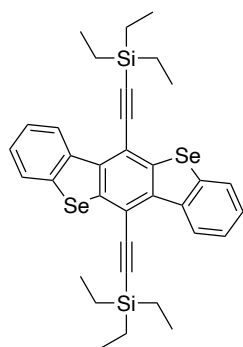


Figure 69: ¹³C NMR (150 MHz, CDCl₃) of compound 1b.



7.96
7.96
7.95
7.95
7.94
7.93
7.47
7.47
7.46
7.46
7.45
7.45 M 7.26

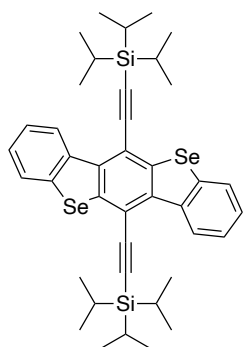


Figure 71: ^1H NMR (400 MHz, CDCl_3) of compound 1c.

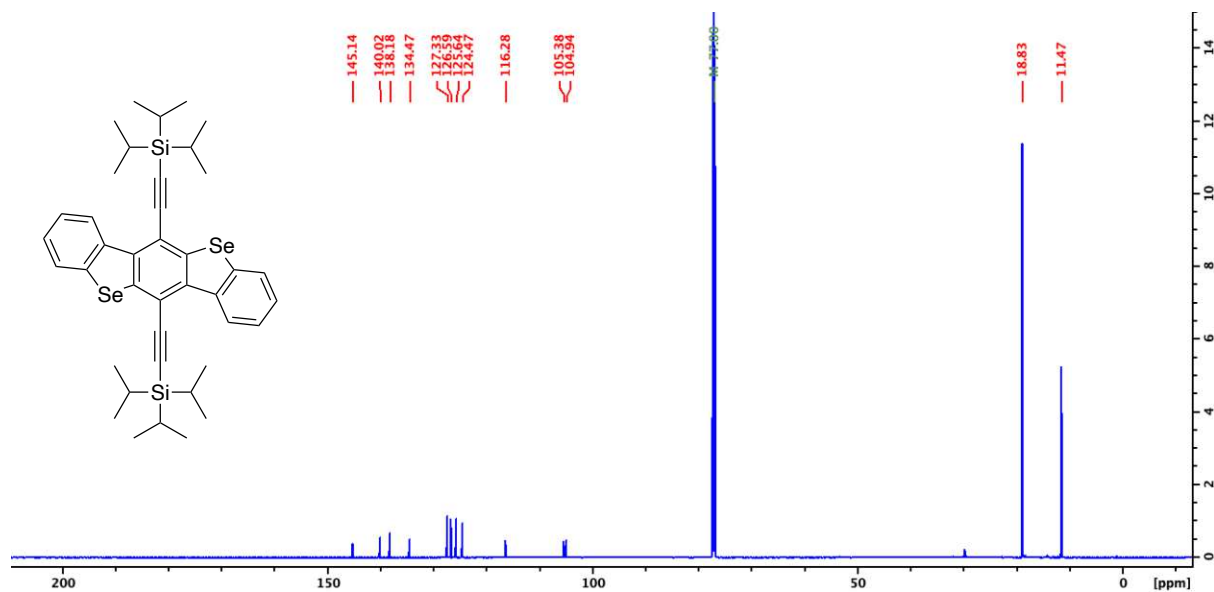


Figure 72: ¹³C NMR (150 MHz, CDCl₃) of compound 1c.

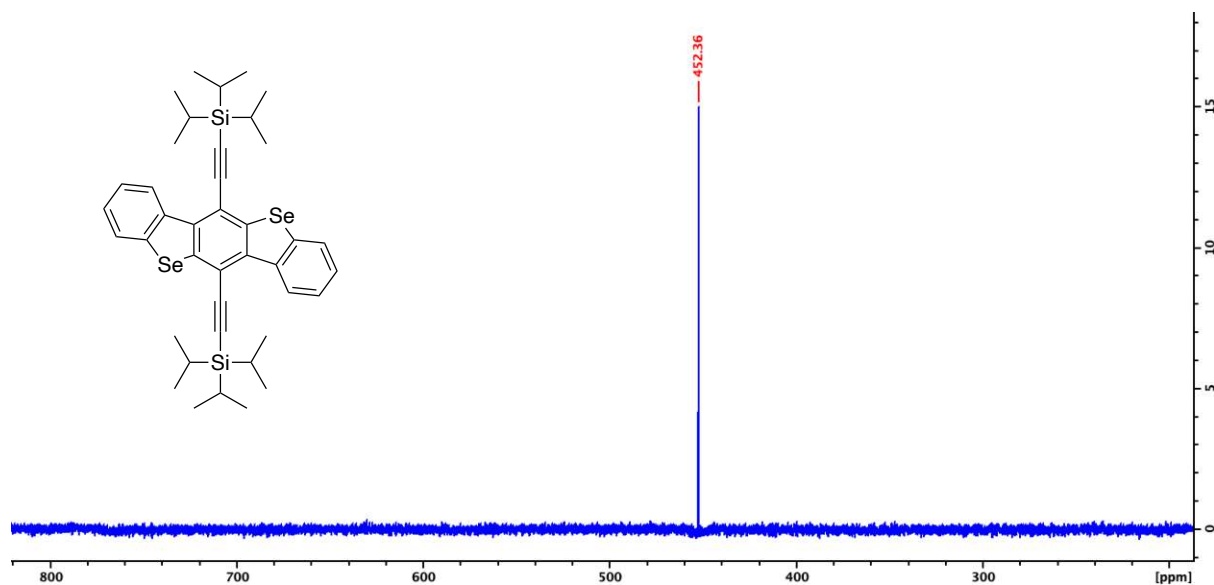


Figure 73: ⁷⁷Se NMR (114 MHz, CDCl₃) of compound 1c.